Atmospheric response to zonally averaged sea surface temperatures in the North Atlantic

-a model study

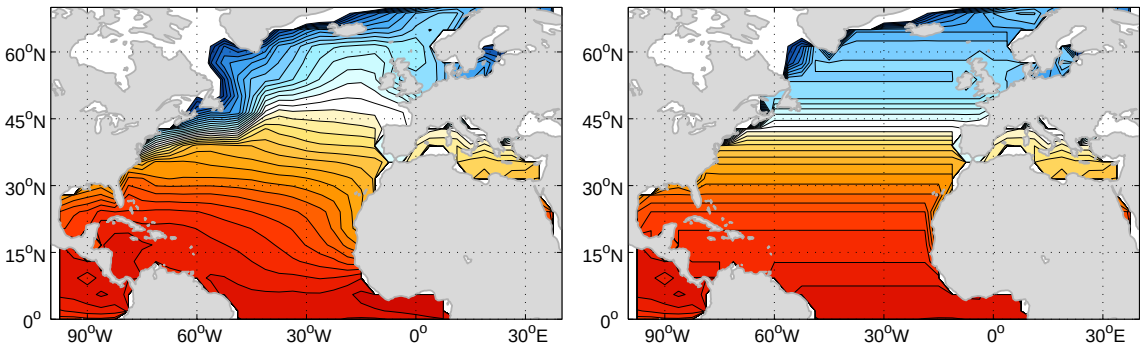

Master Thesis in Meteorology

Stig-Arild Fagerli

May 29, 2008

UNIVERSITY OF BERGEN
GEOPHYSICAL INSTITUTE

Look up, marvel at the ephemeral beauty,
and live life with your head in the clouds.
- *The Cloud Appreciation Society* -

The left figure on the front page show the climatological SSTs in winter. To the right is the hypothesized pattern of winter SSTs in the absence of North Atlantic ocean circulation.

The thesis is written in LaTeX2ϵ, 12 point text, report style and twosided format.

Acknowledgements

Many people have helped me through my time as a student here in Bergen. I feel that here is the place to thank (at least some of) them.

First and foremost I owe my gratitude to my supervisor, Nils Gunnar Kvamstø, for assigning me to this truly interesting (and complex) field of study. My co-supervisor, Jürgen Bader, also deserve my deepest thanks for performing the runs with the SPEEDY model and for the numerous discussions and tips along the way. Without you two, the next pages would definitely be left blank. Our discussions have spanned the whole spectrum, from the more or less intricate climate related topics, to the ones (maybe not less intricate) regarding broken down gearboxes and washing machines. I'm happy to have been included in them all!

I thank Tarjei Breiteig for his willingness to read through my thesis and providing me with invaluable feedback, both through spoken and written words. Tarjei also deserves many thanks for the inspiring lectures he gave in dynamics in the fall of 2006 and for his beautiful handling of the german language. Thanks also to Ivar Seierstad for his general enthusiasm and for developing nice Matlab-scripts. I also acknowledge Christophe Sturm who developed scripts for reading in the data, as well as Justin Wettstein and Camille Li for their comments on the work.

The people at the ICTP is acknowledged for developing the model used in this thesis.

Thanks to the staff at 'Geofysen' and BCCR for making this place a nice arena for learning. I'm grateful for the funds provided by the institute for the EGU-conference in Vienna. Also thanks to Storm Weather Center for letting me use their software when I made my poster.

I'm forever grateful to my family for their neverending support. You have always given me good advice in life!

I owe much to all the great musicians of the world (especially the polka bands of the mighty Finnish woods) who through my entire life have helped me out in times where the world seemed to collapse. Sorry, Berit, Ina and all the rest; I shouldn't have played it that loud. :)

Thanks to all my fellow students at the institute, and in particular the ones at ODD. In the end I guess we'll all miss this room, although it right now would be somewhat nicer with some fresh air.

Finally, I have to thank Helene for her eternal positive attitude and also congratulate her with finishing her master thesis. You ROCK!

Stig-Arild Fagerli

Bergen, May 29, 2008

Contents

1 Introduction **1**
1.1 Motivation . . . 3

2 Background **6**
2.1 Procedure of forcing the atmosphere . . . 6
2.2 Direct linear response to surface heating . . . 7
2.3 Thermal forcing of stationary waves . . . 9
2.3.1 Midlatitudes . . . 11
2.3.2 Tropics . . . 13
2.4 Large-scale patterns of atmospheric variability . . . 17
2.4.1 North Atlantic Oscillation . . . 18
2.4.2 East Atlantic pattern . . . 19
2.5 Observed and modeled impacts of SSTa on atmospheric circulation . . . 20
2.5.1 Earlier model experiments with prescribed midlatitude sea-surface temperature anomalies . . . 21
2.5.2 Large scale co-variability of oceanic and atmospheric circulation . . . 23

3 SPEEDY and statistical methods **29**
3.1 SPEEDY Model . . . 29
3.1.1 General . . . 29
3.1.2 Current resolution . . . 30
3.1.3 Physical parameterizations . . . 31
3.1.4 Validations of SPEEDY . . . 34
3.2 EOF-analysis . . . 37
3.3 Statistical significance tests . . . 39
3.3.1 Student's t-test . . . 39
3.3.2 F-test . . . 40

4 Experimental design **42**

5 Equilibrium atmospheric response **46**
5.1 Mean change of atmospheric circulation . . . 46
5.1.1 Winter . . . 46

5.1.2 Summer . . . 51
5.2 Response in near-surface winds and in the jet . . . 55
5.3 Response in temperature . . . 59
5.3.1 Spatial signature . . . 59
5.3.2 Vertical signature . . . 60
5.4 Sea-surface heat fluxes . . . 62

6 Response in variability **67**
6.1 Mean Sea-Level Pressure . . . 68
6.1.1 Low-frequency variability of the Icelandic Low . . . 68
6.2 Geopotential height . . . 71
6.3 Changes in large-scale variability patterns . . . 72

7 Importance of the tropical and extra-tropical SST forcing **77**
7.1 Description and results from EX-Tr and Tr . . . 77

8 Summary and concluding remarks **86**
8.1 Future work . . . 87

A Derivations and figures **89**
A.1 Upper limit for linear response in Z_{500} . . . 89
A.2 The quasi-geostrophic assumption . . . 90
A.2.1 The momentum equation . . . 91
A.2.2 The thermodynamic energy equation . . . 93
A.3 Linearizing equations 2.4 and 2.5 about the zonally averaged flow . . . 93
A.4 Spatial properties EOFs in CTRL . . . 95

B List of Figures **97**

C List of Acronyms **99**

Chapter 1

Introduction

The world oceans receive more than half of the total solar energy input to the climate system, where most of this energy enters the basins near the equator (Hartmann 1994). The differential energy input between the tropics and extra-tropics results in a meridional large-scale temperature-gradient in both the air- and sea-surface temperatures (SST). The excess radiative energy input in the tropical region is balanced in the atmosphere mainly through temperature advection or adiabatic cooling due to enhanced convection (Holton 2004), whereas in the ocean there is a net oceanic heat transport from low to high latitudes (Bearman 2002). In addition, the atmosphere and ocean are continuously interacting through turbulent fluxes of latent and sensible heat which act to dampen the temperature gradient between the two.

When looking into the climatological state of the ocean currents, there can in many places be seen a zonal asymmetry which tend to induce a basin-wide zonal SST-gradient. In the North Atlantic, this gradient is maintained by the Gulf Stream and the Canary Current in the subtropics, and by the North Atlantic and Labrador currents in mid- to high latitudes. Also, wind-induced divergent oceanic flow act to strengthen this zonal gradient due to upwelling of colder water, especially is this the case in the subtropical East Atlantic.

The topic for the present work is to investigate the effect a dynamical North Atlantic Ocean, and consequently this zonally asymmetric distribution of heat, has on the atmospheric circulation in contrast to a more dynamically passive Atlantic which would have more zonal distribution of SSTs. Doing such a study based purely on observational records is hard, if not impossible, due to the numerous complex intrinsic processes appearing in the coupled climate system (Barsugli and Battisti 1998). It is therefore believed that such a survey demand usage of a somewhat idealized model experiment to enable an analysis of the response. The hope for this kind of research is that a simplification of the problem would lead to a better understanding of the fully coupled system (Kushnir et al. 2002). Therefore, runs with an atmospheric general circulation model (AGCM) with a prescribed SST-distribution over the North Atlantic have been conducted.

The next section gives insight to the motivation for the present thesis, as well as some of the questions hoped to be answered during the work. Chapter 2 is meant to provide a basic back-

ground of the atmosphere's theoretical, observed and modeled response to anomalies in SST or ocean circulation. Here, also an overview of previous work and topics which might be directly or indirectly relevant is given. Chapters 3 and 4 describe the model used and the experimental setup, as well as giving a synopsis of the methods used in this thesis. The results are divided into the mean atmospheric response shown in Chapter 5 and variability changes in Chapter 6. Finally further discussion, with summary and conclusions are provided in Chapters 7 and 8, respectively.

Figure 1.1: Graphical locations of most places referred to in this thesis.

1.1 Motivation

The North Atlantic thermohaline circulation (THC) is a main transporter of heat into the higher latitudes, and is historically believed to be an important factor for the relatively mild winter climate of the European continent. However, the question of whether THC and oceanic heat transport as a whole have a significant impact on European climate has recently been debated in the community. For instance, based on their model-studies, Seager et al. (2002) argue that the principal cause for the zonal asymmetry in atmospheric temperature across the North Atlantic is caused by temperature advection of the prevailing winds. Indeed, they argue that the orographically induced waves from the Rocky Mountains causes the atmospheric component of the total meridional heat transport to be much larger than that of the ocean, saying that the mild winters of Europe could be explained without the inclusion of a dynamical ocean at all.

Rhines and Häkkinen (2003) criticize this view, arguing for example that the latent heat transport conducted by the atmosphere should be treated as an intrinsically coupled ocean/atmosphere mode. Moreover, the view of Seager et al. (2002) stands quite sharply in contrast to the interpretations of paleoclimate records suggesting a sudden spreading of ice-cover in Europe about 13000-15000 years ago; a time period where the ice sheets already had been retreating substantially. Traditionally, this event, which is referred to as *the Younger Dryas*, have been explained as a consequence of the breakdown in the THC and subsequent cooling due to the decreased oceanic heat transport (Hartmann 1994). The abrupt increase in ice packs when oceanic heat transport is switched off are also identified in coupled model integrations (e.g. Winton 2003).

An overview of the ocean currents in the North Atlantic is shown in Figure 1.2 while Figure 1.3(a) show the climatological SST in this basin. It can be seen a clear tendency of the surface water being colder than the zonal average where the currents transport water equatorwards with the opposite being true in the area where the flow is poleward, reflecting the importance of ocean circulation in obtaining the zonal asymmetry of SSTs. It is therefore assumed that the climatological SST-distribution will be more zonally symmetric across the basin when neglecting the advective effects of ocean currents. We refer to this assumption as the *zmean*-hypothesis, and an example of its validity is shown in a model study of Czaja (2003) where the ocean heat transport is excluded, see Figure 1.3(b).

However, it should be noted that this figure also show the presence of an asymmetry across the North Atlantic; in the higher latitudes for example, SSTs tend to be higher in the eastern parts of the basin than in the west. Since all heat transport conducted by the ocean is switched off in this particular environment, the zonal asymmetry could be indicative of the prevailing atmospheric flow's ability in transporting heat communicated to the ocean through heat flux-exchanges. Support for this view is gained by conclusions reached by Seager et al. (2002), namely that stationary waves caused by the Rocky Mountains give rise to a cold north-westerly flow in eastern North America, and relatively warmer south-westerly flow to Europe. Their study show that this orographic feature alone explains almost half of the observed east-west air-temperature contrast across the North Atlantic, and through a thermodynamic relationship this effect could

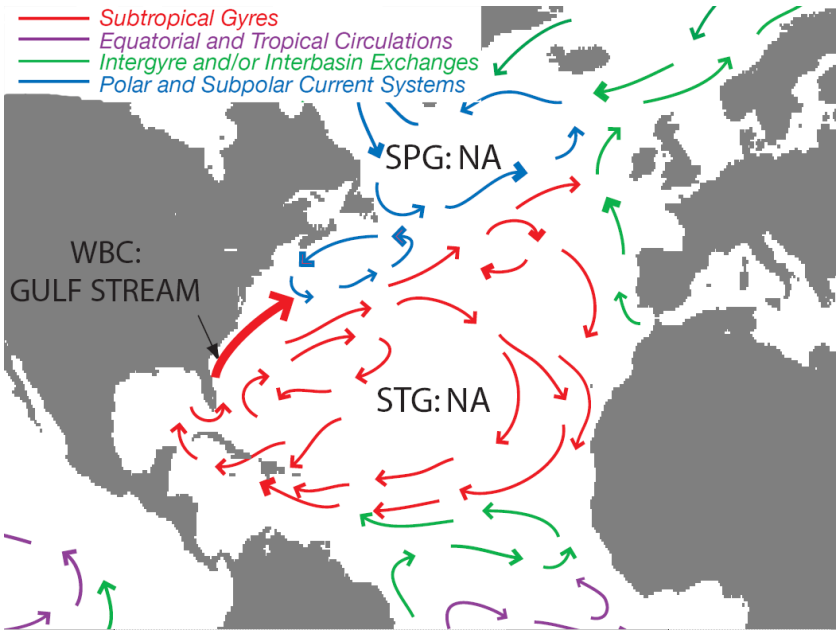

Figure 1.2: Cartoon of the North Atlantic surface ocean currents. WBC is short for western boundary current, and STG and SPG are subtropical and supbolar gyres, respectively. *From Vallis (2006).*

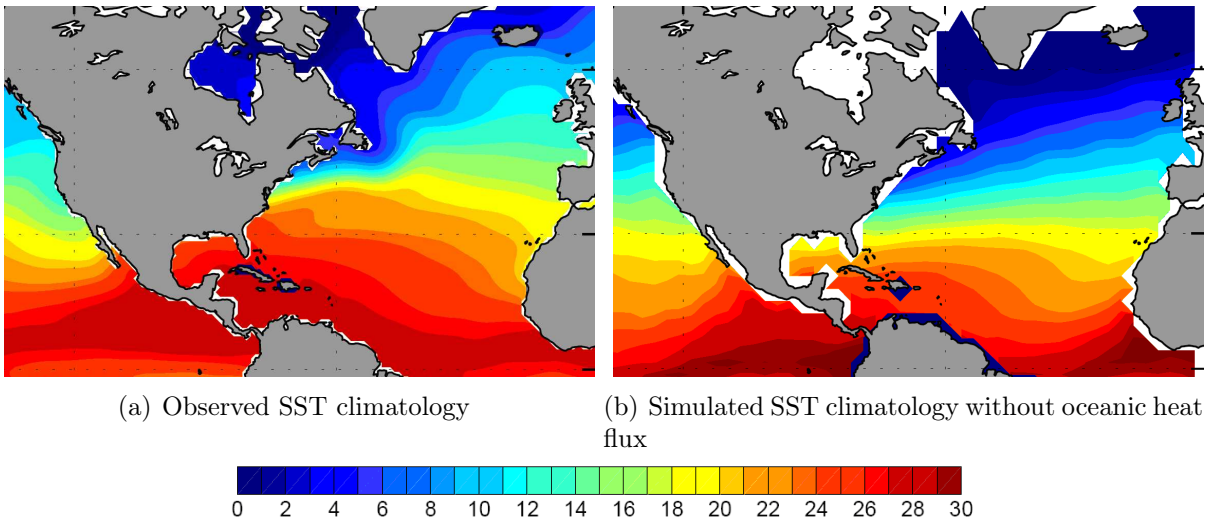

(a) Observed SST climatology

(b) Simulated SST climatology without oceanic heat flux

Figure 1.3: Annual mean sea-surface temperature in the North Atlantic from observed records of da Silva et al. (1994) (a), and from a model run with the CCM3-model without ocean heat transport (b). Contour intervals are 1° C. *Figures obtained through personal communication with Czaja (2003).*

also be reflected in the SST-field of Figure 1.3(b). This discussion about which effect(s) is important for explaining the mild winters of Europe is a motivation for the present study.

Presently, the huge socio-economic interests of anthropogenic climate change obliges the scientific community to work for gaining climate predictability. Since climate often is interperated as the slowly varying component of weather, it is reasonable to believe that the world oceans play a key role in achieving this predictability due to its enormous thermal reservoir. Obviously, the gain in climate (or long-term) predictability would have a large range of applications. Indeed, this view of the oceans role in forecasts has gained some confidence in the community as successful experiments have been applied to the tropical oceans. As an example, Gill and Rasmusson (1983) showed that surface winds might be directly related to the diabatic heating during an ENSO-anomaly in 1982-83, and could be predicted by a simple atmospheric model.

Predictability studies for the midlatitude oceans role were initiated already in the late 1950's by Namias (1959). Although much effort, both through model- and observational studies, has been put into understanding the midlatitude oceans influence on the atmospheric general circulation, several main questions on this topic still remain unanswered. The current lack of a conceptual understanding of large-scale air-sea interaction and its implications is a further motivation for conducting a study such as described in this thesis.

Questions raised in this work

The main questions we would like to consider in this work are the following:

- When represented in a simplified model environment, how sensitive is the atmosphere to North Atlantic ocean circulation, and is the degree of this sensitivity dependent on season?
- How will the absence of ocean currents affect the atmospheric variability patterns as well as the local low-frequency variability?
- To what extent might the atmospheric response be attributed to known dynamical theory?

The following chapter give further background needed in order to answer these questions.

Chapter 2

Background

2.1 Procedure of forcing the atmosphere

The procedure used here to investigate how the atmosphere reacts to a dynamically passive North Atlantic is to impose prescribed anomalies in the sea surface temperatures that is the result of such a situation, according to our *zmean*-hypothesis. To model their implications, these anomalies are put into an AGCM-framework. In the following of the thesis, this procedure is treated as adding or extracting diabatic heat at the lower boundary of the atmosphere. For example, an imposed positive anomaly, $SSTa^{+}$ means input of diabatic heat into the system, thus a positive Q in the thermodynamic energy equation.

In the atmospheric model environment, the prescribed anomaly in SST is communicated from the ocean to the atmosphere through the altering of the heat flux exchange at the ocean/atmosphere interface. Based on simplifications of relevant equations, the next sections provide some basic background of how this potentially could affect the atmospheric circulation.

The discussion is associated with motions in the northern hemisphere unless stated otherwise.

2.2 Direct linear response to surface heating

A linearized and simplified way of showing how the atmosphere can respond to an SST anomaly is by means of the vertically integrated hydrostatic equation between $p = (1000 + p'_{surface})$ and $p = 500hPa$:

$$Z_{500} = \frac{R < T >}{g} ln(\frac{p}{500}) \tag{2.1}$$

where R is the gas constant for dry air, $< T >$ is the vertically averaged temperature of the layer and $p'_{surface}$ is the surface pressure perturbation. To establish a picture of the largest perturbations of the Z_{500}-field that are likely to arise from an imposed anomaly, T'_{SSTa}, the entire lower half of the atmosphere is allowed to thermally adjust to this anomaly. With this assumption, Kushnir et al. (2002) show that Equation 2.1 might be approximated to be written as a response in the height of the 500hPa-surface, as also is shown in appendix A.1:

$$Z'_{500} \approx \bar{Z}_{500}(\underbrace{\frac{T'_{SSTa}}{\bar{T}_a}}_{bc} + \underbrace{\frac{1}{ln2}\frac{p'_{surface}}{1000}}_{bt}) \tag{2.2}$$

where $\bar{Z}_{500}$ and Z'_{500} are the background state and response of the geopotential height of the 500-hPa surface, respectively, while $\bar{T}_a$ denote the unperturbed vertically averaged temperature. For typical values of $\bar{Z}_{500}$ and $\bar{T}_a$ an SST-anomaly of $T'_{SSTa} = 1K$ yields from the bc-term $Z'_{500} \sim 20m$, referred to as the *baroclinic* part of the response. The *barotropic* part of the response (bt-term), will add or subtract $\sim 7m$ for every 1 hPa perturbation of surface pressure, $p'_{surface}$.

The notions *baroclinic* and *barotropic* are most easily explained with the aid of the thermal wind relationship (Holton 2004):

$$\frac{\partial \boldsymbol{V}_g}{\partial lnp} = -\frac{R}{f}\boldsymbol{k} \times \boldsymbol{\nabla}_p T \tag{2.3}$$

where $f = 2\Omega sin\phi$ is the Coriolis parameter and $\boldsymbol{V}_g$ is the geostrophic wind vector.

- *Baroclinic atmosphere:* In a baroclinic atmosphere the density is allowed to change on a surface of constant pressure, hence $\rho = \rho(p, T)$. Thus, horizontal temperature gradients exist, and from Equation 2.3 the geostrophic wind is changing with height, both in direction and strength.

- *Equivalent barotropic (EqBt) atmosphere:* The equivalent barotropic atmosphere is a special case of the above where horizontal temperature gradients still exist, but with the constraint that thickness and height contours everywhere are parallel (Wallace and Hobbs 1977). Consequently, the strength of the geostrophic wind remains height dependent whereas its direction is constant throughout the atmosphere.

- *Barotropic atmosphere:* In a barotropic atmosphere the surfaces of constant pressure are coincident with surfaces of constant temperature, hence there exist no horizontal temperature gradients[1], $\nabla_p T = 0$. Through the thermal wind relationship, this is corresponding to the geostrophic wind being independent of height.

The direct and linear response to surface heating (cooling) features a surface low (high) with an upper-level high (low) above (Kushnir et al. 2002). Experiments with linear quasigeostrophic models, however, show that the surface response is situated downstream of (or east to) the imposed heat anomaly with the upper-level situated above.

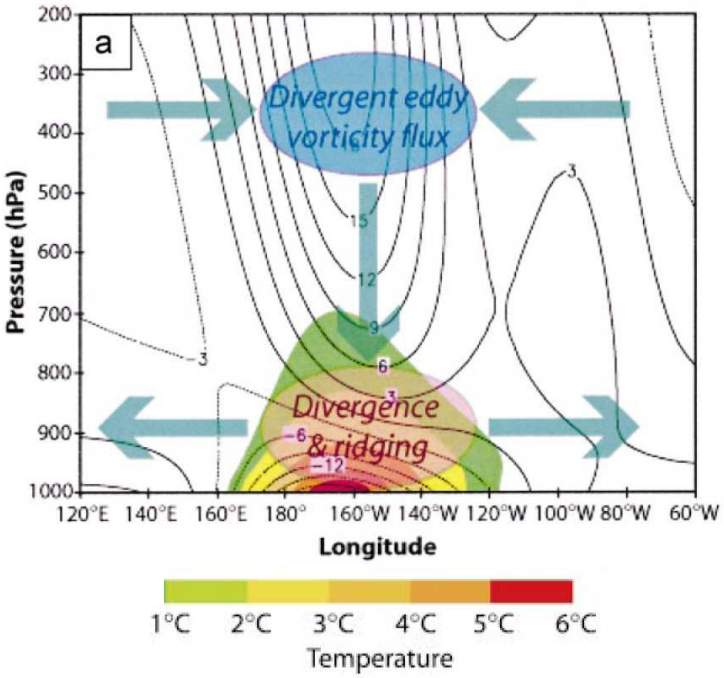

Figure 2.1: The response to shallow heating (centered at 180°) in a linear quasigeostrophic model in a wide β channel. The underlying colors show the temperature perturbation with values smaller than $1K$ shaded white. The contours indicate the geopotential height response with a contour interval of 3 m. The quasigeostrophic secondary circulation (wide arrows) resulting from the eddy vorticity fluxes (colored ellipses) shows how the positive SST anomaly might lead to development of a surface ridge, see Section 2.3 for a further discussion. *From Kushnir et al. (2002)*

This can be explained from simplifications of the basic equations (see equations A.4 - A.7) where it can be shown that induced divergent/convergent atmospheric flow, with subsequent secondary circulation patterns, might have the ability to reverse the sign of the linear response proposed by basic atmospheric models, such as schematically shown in Figure 2.1, where also the response situated downstream of the imposed anomaly is indicated.

Bearing this in mind, the following subsection will make usage of a slightly more dynamical approach in discussing the atmosphere's adjustment to imposed SST-anomalies. In order to obtain a theoretical basis of how the atmosphere can respond to such a change, a brief investigation of the governing equations are necessary. The basis for such considerations were developed by

[1]'Horizontal' is here referred to as parallel to a surface of constant pressure.

Charney and Eliassen (1949), but a full theory which is globally applicable still does not exist. Therefore, the following section should not be treated as a complete description of all processes going on, but merely an introductory overview.

2.3 Thermal forcing of stationary waves

The theory and most considerations are mostly based on Hoskins and Karoly (1981, from from now referred to as HK81), Nigam and DeWeaver (2003) and Holton (2004). For the part regarding the tropics, it is also referred to the work of Gill (1980).

In the presence of a positive heat source influencing the atmosphere, it will respond to this source by (a combination of) increasing the local temperature, advecting colder air into the area of heating, or increasing the convection which balances the heating by adiabatic cooling due to the enhanced upward motion. However, the extent of which anomalies in these heat patterns are able to produce large-scale atmospheric responses depends on their ability to generate Rossby-waves (Holton 2004). Some basic dynamical features of this is therefore established in the following part.

For the large-scale atmospheric circulation in the midlatitudes, the assumptions of hydrostatic and quasi-geostrophic (QG) balance are generally valid (Nigam and DeWeaver 2003). In isobaric coordinates, these assumptions state the following:

- The hydrostatic balance:
$$\frac{\partial \Phi}{\partial p} = -\frac{1}{\rho} = -RT/p$$
where $\Phi = g_0 z$ is the geopotential and R is the gas constant of dry air. The above equation describe the balance between the upward force felt by an air parcel due to the vertical pressure gradient, (in cartesian coordinates: $-\frac{1}{\rho}\frac{\partial p}{\partial z}$) and the downward force due to gravitation.

- QG-balance:
$$f\boldsymbol{k} \times \boldsymbol{V} \approx -\boldsymbol{\nabla}\Phi \Rightarrow \boldsymbol{V} \approx \boldsymbol{V}_g$$
where f is the Coriolis parameter, and $\boldsymbol{V}_g = u_g\boldsymbol{i} + v_g\boldsymbol{j}$ and $\boldsymbol{V} = u\boldsymbol{i} + v\boldsymbol{j}$ are the geostrophic and real horizontal wind vectors, respectively. The QG-assumption acknowledge the near-balance between the Coriolis force, $f\boldsymbol{k} \times \boldsymbol{V}$ and the horizontal pressure gradient $-\boldsymbol{\nabla}\Phi$ in all layers.

The reader is referred to Appendix A.2 or Section 6.2 in Holton (2004) for a more thorough review of the QG-assumption and its implications to the basic equations.

To see what general implications an anomalous heating pattern might have on the atmospheric circulation, an investigation of the evolution of the QG-flow can be performed. In the following,

this will be done by examining the QG-vorticity equation (see Appendix A.2.1):

$$\underbrace{\frac{\partial \zeta_g}{\partial t}}_{A1} + \underbrace{\boldsymbol{V}_g \cdot \boldsymbol{\nabla} \zeta_g}_{B1} + \underbrace{\beta v_g}_{C1} = \underbrace{f_0 \frac{\partial \omega}{\partial p}}_{D1} \tag{2.4}$$

term A1 being the local rate of geostrophic vorticity, ($\zeta_g = \frac{\partial v_g}{\partial x} - \frac{\partial u_g}{\partial y}$) change with time, while term B1 and C1 are the horizontal advection of relative and planetary ($\beta = \frac{df}{dy}$) vorticity, respectively. In term D1, $\omega \equiv \frac{Dp}{Dt}$ is the vertical velocity in pressure coordinates. This term describe the change of the relative vorticity due to the Coriolis force acting on divergent/convergent motions and is often called the *stretching*-term. This is because convergent flow leads to stretching of vortex tubes (Nigam and DeWeaver 2003). It should also be noted that this term in the literature often is written as $(f_0 + \zeta_g)\frac{\partial \omega}{\partial p}$. Outside centers of low-pressures (and, on the smaller scale; fronts), however, $\zeta_g << f_0$ and could therefore be neglected (Holton 2004).

It is evident that the evolution of the thermodynamic state also is of importance for our purpose. The potential temperature, which is the temperature an air parcel will achieve if lowered adiabatically from a level of pressure p to the surface pressure $p_0 = 1000hPa$ is written as:

$$\theta = T(p_0/p)^{R/c_p}$$

where c_p is the specific heat of air with constant pressure and T is the temperature of the air parcel at pressure p. The potential temperature is conserved through an adiabatic process, therefore only a diabatic heat source (for instance an SST-anomaly) might affect its state. Therefore, θ is used as the variable in the thermodynamic energy equation (see Appendix A.2.2):

$$\underbrace{\frac{\partial \theta}{\partial t}}_{A2} + \underbrace{\boldsymbol{V}_g \cdot \boldsymbol{\nabla} \theta}_{B2} + \underbrace{\omega \frac{\partial \theta}{\partial p}}_{C2} = \underbrace{\frac{Q}{c_p}\frac{\theta}{T}}_{D2} \tag{2.5}$$

Terms A2 and B2 denote the local rate of change of θ with time and the horizontal advection of θ, respectively. Term C2 is the vertical advection of θ and is related to the stability of the air column. The diabatic heating term, D2, is often referred to as the *residual*-term since the diabatic heat, Q, is hard to quantify from objective measurements. From this term, physically meaningful properties of the atmosphere can be investigated, such as for instance the release and uptake of latent heat. An overview of how this term is distributed throughout the atmosphere is presented in Figure 2.2.

The generation of Rossby-waves is, as mentioned above, the atmosphere's key to create large-scale and nonlocal responses when a thermal forcing is present. Waves of the scale in question are represented as the zonally varying component of the flow, and their dynamics can therefore be studied to the 1st order by linearizing equations 2.4 and 2.5 about the zonal-mean circulation. This is the equivalent of saying that a variable, $A(x, y, p, t)$ can be expressed as a sum of the zonally and temporally averaged part, $\bar{A}(y, p)$ and its deviation, $A'(x, y, p, t)$. If applying this

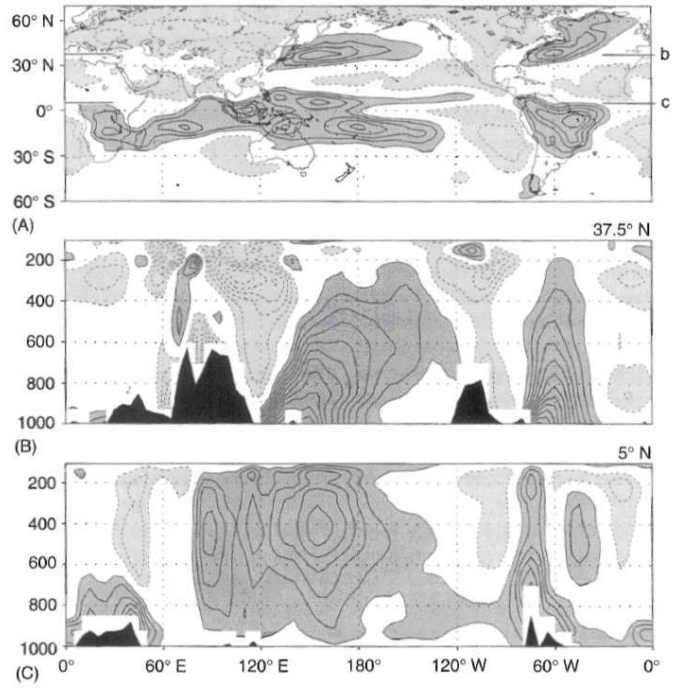

Figure 2.2: Diabatic heating, calculated as the residual of the thermodynamic equation. Mass-weighted vertically integrated geographical distribution (a), zonal-vertical cross-section of the diabatic heating at 37.5N (b) and 5N (c). The contour interval is $0.5Kday^{-1}$, with dark (light) shading for positive (negative) values in excess of $0.5Kday^{-1}$. The diagnosis is based NCEP-reanalysis fields from 20 winter-seasons (DJFM) in the period 1979/80-1998/99. *From Nigam and DeWeaver (2003)*

on the steady-state of the above equations while replacing the $_g$-subscript denoting geostrophy with subscripts indicating derivatives (i.e. $_x = \frac{\partial}{\partial x}$), they may be written (see appendix A.3):

$$\bar{u}\zeta'_x + v'(\beta - \bar{u}_{yy}) = f_0\omega'_p \tag{2.6}$$

and

$$\bar{u}\theta'_x + v'\bar{\theta}_y + \omega'\bar{\theta}_p = \frac{Q}{c_p}\frac{\theta}{T} \tag{2.7}$$

These equations form a basis for discussing the atmosphere's adjustment to thermal forcing, as has been done in HK81 and Nigam and DeWeaver (2003). The rest of this subsection will provide parts of their discussion regarding thermal forcing, first considering the midlatitudes.

2.3.1 Midlatitudes

In the midlatitudes, the process generally being most effective in balancing a heat source is horizontal temperature advection. This can be seen from the fact that large temperature gradients might have its presence here, as well as the convection not being as deep here as in the tropics (Holton 2004). The latter can be visualized from the monotonically decreasing diabatic heat rate with height in the middle panel of Figure 2.2. The upper panel show that the midlatitude diabatic heating in the northern hemisphere is directly linked to heat exchanges with the ocean, as the amplitude of the residual is small over the continents.

Although one would from this deduction expect that the midlatitude response to input of diabatic heat at the surface is of relatively shallow character, forcing from SSTa might on some occasions display a deep structure communicated through upward eddy heat fluxes by transient eddies of many scales (HK81). More specifically, it could be hypothesized that midlatitude SSTa could have the potential to directly affect latent heat release higher in the atmosphere in terms of changed baroclinicity and, as a consequence, changed storm activity. This direct relationship is indeed the topic in Minobe et al. (2008), and some of their results are given attention later in this chapter. Therefore, in the footsteps of HK81, a discussion of both the deep and shallow midlatitude thermal forcing are provided.

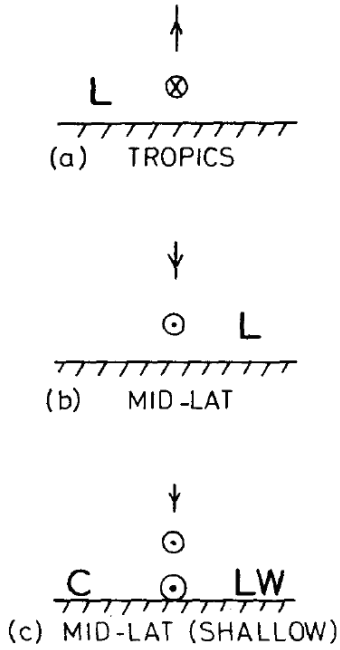

Figure 2.3: Schematic overview of the longitude-height response forced by a tropical heating (a), a (deep) midlatitude heating (b), and a shallow midlatitude heating (c). The arrows indicate the vertical motion induced by the forcing, while the circled dots and crosses denote equatorward and poleward flow, respectively. Their longitudonal position also designate the center of the initial forcing in the different regimes. L indicate the pressure trough, and C and W are relatively cold and warm air, respectively. *From HK81.*

When considering the steady-state linearized thermodynamic energy equation (Equaton 2.7), the heating must be offset by zonal ($\bar{u}\theta'_x$), or meridional ($v'\bar{\theta}_y$) temperature advection. Firstly, considering the case of a deep forcing, heating is balanced by $v'\bar{\theta}_y > 0$ (HK81). Noting that $\bar{\theta}_y < 0$, one must have equatorward motion, or $v' < 0$, above the heating, implying a surface low to the east of the heat source according to the quasi-geostrophic assumption.

Interestingly (and quite counter-intuitive), the induced vorticity from $\beta v' < 0$ in Equation 2.6 causes air to descend in the vicinity of the forcing. This is because the induced vorticity anomaly must, in the absence of strong advection of relative vorticity, be balanced by $\omega'_p = \frac{\partial \omega'}{\partial p} < 0$. As ω' increases with decreasing pressure this descent could be seen from the boundary condition of

$\omega'_{surf} = 0$ at the surface[2], yielding $\omega' \equiv \frac{Dp}{Dt} > 0$ above it. An increase in pressure with time is in this framework characterized by downward motions, which also explains the induced secondary circulation in Figure 2.1.

The induced vorticity anomaly at the upper levels can be balanced either by zonal advection of relative vorticity, or meridional advection across the mean potential vorticity gradient. Due to the spatial scale of typical SST-anomalies, the zonal advection is the most relevant (Kushnir et al. 2002), thus $\bar{u}\zeta'_x < 0$. As the flow generally is westerly, this will require $\zeta'_x < 0$ which is equivalent to cyclonic vorticity, hence a mid- or upper-level low west of the forcing, and anticyclonic vorticity or a high downwind. This could also be seen in results from quasi-geostrophic model runs (for instance HK81; Hendon and Hartmann 1982), and the upper-level high might also be identified in Figure 2.1.

In the case of a shallow heat source in the midlatitudes, the heating is balanced in the lower atmosphere partly by zonal advection of heat, $\bar{u}\theta'_x$ (HK81). Thus, the effect of the heating is advected downstream, and consequently $\theta'_x > 0$ in Equation 2.7 (Vallis 2006). For this mechanism to work, it will therefore require relatively cooler low-level air upstream of the heating anomaly. In the lower panel of Figure 2.3, these patches of relatively warmer and cooler air are denoted by 'W' and 'C', respectively. Thus, the mid- to upper-level high downstream of the imposed heating discussed above could also be explained by simply looking at the vertically integrated hydrostatic equation, referred to as the hypsometric equation:

$$\Delta Z = \frac{R < T >}{g} ln(\frac{p_1}{p_2}) \tag{2.8}$$

This would assume, however, that the downstream warm patch acts to sufficiently increase the mean temperature, $< T >$ of the layer between the two pressure surfaces, $p_1 > p_2$, in order to expand the layer thickness, $\Delta Z = Z_2 - Z_1$.

2.3.2 Tropics

Due to the weak effect of the earth's rotation on the atmospheric motions in tropical areas, the appliance of quasi-geostrophic theory remains a matter of controversy, at least in the vicinity of the equator, as also argued in (Vallis 2006). For completeness, however, a discussion of the tropical atmosphere balancing the thermal forcing is presented where the assumptions of quasi-geostrophic and hydrostatic balance are assumed to hold. Support for the near-geostrophic flow regime to occur also close to the tropics could be found in the literature, for instance in the model study of Lindzen and Nigam (1987). It is to be emphasized that several other features than those mentioned here might be important in the aspect of tropical SST-forcing.

Close to the equator where the Coriolis force is weak, horizontal gradients in the geopotential, Z is more quickly broken down than is the case for the midlatitudes (Nigam and DeWeaver 2003). As seen from Equation 2.8, Z or more precisely the layer thickness, ΔZ, between two

[2]Valid in the absence of strong temporal pressure trends.

pressure surfaces is linearly related to the mean temperature of the layer. Thus, small horizontal gradients of ΔZ implies small horizontal gradients of $< T >$. Consequently, horizontal advection of heat is a rather inefficient mechanism to balance the diabatic heating (Holton 2004). Hence, the terms $\bar{u}\theta'_x$ and $v'\bar{\theta}_y$ of Equation 2.7 could be treated as relatively small and, away from the surface, heating must therefore be balanced by adiabatic cooling due to increased vertical motion.

When inducing vertical motions, the mid- to upper troposphere might experience a substantial and indirect temperature response due to changes in the release of latent heat, as depicted in the lower panel of Figure 2.2 (also, see a short discussion of this matter below). Subsequently, this will alter the stability of the air column, with the level of greatest vertical velocities associated with the level of maximum heating (Nigam and DeWeaver 2003). In the atmosphere below (above) this level, a convergent (divergent) wind field is required as can be seen from the continuity equation:

$$\frac{\partial u}{\partial x} + \frac{\partial v}{\partial y} = -\frac{\partial \omega}{\partial p} \tag{2.9}$$

and it could be explained by the following argument:

Remembering that upward motion in isobaric coordinates is designated by $\omega \equiv \frac{Dp}{Dt} < 0$ and once more that the boundary condition ω'_{surf}=0 applies at the surface, the result in the atmosphere below the level of maximum heating is that ω' must decrease by decreasing pressure; $-\omega'_p = -\frac{\partial \omega'}{\partial p} < 0$. When this apply, Equation 2.9 demands the horizontal wind field to be convergent. As the strong stability of the tropopause acts to suppress vertical motions at this level, one might apply the boundary condition of ω'=0 also here, with the consequence that the opposite is true for the levels above maximum heating. From this argument, the wind above the level of maximum heating characterized by a horizontally divergent flow.

Looking at the low-level atmosphere north of the equator, the enhanced vertical motion following the thermal forcing gives a positive term on the right hand side of the linearized QG-vorticity equation, $f_0\omega'_p > 0$. For large-scale motions this vorticity anomaly is balanced by poleward advection of planetary advection, $\beta v' > 0$ in the area of the heating (HK81; Nigam and DeWeaver 2003). This will then be indicative of a surface low to the west of the imposed forcing as shown in Figure 2.3(a).

Figure 2.4 show changes in atmospheric circulation in the presence of a positive forcing situated mainly north of the equator. Based on an analytical approach by Gill (1980), these panels show many of the characteristics also found from the quasi-geostrophic considerations of (Hoskins and Karoly 1981) and are therefore included here for reference.

Looking at Figure 2.4(a) the induced meridional flow is observed as wind vectors with a positive meridional component in the vicinity of the forcing, and extending northwards. It can be seen from the response in winds that the zonal component is the main contributor to the induced

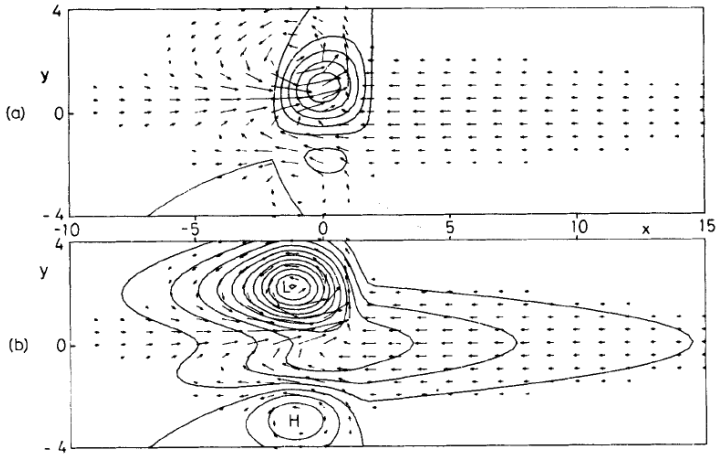

Figure 2.4: Solution of the forced shallow water equations for heating confined to $|x| < 2$ with the main heating concentrated to the north of the equator ($y > 0$). (a) Contours of vertical velocity, w with an interval of 0.3 m/s. Arrows denote the induced horizontal winds. (b) Contours of perturbation pressure p, with contour interval of 0.3 hPa, showing the surface low placed west of the forcing. *Figure from Gill (1980).*

convergent regime, acting to replace the heated and rising air in the vicinity of the heating. One could also observe that the results of Gill (1980), which is based on simplifications of the shallow water equations with the inclusion of simple form of dissipation, give a qualitatively comparable picture to that proposed by HK81, with the rising air above the heating and induced meridional flow associated with the induced low pressure system to the west of the heat source. However, in Gill's framework this low pressure is displaced northwestwards compared to the forcing.

To give a summary of this section, table 2.1 show the results from numerous experiments presented in HK81 with positive thermal forcing varied both in position, shape and depth. Focusing first on the midlatitude results, it can be seen that the zonal displacement and strength of the pressure response is strongly dependent on the depth of the forcing. This is also the case for T_{900} which, interestingly, show a negative response in the vicinity of a deep forcing, with the opposite being true for the shallow case. Also, the induced meridional flow is larger when the shallow forcing is imposed at 60° N compared to the one at 45° N. This is because the meridional temperature gradient is weaker at 60° N therefore requiring a larger compensating meridional wind (HK81).

The tropical scenarios, taken here to be the cases where the forcing occur south of 20°N, show the increased upward motion when moving away from the equator as well as the temperature response having the same sign as the forcing, implying decreased static stability. It is also observed that the model of HK81 do not induce poleward flow when the forcing is centered at the equator.

Table 2.1: Experiments with different heat source distributions. The sources are denoted by the latitude of their maxima, their eccentricity, latitudinal extent and vertical distribution with D and S representing a deep and shallow source, respectively. The values given for surface pressure trough (p_{*min}), 500 hPa vertical velocity (ω_{500}), 900 hPa meridional wind (v_{900}) and temperature (T_{900}) are the extrema in the vicinity of the source. Where no value is given, there is no definite extremum in that vicinity. The pressure trough position is its longitude from the heat source with negative values indicating a westward position relative to the imposed forcing. The last rightmost column is a subjective measure of the strength of the polar wavetrain at 300 hPa. *Table from HK81.*

Latitude (deg)	Eccentricity	Latitudinal extent (deg)	Vertical distribution	p_{*min} (hPa)	p_{*min} position (deg)	ω_{500} hPa day^{-1}	v_{900} m s^{-1}	T_{900} (K)	Polar wave
0	4	16	D	0.5	0	-45	-0.3	0.8	0.1
10	4	16	D	1.3	-11	-50	1.3	1.1	0.5
15	4	16	D	2.6	-14	-67	2.2	2.1	1.0
20	4	16	D	5.3	-13	-79		3.9	1.0
30	4	16	D	9.1	+25		-3.9	-5.2	0.8
45	4	16	D	7.0	+25		-2.7	-2.3	0.8
45	1	32	D	6.5	+21		-3.7	-2.9	0.8
45	1	64	S	12.6	+14		-5.8	5.2	0.7
45	1	32	S	18.7	+11		-5.8	10.6	1.8
60	1	32	S	22.1	+15		-8.2	8.4	0.9

The sensitivity of the atmosphere to tropical SSTa

Based on the principles of quasi-geostrophy and hydrostatic balance, it has been provided parts of a framework of how the atmosphere responds to a diabatic heat source. However, since a large part of the diabatic heating in the tropics results from deep convection (see lower panel of Figure 2.2), it is plausible that the enhanced vertical motion due to the thermal forcing might give rise to an increase in the release of latent heat higher up in the atmosphere, which might be identified by investigating changes in precipitation rates. It is in this matter worth mentioning that the relationship between the forcing at the surface and the release of heat due to condensation in mid- to upper troposphere might be sensitive if considering an atmosphere that adjusts thermally to the heating anomaly. In particular, this can be seen from the strong temperature dependency of the air's ability

to contain water, as stated in the Clausius Clapheyron equation (Hartmann 1994):

$$\frac{de_s}{dT} = \frac{L}{T(\alpha_v - \alpha_l)} \tag{2.10}$$

where e_s is the saturation water vapor pressure, L is the latent heat of condensation and (α_v, α_l) are the specific volume of the vapor and liquid phases, respectively. By dividing Equation 2.10 by the ideal gas law for water vapor ($e_s = \frac{R_v T}{\alpha_v}$) and neglecting the specific volume of the liquid phase, α_l, it can be re-written as:

$$\frac{de_s}{e_s} \approx (\frac{L}{R_v T})\frac{dT}{T} \tag{2.11}$$

Since the assumption of constant relative humidity[3] is thought to be plausible during a change of temperature (Hartmann 1994), e is linearly related to e_s by a factor 1. The scaling factor $\frac{L}{R_v T} \sim \frac{2.5\times10^6 JK^{-1}}{461 JK^{-1}kg^{-1}\times270K} \approx 20$, therefore Equation 2.11 suggest that a 1 % increase of temperature ($\approx 3K$) give a ≈20 % increase in the water vapor pressure, or water content. Hence, only a small change in temperature might greatly affect the potential for releasing heat through condensation.

Having established some basic principles of how the atmosphere might respond to thermal forcing in a simplified environment, the rest of this chapter will focus on a more complex one, firstly introducing the large-scale patterns of atmospheric variability.

2.4 Large-scale patterns of atmospheric variability

Studies show that there is a tendency of the atmospheric response to low-level forcing[4] to be related to the leading mode, or patterns, of intrinsic atmospheric variability (e.g. Peng and Robinson 2001; Czaja et al. 2003; Deser et al. 2004). The reason for these observations could be related to the strength of the internal atmospheric variability, enabling the atmosphere to respond to such a forcing by altering the statistics of its variability patterns.

The implications of such patterns have been widely studied; conclusions being that they are both significant and diverse (Hurrell et al. 2003). Based on this fact, these patterns and their implications are of importance when analysing the response to a dynamically passive North Atlantic, which obligates for a brief survey of some of these large-scale modes in the North Atlantic region.

[3] Relative Humidity, $RH \approx \frac{e}{e_s}$, where e is the actual partial pressure of water vapor.

[4] 'Low-level forcing' might here be interperated as both forcing due to SSTa and changes in sea-ice cover.

2.4.1 North Atlantic Oscillation

The most well-known pattern of internal variability in the Atlantic region is that of the North Atlantic Oscillation (NAO). The pattern is characterized by a dipole structure in the surface pressure field, where the combined strengths of the Icelandic low and Azore high determine the mean westerly winds and the latitude of the jet. Some of the direct climatic impacts when the NAO-index is positive or negative are shown in Figure 2.5.

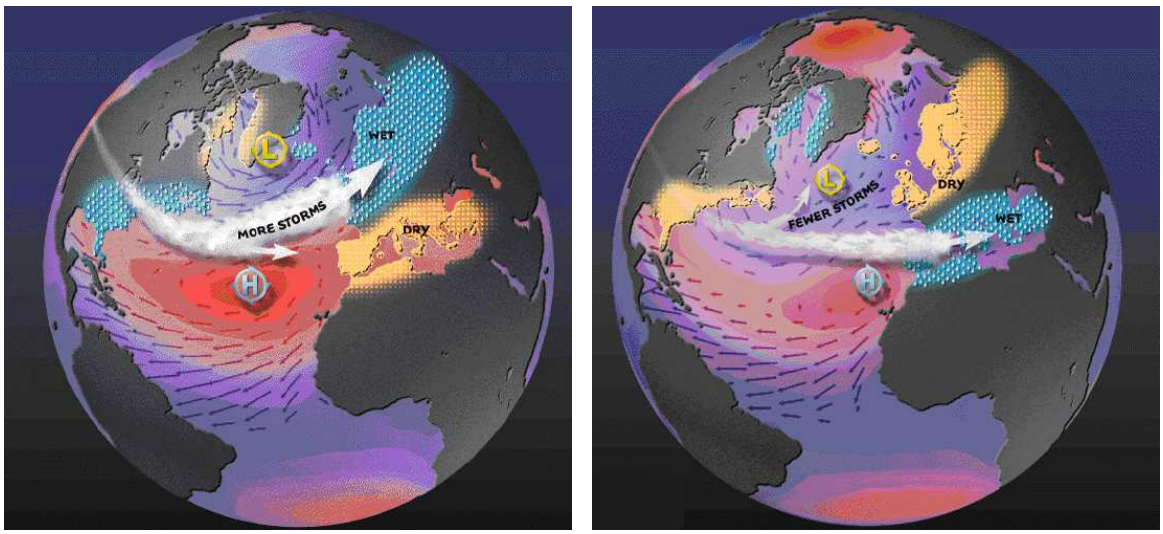

(a) Implications of a positive NAO (b) Implications of a negative NAO

Figure 2.5: Overview of some climatic responses to the positive (a) and negative (b) phase of the North Atlantic Oscillation. *Figure from the NAO-webpage 2007: http://www.ldeo.columbia.edu/NAO, visited May 2007.*

NAO, as opposed to the Southern Oscillation in the tropical Pacific, does not have a significant periodicity, and the mechanisms that account for its variability and trends are still not entirely understood (Hurrell et al. 2003). One theory of its emergence is that of nonlinear dynamics and interactions intrinsic to the extra-tropical troposphere (Thompson et al. 2003). Downward propagating signals from the lower stratosphere to the troposphere have been proposed as a possible explanation for the observed positive trend in the last decades (Thompson et al. 2000; 2003). Also, changes in sea ice extent in the Labrador Sea has been found to affect the index statistics (Kvamstø et al. 2004). Several studies have also shed light upon the impact of SST-anomalies on the NAO (e.g. Sutton et al. 2001; Hoerling et al. 2001; Czaja et al. 2003), which also will be our main focus (see Section 2.5).

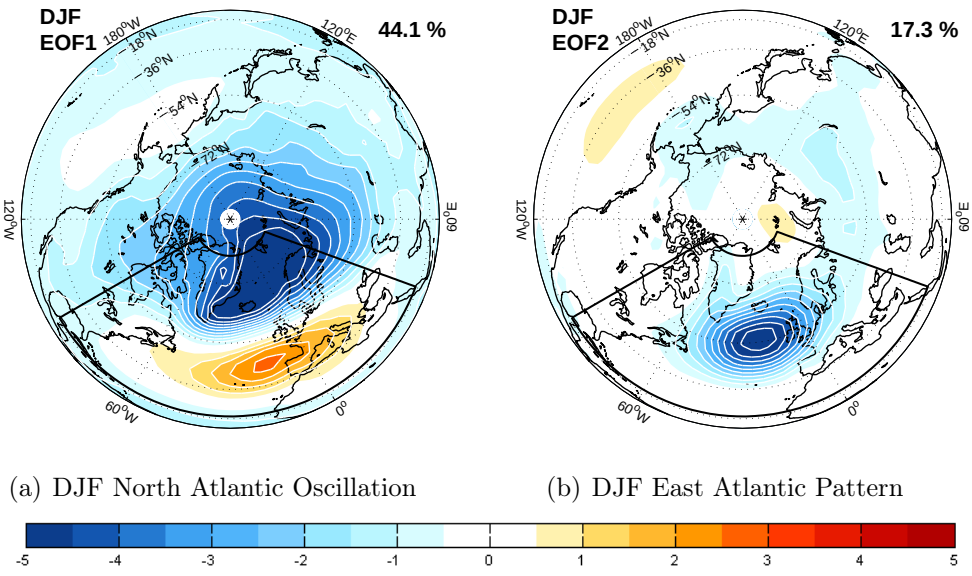

(a) DJF North Atlantic Oscillation (b) DJF East Atlantic Pattern

Figure 2.6: The winter (DJF) Mean Sea-Level Pressure anomaly-patterns of NAO (a) and East Atlantic Pattern (b) calculated by regressing the anomaly field onto the principal component as described in section 3.2, but here with trends removed. The percentage count tells the fraction of the total variance explained by the pattern, and the sector enclose the area of data used as basis for computing the PCs. Contour intervals are 0.5 hPa, with all anomalies smaller than |0.5 hPa| colored white. An interpolation to a T30-resolution of the reanalysis-data have been performed prior to the calculation of the EOFs in order to gain consistency with that of the model used in this thesis (see Section 3.1.2). *Data obtained from the NCEP/NCAR reanalysis (Kalnay et al. 1996).*

A graphical overview of the winter-time spatial characteristics of the positive phase of the NAO and East Atlantic Pattern (EAP), which is the other pattern in focus here, is shown in Figure 2.6. The calculation of the patterns are based on reanalysis data from the National Centre of Atmospheric Research (NCAR) and National Centers for Environmental Prediction (NCEP).

2.4.2 East Atlantic pattern

Identified in the early 1980's (Wallace and Gutzler 1981), the East Atlantic pattern (EAP) is the second most prominent pattern of atmospheric variability in the Atlantic sector. As shown in Figure 2.6(b), the East Atlantic pattern display, in terms of the MSLP-field, a monopole structure with a maximum anomaly confined to the region just west of the British Isles, more precisely 55°N, 20°-35°W as found by Barnston and Livezey (1987). In its positive phase, EAP^+, the East Atlantic pattern is adjunctive to stronger zonal winds than normal, whereas EAP^- introduce a more blocked flow (Dole 1989). This pattern is

also a robust feature of the atmospheric circulation in the North Atlantic region, although explaining considerably less of the overall atmospheric variability, compared to the NAO.

Although not by far as extensively studied nor well-known as the NAO, EAP has also been found to have implications on climate. For example, it has been found to be a main contributor to variability in the storminess in the middle parts of the North Atlantic not covered by the NAO dipole (Seierstad et al. 2007).

Park and Latif (2005) investigated ocean dynamics and its relationship to atmospheric circulation by performing two model runs; one fully coupled, and one where the atmospheric component is coupled to the ocean only through a thermodynamic model. An index based on SSTs from the coupled run within the region [40°-60°N, 50°-10°W], used in a earlier work of Latif et al. (2004) as a representation of the THC, was attributed in a correlation analysis with the MSLP-fields in both model runs. Through this analysis they found that the fully coupled model integrations produced a correlation pattern resembling that of EAP (a maximum correlation of 0.6), thus bringing forward a hypothesis that the presence of EAP is significantly affected by the inclusion of ocean dynamics. In the case where their model is coupled thermodynamically to the ocean this correlation pattern, still significant, resembled the NAO-pattern.

They also found the decadal standard deviation of the MSLP field to be increased by 20% when including ocean dynamics in their model. This weak response has often been used to argue that the impact of ocean circulation on the atmospheric low frequency variability is not very pronounced. However, do their results indicate that the air-sea interactions and the presence of a dynamical ocean modulate the spatial structure of the atmospheric response.

These results indicate the complex relationship(s) between atmospheric and oceanic low frequency variability when modeled in different environments and that caution should be made when ascribing cause and effects such a framework. The next section illuminates some aspects of this complexity of the coupled climate system, both from the observational, and modeling point of view.

2.5 Observed and modeled impacts of sea surface temperatures anomalies on the general atmospheric circulation

As discussed in Section 2.3, it might be possible to predict a general outcome of a heating anomaly in the lower atmosphere or in its lower boundary, based purely on linearizations

and simplifications of the equations of motion and thermodynamics. However, the atmospheric circulation include several and often unknown nonlinear processes not resolved by the approximations of these basic equations. In a general circulation model environment, as well as in the natural system, nonlinear processes tend to break down the deterministic view, and the following subsection provide an overview of model studies addressing this topic.

2.5.1 Earlier model experiments with prescribed midlatitude sea-surface temperature anomalies

The outcome of different general circulation models (GCMs) with prescribed midlatitude SST anomalies often suggests nonlinear atmospheric responses in both sign and amplitude (Robinson 2000; Kushnir et al. 2002; Sutton and Hodson 2007). Often contradictory results from different models occur, which complicates the analysis of the dynamical cause and effect of the atmospheric response. The position of the extratropical SST anomalies relative to the storm track as well as its climatological characteristics could be particularly important in shaping the GCM response, as discussed for instance by Peng and Robinson (2001). Table 2.2 shows an overview of previously conducted model experiments, and addresses this diversity in the results.

It can be seen that the atmospheric response in the models mostly occur as *equivalent barotropic*, but often with a varying size or amplitude. In addition, some of the studies suggest a dependency of the response upon which month the data is analysed. This is also the case in a study by Seierstad and Bader (2008) where the model response to arctic sea-ice perturbations showed significant dependency upon the background flow (i.e. season).

Some of the experiments shown in table 2.2 also suggest a baroclinic response with a surface low downstream of a positive anomaly, which in general terms is consistent with quasi-geostrophic theory. The spread of the results might be explained by a model-dependence on the response, however, positions and size of the anomalies as well as the background flow might also account for this observed diversity in the model results (the reader is referred to Robinson (2000) and Kushnir et al. (2002) for reviews on these topics).

In the last decades, effort has been put into understanding and identifying features which might account as an explanation of the long-term variability of the climate system, emphasizing the (often complex) dynamical feedback mechanisms of different time-scales involving ocean-atmosphere interactions. Examples of such works are the topic for the rest of this section.

Table 2.2: Overview of some earlier idealized GCM experiments with fixed and prescribed SST anomalies. The terms m K^{-1} and hPa K^{-1} are meant as a relative measure of the response amplitude, where K^{-1} denote the imposed anomaly in sea-surface temperature. EqBt stands for equivalent barotropic. The table is extracted from Kushnir et al. (2002).

Reference	SST anomaly (location and size)	Response pattern
Palmer and Sun (1985)	Western North Atlantic; 3 K	EqBt high downstream of positive SSTA; 20 m K^{-1} at 500 hPa; 1.5 hPa K^{-1} at SLP
Pitcher et al. (1988)	North Pacific; 2 and 4 K	EqBt low downstream of both positive and negative SSTA; 25 m K^{-1} or 1.2 hPa K^{-1}
Kushnir and Lau (1992)	North Pacific; 2 K	EqBt low downstream of both positive and negative SSTA; slow transient adjustment; 20 m K^{-1} or 2 hPa K^{-1}
Ferranti et al. (1994)	Northwest Pacific and North Atlantic; 2 K	High (low) downstream of positive (negative) SSTA; 20 m K^{-1}
Peng et al. (1995)	Western North Atlantic; 3 K	Downstream of positive SSTA EqBt high in Nov, but EqBt low in Jan; 30-40 m K^{-1} or 3 hPa K^{-1}
Kushnir and Held (1996)	Central North Atlantic; 4 K	Weak baroclinic response with surface low and upper level high downstream of positive SSTA
Latif and Barnett (1994; 1996)	North Pacific Basin; 1 K	Positive-negative composite has strong EqBt high downstream of positive SSTA; 5 hPa K^{-1}
Peng et al. (1997)	Central North Pacific; 2.5 K	Downstream of positive SSTA EqBt high (10 m K^{-1}) in Feb but baroclinic low (1 hPa K^{-1} in Jan

2.5.2 Large scale co-variability of oceanic and atmospheric circulation

The research on the concrete problem of decadal large-scale climate variability due to midlatitude ocean-atmosphere interactions starts out with Bjerknes (1964). It was herein stated that:

> *(...) any specific theory for climatic change during geologic time has to include the consideration of ocean-atmosphere interaction.*

This conclusion was based on his observational analysis that an interdecadal basin-wide warming, believed to be caused by changes in the ocean circulation of the North Atlantic from 30°N to 50°N, led to a positive anomaly in mean sea-level pressure (MSLP) at 30°N and a negative anomaly at 50°N. This is consistent with a strengthening of the overlying westerly winds, what could be referred to as an increase in the index of the North Atlantic Oscillation (NAO) (see Section 2.4.1). On the interannual time scale, however, the general picture that a warmer ocean surface is associated with stronger westerlies is, according to Bjerknes, completely reversed, with the SSTs and wind speed displaying a local negative correlation, as shown in Figure 2.7.

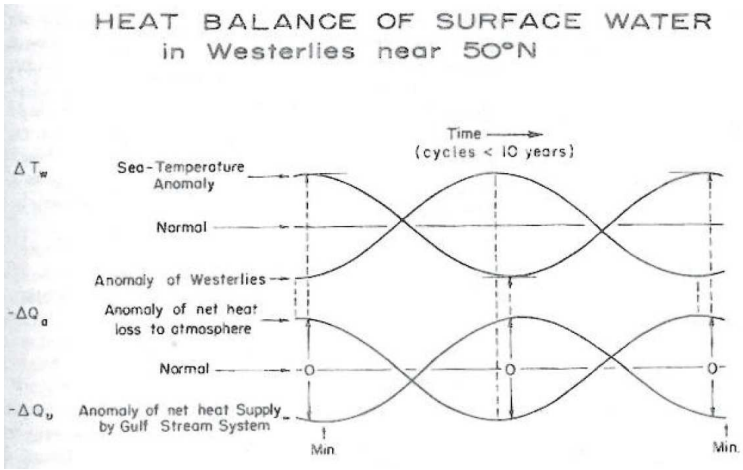

Figure 2.7: Schematic model of the interannual relationship between cycles (less than 10 years of length) of atmospheric indices and ocean surface temperatures near 50°N. The SST anomalies, ΔT_w result from cycles of the transfer of net oceanic heat loss to the atmosphere, $-\Delta Q_a$ and the anomaly of the oceanic heat flux convergence, $-\Delta Q_v$. When concerning the anomaly in the westerlies it is related without lag to $-\Delta Q_a$, whereas the index for ocean circulation, $-\Delta Q_v$, operates with a lag. *From Bjerknes (1964).*

The hypothesis for this relationship is that stronger winds increases the evaporation, resulting in a greater heat loss ($-\Delta Q_a$) from the sea surface, followed by a lagged decline in SST, (ΔT_w) due to the great thermal capacity of the oceanic mixed layer (Bjerknes 1964).

When the anomalies of the westerly winds are positive (hence a NAO^+ situation) the loss of heat from the ocean to the atmosphere is, according to Bjerknes, on the interannual time scale compensated to some degree by an induced increase of the oceanic heat flux, but with a lag compared to the curve of (ΔT_w).

The implications of this hypothesis are intriguing, suggesting a compensational effect between the atmospheric and oceanic parts of the total meridional heat transport, or in Bjerknes' own words:

> *The (above) hypothesis concerning quasi constant total meridional heat flux and opposite fluctuations of its oceanic and atmospheric parts, does explain the possibility of relatively big variations in climates without having recourse primary to solar changes.*

In summary, these observations led to the notion that the North Atlantic SSTs basically are driven directly by the atmosphere at interannual (shorter) time scales, while ocean dynamics play a crucial role at longer timescales. Thus, the air-ocean interactions in the North Atlantic displays two time-dependent modes of co-variability. This quite impressive deduction is still somewhat consistent with more recent observational studies such as that of Kushnir (1994), and modelling studies (Timmermann et al. 1998), although the latter relates the observed interdecadal variability more to the thermohaline circulation rather than ocean dynamics as a whole. Their proposed negative feedback mechanism of this low frequency variability is shown in Figure 2.8.

Knowing from the above mentioned studies that the atmospheric influence on the upper-level thermal properties of the ocean is the leading mechanism on shorter time scales, it is still of importance to investigate the eventuality of the latter's ability to feedback onto the former since such knowledge might result in increased skill of regional climate predictability.

An example of a work demonstrating that there might be signals of the SSTs which could be related to atmospheric circulation responses, and hence increased long-term predictability, is that of Rodwell et al. (1999). They showed that ensembles of their atmospheric model was able to reconstruct much of the observed low frequency variability of the NAO from knowledge of the global SSTs from the last half decade. Being in a model environment uncoupled to the ocean, they claimed that their analysis could be performed without considering the forcing onto the ocean from the atmosphere, implying that the skill of their NAO-simulation had to be attributed to the SSTs, and not to the indirect effects of ocean-atmosphere coupling.

Care should, however, be taken when attributing such results directly to the predictive

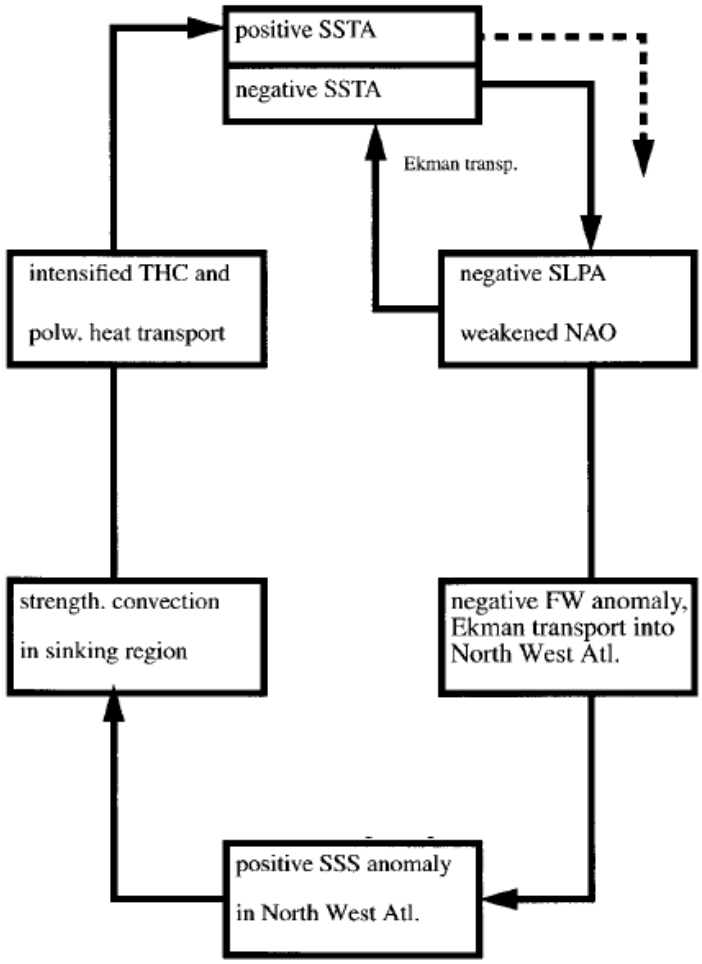

Figure 2.8: Schematic diagram of the interactions that lead to an interdecadal cycle. Considering a negative SSTa, which involves a weakened North Atlantic Oscillation causing anomalous freshwater (FW) fluxes and wind induced Ekman transport off Newfoundland and in the Greenland Sea. This results in a positive anomaly in the distribution of sea surface salinity (SSS) which increases the density, thus enhancing deep convection in the oceanic sinking regions. This is followed by an increase in the THC and poleward heat transport leading to positive SST anomalies, which completes the negative feedback loop and constitutes an oscillation. *Figure obtained from Timmermann et al. (1998).*

skill of climate indices such as the NAO, as also is discussed in the studies of Bretherton and Battisti (2000) and Czaja and Marshall (2000). For example, the AGCM of Rodwell et al. (1999) is successful in reproducing the observed phase of the NAO while its simulated amplitude is greatly damped in the model environment. Moreover, as far as climate predictability is concerned, one would need the SSTs themselves to be predictable, being a hard task when remembering the observed (and timescale-dependent) interactions determining the SST-field discussed above.

The SST pattern, shown by Rodwell et al. (1999) to be the one associated with the NAO is shown in Figure 2.9 and is referred to as the North Atlantic SST tripole. This pattern is also shown by Deser and Blackmon (1993) to be a prominent pattern of natural North Atlantic SST variability. As could be seen it is constituted by SST anoamlies both in the tropical as well as the extratropical parts of the basin.

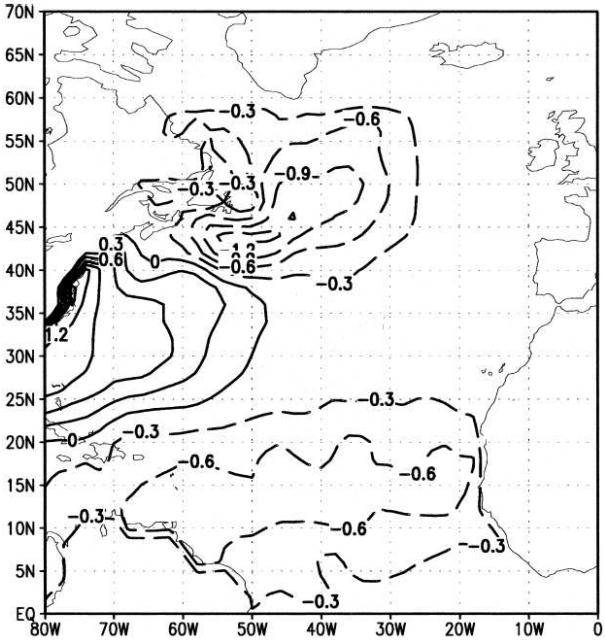

Figure 2.9: The tripole pattern of SST in the North Atlantic associated with the leading empirical orthogonal function of SST variability. *From Peng and Li (2002).*

The general importance of the midlatitude SST-anomalies have, however, been debated when it comes to SST-influence on the NAO and atmospheric circulation in general. When forcing their model with the SST-tripole, Sutton et al. (2001) found that the tropical part (south of 30° N) of the tripole was the main contributor to atmospheric circulation changes both locally in the tropics, and in the midlatitudes. The extra-tropical influence on the atmospheric circulation was weak, and displaying a nonlinear nature. They found this nonlinearity hard to explain in other than more general terms. For instance, they considered the extra-tropical atmosphere's sensitivity to small perturbations in the presence of baroclinic and barotropic instabilities, as well as the nonlinearity in moist processes to be possible explanations for it.

Investigations of the linearity of the atmospheric response due to SST-forcing is followed up in a later study by Sutton and Hodson (2007), where also an investigation of the seasonal cycle of the climate impacts were conducted. The focus here was on the atmosphere's adjustment to a general warming or cooling of the North Atlantic. They found the atmospheric response to be highly dependent on season, and thus on background flow. Here, extra-tropical SST-forcing were found to induce a robust response in atmospheric circulation only in summer[5], displaying only very weak changes in the other seasons.

[5]In terms of the signal-to-noise ratio, which they defined as the mean response divided by the inter-annual variability

When tropical anomalies in SST also were introduced, however, the amplitude of the response were enhanced, once more indicating the importance of the tropical SST-forcing.

Hoerling et al. (2001) also argued that the specific SST-signal forcing the NAO originated from the tropics. They reached to this conclusion as their model reproduced around half of the observed NAO-variability both when forced by observed global SSTs, and when only observed SSTs inside the latitudinal band of 30° S - 30° N were included. Outside this region, they employed an annual cycle of climatological SSTs. This, they claimed, left out the extra-tropical SSTs influence on the NAO. The success of the model in simulating the observed NAO-variability persisted when they introduced climatological SSTs also to the tropical Atlantic, suggesting that the NAO-signal actually has its origin in the tropical Pacific and Indian Oceans.

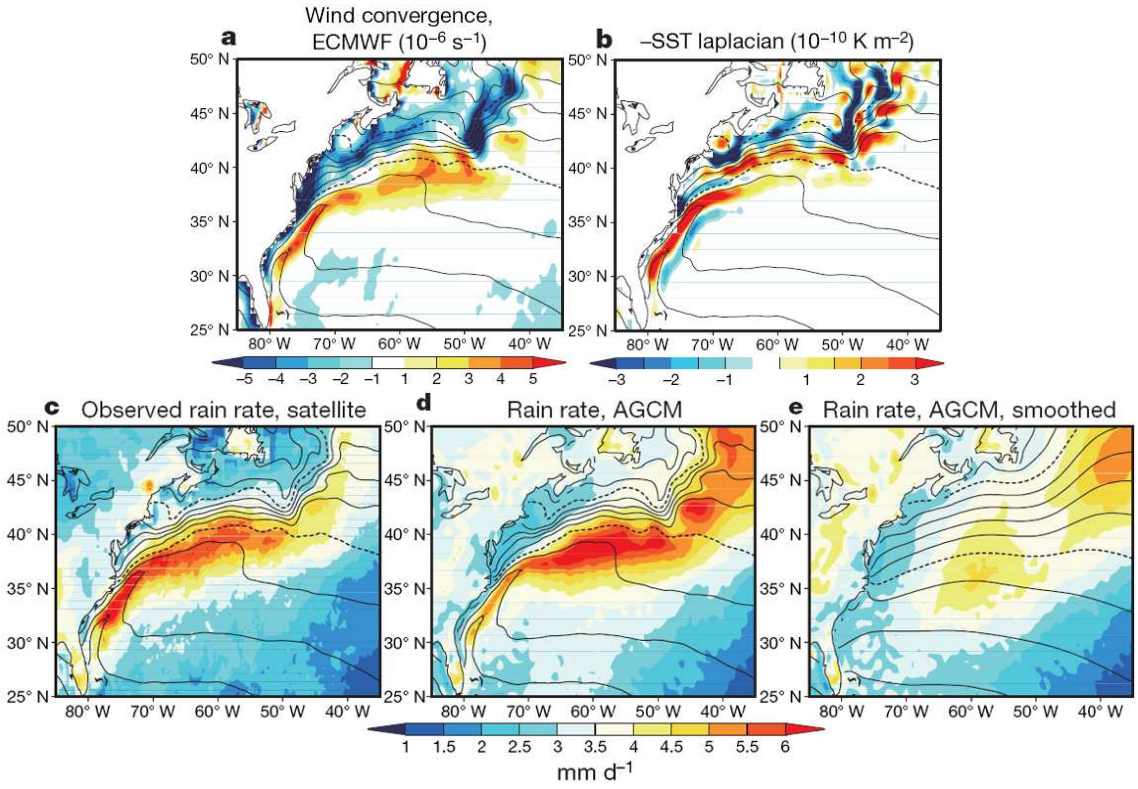

Figure 2.10: Annual climatological fields of the wind convergence (a), and the negative laplacian of SST (b), from ECMWF-reanalysis. The rain rates as observed by satellites are shown in (c), whereas the precipitation as represented in an AGCM forced with observed and smoothed SSTs are shown in (d) and (e), respectively. In all figures, the SST-field is indicated as contours with an interval of 2K with the contours of 10°C and 20°C dashed. *From Minobe et al. (2008).*

However, a study by Minobe et al. (2008) propose that the Gulf Stream through its maintenance of sharp SST-gradients (shown as the negative laplacian[6]) entailed by surface wind convergence (figures 2.10(a-b)) is associated directly to the narrow band of precipitation (figures 2.10(c-d)). Their high-resolution model is not able to reproduce this precipitation pattern when SSTs are smoothed (Figure 2.10(e)), which, they claim, is an indication of this precipitation band resulting from forcing by the sharp SST front. It is believed that such precipitation anomalies following Gulf Stream changes might have the ability to adjust planetary waves and storm tracks, hence inducing atmospheric circulation changes (Minobe et al. 2008). It could also be mentioned here that the presence of the strong SST-gradients (and hence strong atmospheric baroclinicity) has been proposed by Hoskins and Hodges (2002) to be a main contributor to the North Atlantic storm track.

Following this deduction, the Gulf Stream, being the upper branch of the Atlantic meridional overturning circulation (AMOC), might act as a direct pathway for the atmospheric circulation to respond to changes in ocean dynamics. The work of Minobe et al. (2008) constitute the most recent results supporting the hypothesis that changes in midlatitude SSTs associated with ocean circulation might have the ability to affect the atmospheric circulation.

[6]The negative laplacian can be written as: $-\nabla^2 SST = -(\frac{\partial^2 SST}{\partial x^2} + \frac{\partial^2 SST}{\partial y^2})$

Chapter 3

SPEEDY and statistical methods

3.1 The SPEEDY model

The model used for the experiments in this thesis is the SPEEDY-model (nicknamed after Simplified Parameterizations, primitvE-Equation DYnamics). The model is an AGCM (Atmospheric General Circulation Model) of intermediate complexity. The model runs themselves are performed by dr. Jürgen Bader, and the data are read into Matlab through scripts provided by Christophe Sturm, available for download at *http://www.mathworks.com/matlabcentral/files/15326/read_grads.m*, (Visited September, 2007).

3.1.1 General

SPEEDY is a hydrostatic, σ-coordinate, spectral transform model in the vorticity - divergence form described by Bourke (1974). SPEEDY is developed by Molteni (2003b) and Kucharski et al. (2006), and employs a spectral dynamical core developed at the Geophysical Fluid Dynamics Laboratory by Held and Suarez (1994). The basic prognostic variables of SPEEDY are vorticity ($\zeta = \frac{\partial v}{\partial x} - \frac{\partial u}{\partial y}$) and the divergence ($\boldsymbol{\nabla} \bullet \boldsymbol{V} = \frac{\partial u}{\partial x} + \frac{\partial v}{\partial y}$) of the wind field, absolute temperature (T) and the logarithm of surface pressure ($\log p_s$). In addition, the model computes the evolution of other variables which are advected in the dynamical core, such as specific humidity (q). For the T30-resolution (see Section 3.1.2), the time-step is around 30 minutes[1], and the integration is done by means of a leapfrog-scheme with the appliance of a time filter to reduce the computational mode.

The vertical σ-coordinate is by definition the pressure normalized by ground pressure, $\sigma = \frac{p}{p_s}$(Hartmann 1994). The term 'spectral' is associated with the fact that the fields

[1]According to the Courant Friedrich Lewy (CFL) criterion the length of the time-step is dependent on the model resolution in order to maintain numerical stability (Press et al. 2003)

of the variables are transformed into the wavenumber-domain prior to solving the differential equations included in the dynamical core of the model. Therefore, the differential equations of the dynamical core of the model are solved in this domain rather than in the physical domain.

A 2-dimensional field in the physical domain is represented as simply:

$$f = f(x, y)$$

whereas in the wavenumber-domain the data is represented as spatial Fourier-components, e.g.:

$$f = \sum_{j=1}^{N_x} \sum_{k=1}^{N_y} a_{(j,k)} e^{ijx+iky}$$

Where j and k are the zonal and meridional wavenumber, respectively. x and y are the zonal and meridional cartesian coordinates of a given data point.

The horizontal resolution of the model decides the size of N_x and N_y. An increased resolution yield higher N_x and N_y, which means that shorter wavelengths can be resolved in the model.

An advantage of applying the spectral method in a global model is briefly discussed in Press et al. (2003). Here it is pointed out that spectral schemes converges more rapidly than is the case for finite-difference methods. An apparent drawback with spectral methods is the Gibbs phenomena, shown in Figure 3.1, stating the impossibility of representing a discontinuous function in the spectral domain (Emery and Thomson 2001). This might affect the accuracy of spectral models.

3.1.2 Current resolution

SPEEDY is defined on a grid corresponding to the triangular truncation of spatial spectral fields at total wavenumber 30. This resolution is referred to as T30. The largest wavenumber, k, and thereby the shortest wavelengths (since $k \propto \frac{1}{L}$, where L is the wavelength) of the fields resolved by the model is 30. In practice, this yields an approximate distance between grid points of 3.8° corresponding to a grid of 96 and 48 points in the zonal and meridional directions, respectively. The SPEEDY-version used in this thesis have 8 vertical layers, and is referred to as Version 40 (see fig. 3.2).

The 8 σ-layers have values of 0.025, 0.095, 0.20, 0.34, 0.51, 0.685, 0.835 and 0.95. The output-data from the model integrations are then post-processed on the pressure levels: 30, 100, 200, 300, 500, 700, 850 and 925 hPa. The the bottom and the two upper lay-

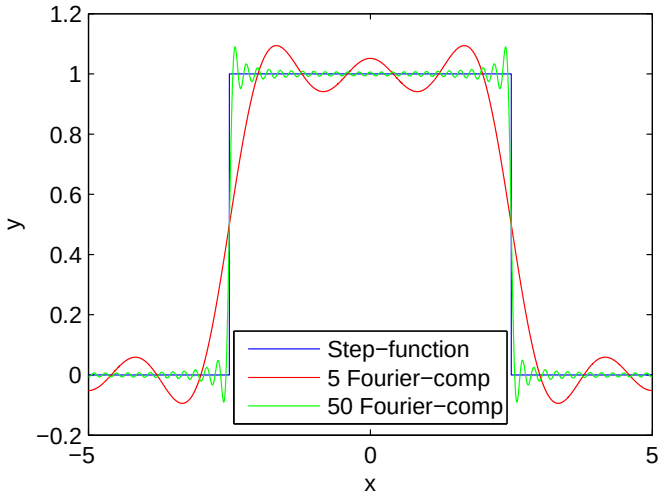

Figure 3.1: The Gibbs phenomena, showing that a discontinuity in physical space (blue) will provide a bias in the spectrum space, represented by Fourier-components, and that this bias will still exist with the same amplitude, even if the number of Fourier components used are increased. Examples of this are shown for 5 (red) and 50 (green). The figure is made with statistical tools in MATLAB.

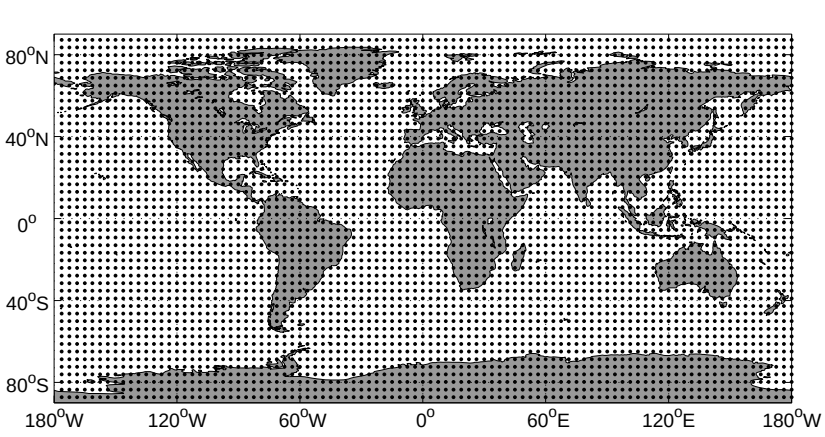

(a) Horizontal resolution

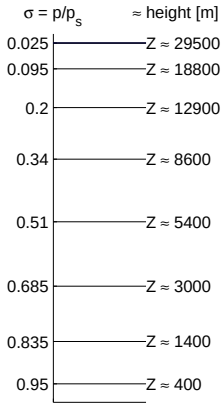

(b) Vertical resolution

Figure 3.2: Schematic view of horizontal (a) and vertical (b) resolution of the SPEEDY-version used in this thesis. Figures are obtained through plotting routines in Matlab.

ers are thought as a bulk presentation of the planetary boundary layer and stratosphere, respectively (Kucharski et al. 2006).

3.1.3 Physical parameterizations

All models used, both in weather forecasting and climate research, have a finite distance between their computational points. Numerous relevant phenomena of the atmosphere

act, however on scales much smaller than the resolution of the model, and are therefore not captured directly. In nature, these unresolved features are important since they will feedback to the resolved features, thus increasing the model bias significantly. In order to account for the small-scale processes, models are computing such phenomena in a parameterized way, where equations of known resolved variables are solved in order to obtain estimates for the impact of subgrid-scale features. Especially, coarse resolution GCMs, such as SPEEDY, are dependent on having robust parameterizations.

The parameterizations of SPEEDY, handling these sub-grid features of the atmosphere, are designed and optimized for working in models with few vertical layers (Molteni 2003b). The parameterization schemes include the calculation of convection, large-scale condensation, clouds, short wave radiation, long-wave radiation, surface fluxes of momentum and heat, and vertical diffusion. A detailed description of the physical parameterizations of SPEEDY are given in Molteni (2003a). Also a shorter, but updated description are given in Kucharski (2007).

Boundary conditions

SPEEDY requires the following climatological fields of variables as boundary conditions:

1. Monthly Sea Surface Temperature (SST)
2. Monthly Sea ice fraction
3. Monthly Surface temperature in the top soil layer (about 10 cm)
4. Moisture in the top soil layer and the root-zone layer
5. Snow depth
6. Bare surface albedo (in the absence of snow or sea ice)
7. Fraction of land-surface covered by vegetation.

In addition, SPEEDY incorporates the topographic height and a fractional land-sea mask into the computations. The climatological fields used as boundary conditions in SPEEDY are obtained from the European Center for Medium-range Weather Forecast's (ECMWF) reanalysis, ERA15 (Gibson et al. 1997).

Why the SPEEDY Model?

During the last years, state-of-the-art GCMs have being increasingly able to reproduce several important aspects of the atmospheric general circulation (Randall et al. 2007). However, the degree of complexity in these models can make the interpretations of simulations equally difficult as analysing real observational data (Robinson 2000; Molteni 2003a). In addition, they claim that the comprehensive and advanced code structures sometimes are hard for scientists to understand in order to perform different sensitivity experiments.

One main advantage for using SPEEDY in the experiments described in this thesis, is the extremely short computation time. SPEEDY requires an order less computation time than an state-of-the-art GCM with the same resolution (1 year of simulation can be run in 12 minutes on a Pentium 4 (3.40GHz) processor). This short computation time opens the possibility for long model-runs in which studies of inter-decadal or even inter-centennial variability can be performed. Also, the robustness of the atmospheric response will increase when performing a large number of ensembles.

In the setup used in the present work, SPEEDY is uncoupled from the ocean in the sense that the underlying SST is not altered by the atmosphere's back interaction during the model integrations. However, SPEEDY has the opportunity to be coupled to a slab/mixed layer ocean. The reasons for not employing this option is mainly due to the wish of preserving simplicity when analysing the response. In addition, in order to obtain an equilibrium response of the atmosphere to the passive ocean, such a simplification is believed to be necessary, since a coupled model environment will constitute a time-dependent response (Kushnir et al. 2002). However, it is important to briefly discuss the constraints of decoupling the atmosphere from the ocean, as is done below.

In this thesis, the model is uncoupled to the ocean with the thermal forcing consisting of prescribed SST-anomalies both in the tropics and midlatitudes. When forcing the tropical ocean this way, one should remember the discussion of the sensitivity of the atmospheric response to such anomalies from Section 2.3.2. It can be argued that this effect is particularly strong in a model environment such as used here because of the following:

The ocean surface temperature is by definition prescribed, with the consequence that the atmosphere is unable to affect the upper-level properties of the ocean surface temperature, inconsistent with the observations and the considerations of Bjerknes (1964). Consequently, the expected increased evaporative cooling of the ocean surface as a consequence of an imposed positive SST anomaly is not taken into account. In the natural system, this mechanism, known as the *negative evaporation feedback*, effectively acts to attenuate anomalies, and is indeed thought to be part of the explanation for the observed

stability of the tropical SSTs through glacial and interglacial eras, when compared to the large SST-variability in the midlatitudes through such climate transitions (Hartmann 1994). Hence, when neglecting this mechanism, there is a possibility for the modeled atmosphere to 'see' a stronger forcing than what would be the case in the fully natural system, and this is a constraint which should not be neglected when analysing the atmospheric response.

3.1.4 Validations of SPEEDY

For the first version of SPEEDY, Molteni (2003b) gives an overview of the models ability to reproduce properties of the atmospheric general circulation. In general, the validation showed that the systematic errors in SPEEDY are typical for many GCMs, but that the amplitudes of SPEEDY tended to be higher than in state-of-the-Art GCMs. This might be expected given the simplicity of SPEEDY compared to the most complex GCMs, in addition to its relatively coarse resolution. Nonetheless, the increase of the number of vertical layers from 5 to 7 (Bracco et al. 2004) and from 7 to the present 8 (Kucharski et al. 2006) have proved to significantly improve the models ability to reproduce the observed climatological state of the atmosphere, and it is of interest to investigate this more thoroughly.

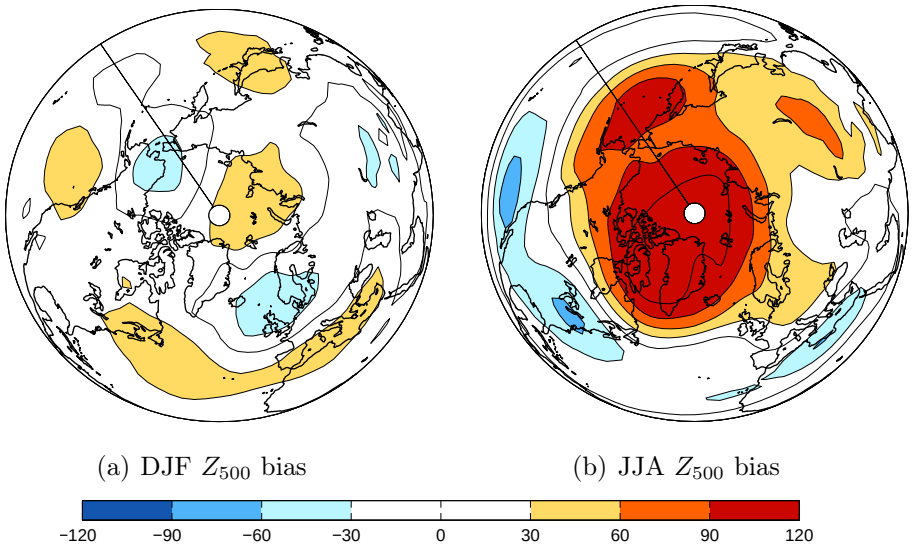

Figure 3.3: Bias in the northern hemisphere geopotential height of the 500hPa-surface in winter (a) and summer (b). Biases are computed as the DJF and JJA mean difference between model and NCEP/NCAR re-analysis (Kalnay et al. 1996). SPEEDY data are obtained from the 260-year long control run described in Chapter 4. Contour intervals are 30 m.

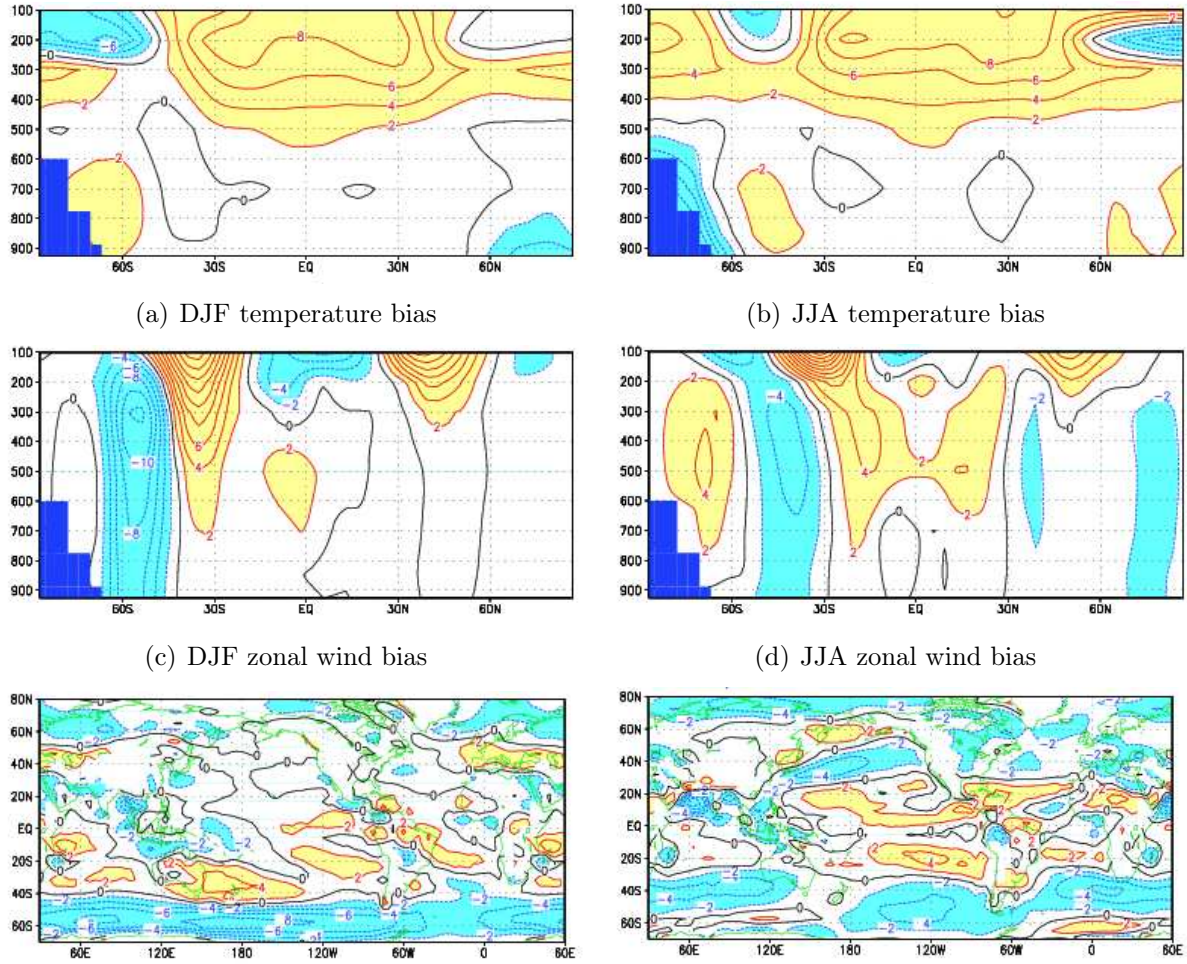

(a) DJF temperature bias

(b) JJA temperature bias

(c) DJF zonal wind bias

(d) JJA zonal wind bias

(e) DJF zonal wind at 925 hPa bias

(f) JJA zonal wind at 925 hPa bias

Figure 3.4: Zonal mean model bias in SPEEDY. (a) DJF temperature, (b) JJA temperature, (c) DJF U-wind, (d) JJA U-wind, (e) DJF U-wind at 925 hPa and (f) JJA U-wind at 925 hPa. Contours in 2K(a-b) and 2m/s(c-f), negative values shaded blue, positive values shaded red. *Figures from Kucharski (2007).*

Figure 3.3 gives an overview of the model bias in representing the geopotential height of the 500hPa-surface, Z_{500}, in the Northern Hemisphere. It is evident that a large positive bias (exceeding 120 m) exists over large regions of the polar region during summer. In the winter case, however, the model reproduces the atmosphere's mean state better. 2 negative and 4 positive bias regions are seen, none of them having amplitudes larger than 60m.

Figure 3.4 shows the 8-layer SPEEDY model bias for zonal mean temperature and zonally averaged U-wind for the winter (DJF) and summer (JJA) seasons when compared to

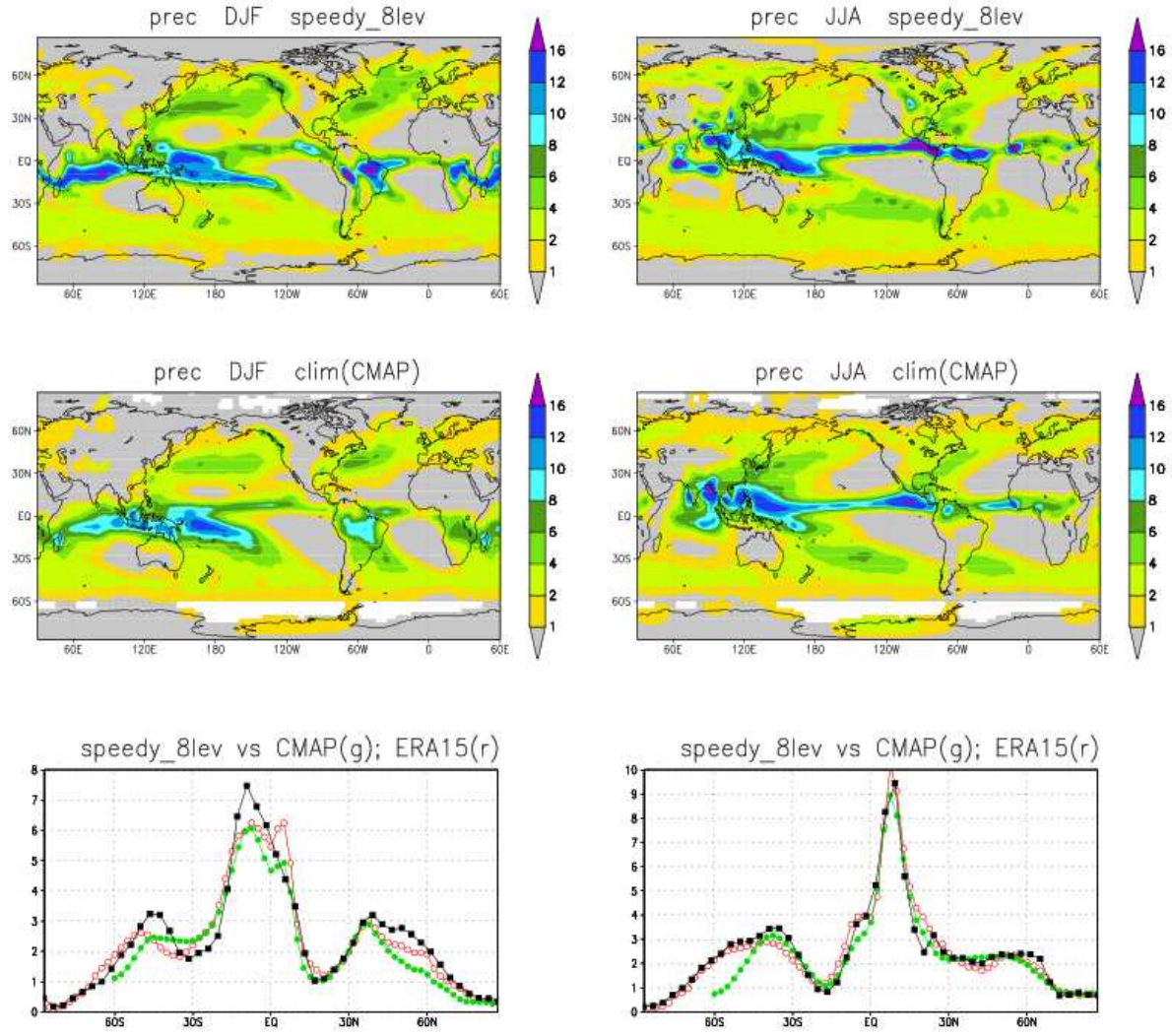

(a) DJF precipitation

(b) JJA precipitation

Figure 3.5: Precipitation in winter (a) and summer (b). The upper panels show precipitation in SPEEDY with the corresponding observed precipitation rates obtained from the CMAP-database (Xie and Arkin 1997) in the middle panel. The zonally averaged precipitation of SPEEDY (black), CMAP (green) and ERA15 (red) are shown in the lower panel. *Units in mm/day.* Figures from Kucharski (2007).

the observed climatology. Generally, it can be seen that amplitudes are greatest in the Southern Hemisphere. The upper troposphere (above ∼500 hPa) in SPEEDY are generally too warm. A negative bias in the zonal wind, extending throughout the troposphere and lower stratosphere can be identified at ∼60°S. The main zonal wind biases seem to

be associated with an equator-ward shift in the southern subtropical jet. The low-level temperature and surface winds in the Atlantic sector are fairly well simulated.

Figure 3.5 shows the global distribution of precipitation in SPEEDY compared to the observed. SPEEDY overestimates the precipitation in midlatitudes and in the equatorial areas during boreal winter. In summer, this seems to be a smaller problem. Since precipitation is generally a difficult parameter to handle, also for the more advanced circulation models, one could say that SPEEDY is able to represent the global precipitation in a quite realistic way.

The systematic errors in SPEEDY are assumed to be the same in the experiments described in Chapter 4. Therefore, the response addressed in this thesis will primarily focus on the deviations of the perturbed run compared to the control-run, a procedure common in analysing output from GCMs.

3.2 EOF-analysis

Empirical orthogonal functions (EOF) are widely used in the field of geophysics, especially since the commencement of numerical computing. The application of EOF-analysis in the geophysical sense goes back to the mid-1950s when Lorenz (1956) developed a statistical technique for forecasting the weather. This has later become a usual way to represent and analyse output from GCMs and reanalysis-data.

The EOF-analysis is a way to split up the variance in a dataset into independent spatial modes of variability (Emery and Thomson 2001). The output of the EOF-analysis are the different modes, showing anomaly-patterns in the spatial domain and the time-series of the principal components (PCs) which visualize the time-evolution of the belonging pattern. For example, a high and positive (negative) value in a timestep of the PC-timeseries would imply that the corresponding pattern have a relatively large and positive (negative) amplitude at that particular timestep.

Also, each mode have an eigenvalue telling how much of the total variability of the field is explained by the corresponding EOF. This is also the usual way of sorting the different patterns, with the 1st mode (EOF1) explaining most of the variance, and the 2nd (EOF2) explaining the second most, etc.

In this work the method used for obtaining the EOFs is the Singular Value Decomposition (SVD) with the appliance of the *svd*-routine in MATLAB. Data within the box (20-80N, 90W-40E) have been used as basis for the analysis. This box is chosen as it covers the area of the SST-forcing and since it also is defined by Hurrell et al. (2003) to constitute

the data used for calculating the EOF-based NAO-index.

Prior to the decomposition the following procedures are performed:

1. The monthly data of both the control run and the perturbed run are averaged to separate seasonal components.
2. The timeseries of both runs are combined into one data matrix, $\boldsymbol{A}$.
3. In each grid point of $\boldsymbol{A}$ the corresponding total long-term mean is subtracted, yielding an anomaly matrix, $\boldsymbol{A'}$
4. Finally, anomalies are weighted by the square-root of cosine to latitude ($\sqrt{\cos\phi}$).

The last procedure is done in order to remove the area dependence of the data since the model grid points are unevenly spaced in the zonal direction when moving meridionally.

It is here to be mentioned that trends in the timeseries also should be removed according to conventional EOF-analysis (Emery and Thomson 2001). The main reason for not detrending the time series, is to enable an investigation of any regime shifts of the indices in the experiments. If a mean shift or change in the variance of one index is found, this can be ascribed to one spatial EOF-pattern, only. Moreover, probably due to the absence of forcing trends, the simulations show stability with no observed significant trends of PCs within each experiment.

After the decomposition, the PCs are normalized to unity standard-deviation and zero mean. The anomaly data matrix, $\boldsymbol{A'}$, are then regressed back onto the principal components, resulting in spatial variability patterns scaled to original data units. Consequently, the units of each EOF-pattern for MSLP (Z_{500}) might be interperated as hPa (meters) pr. standard deviation of the corresponding principal component.

Advantages

The advantages of EOF-analysis in large datasets are several, one big asset being the data reduction. In fact, this method constitute the most efficient statistical compression of the data field (Emery and Thomson 2001). Also it constitute as a powerful tool to identify causal spatial relationships of the circulation.

Also, a large portion of the total variance in a spatial field is usually explained by only the first few modes, opening for the opportunity to address the variability to different dynamical features. As is discussed in Section 2.4, these patterns proves to significantly impact and interact with various aspects of climate. Hence, the output from such an analysis might in some cases form a basis for discussing which physical processes are interconnected to the pattern, and might also be used as a tool in predictability studies.

Disadvantages

Even though this kind of analysis can be applied to describe physical features, the procedure of EOF-analysis remain purely statistical and it is therefore important to remember that there is no guarantee that EOFs really reflect physical processes. As an example, one distinct physical mechanism might be spread over several EOFs, or many different physical processes might contribute to the variance contained in only one EOF (Emery and Thomson 2001). The interpretation of EOFs should therefore always be done with caution. Another property which escalates the difficulties of interpretation is the fact that EOFs might be quite sensitive to the choice of the spatial domain and/or time period chosen as basis for the analysis.

For a recent review on EOF analysis and related techniques in atmospheric sciences the reader is referred to Hannachi et al. (2007).

3.3 Statistical significance tests

In order to statistically quantify whether a difference in the mean state or variability of a population might occur just by chance (*e.g. random)*, a statistical test has to be applied. In this section the basics of the tests used in the thesis are explained.

3.3.1 Student's t-test

The test used for calculating the statistical significance of the temporal mean response is the two-tailed Student's t-test. The aim of the test is to estimate a possibility of the real mean of one population, μ_x, to be equal to the real mean of another population, μ_y.

Let X and Y be time series consisting of N_x and N_y samples, respectively, $X = x_1, x_2, \ldots, x_{N_x}$ and $Y = y_1, y_2, \ldots, y_{N_y}$. Further, assume that the samples of X and Y are independent and normally distributed, with respective population variances[2], s_x^2 and s_y^2, and that the sample means[3], $\overline{X}$ and $\overline{Y}$, themselves are normally distributed as given by the *central limit theorem* (Emery and Thomson 2001, pages 211-214).

The first step of the test is to state two hypotheses:

- H_0: $\mu_x = \mu_y$

[2] i.e. $s_x^2 = \frac{1}{N_x} \sum_{i=1}^{N_x} (x_i - \overline{X})^2$

[3] i.e. $\overline{X} = \frac{1}{N_x} \sum_{i=1}^{N_x} x_i$

- H_a: $\mu_x \neq \mu_y$

The above hypotheses are suggesting a two-tailed test. The next step is to state a maximum threshold of the probability to reject the H_0-hypothesis when it in fact is true. This threshold is called the *significance level*, designated by α. For instance, if H_0 could be rejected at the $\alpha = 5\%$-significance level, one might say that the hypothesis H_a is true with a confidence level of $1-\alpha = 95\%$. However, the possibility of erronously rejecting the H_0-hypothesis would in this case still be $\alpha = 5\%$, which is referred to as the possibility of making a $type-1$ error. In the present work, this possibility is also denoted as the *p-value*.

In order to perform the test itself a critical quantity is needed. This critical quantity, $t_{crit(\frac{\alpha}{2},\nu)}$, where ν is the degrees of freedom (DOF), could be found in tables from Emery and Thomson (2001). Also, the calculation of a test-statistic, t is needed:

$$t = \frac{\overline{X} - \overline{Y}}{\sqrt{\frac{s_1^2}{N_x} + \frac{s_2^2}{N_y}}} \tag{3.1}$$

When the two-tailed test is applied, the H_0-hypothesis can be rejected at the $(1-\alpha)$ confidence level in the cases where $|t| > t_{c(\frac{\alpha}{2},\nu)}$.

Unlike the normal-distribution (*Z-distribution*), the t-distribution depends on the size of the sample, and thereby on the above-mentioned DOF. For cases where the population time-variances of the fields can be assumed to be the same, $DOF = N_1 + N_2 - 2$. When this assumption fails, the DOF (now denoted with a prime, ν') has to be approximated in the following way (Walpole et al. 2002):

$$\nu' = \frac{(w_x + w_y)^2}{\frac{w_x^2}{N_x - 1} + \frac{w_y^2}{N_y - 1}} \tag{3.2}$$

where $w_x = \frac{s_x^2}{N_x}$ and $w_y = \frac{s_y^2}{N_y}$.

In this work, the degrees of freedom have been approximated to that of Equation 3.2. However, it is found that this approximation will not comprehensively affect the outcome of the hypothesis test due to the large sample size. The specific routine for the appliance of the t-test in this work is the MATLAB-function *ttest2*.

3.3.2 F-test

A statistical test is conducted to measure if a change in variance, σ^2, between the experiments can be ascribed to randomness only. For the statistical test of equal sample variances, the F-test based on Walpole et al. (2002) is employed. Again, considering the

two timeseries X and Y which consist of normally distributed and independent samples with ν_x and ν_y DOF, respectively.

The first procedure for the test is similar to the t-test, which is to state two hypotheses, e.g:

- H_0: $\sigma_x^2 = \sigma_y^2$
- H_a: $\sigma_x^2 \neq \sigma_y^2$

Then, the desired α-level for the test is to be defined. The above hypotheses state a two-tailed test, which is the one used in this thesis. In this case, the critical region is (Walpole et al. 2002, page 331 and theorem 8.7):

$$F_{c1} = F_{\frac{\alpha}{2}}(\nu_x, \nu_y) < F < F_{\frac{1-\alpha}{2}}(\nu_x, \nu_y) = \frac{1}{F_{\frac{\alpha}{2}}(\nu_x, \nu_y)} = F_{c2}$$

This critical region can be found from tables in Emery and Thomson (2001). Finally, a computation of the test statistic, $F = \frac{s_x^2}{s_y^2}$, is to be performed in each grid point. In the grid points where F lies outside the region spanned by F_{c1} and F_{c2}, the H_0 hypothesis can be rejected with a confidence of (1-α)%. In general, it can be said that the more the test statistic deviates from 1, the stronger is the evidence for unequal population variances between X and Y. The specific routine for the appliance of the F-test in this work is the MATLAB-function *vartest2*.

Chapter 4

Experimental design

As mentioned in the introduction of the thesis, the aim of our work is to establish a picture of the equilibrium atmospheric response to a reduction in ocean circulation, when hypothesizing that the latter will induce a more zonally oriented SST-field (the so-called *zmean-hypothesis*). In the present study, this is done by performing model simulations, and the setup of these is the topic of the current chapter.

Two model simulations have been performed, referred to as the control or CTRL, and ZMEAN experiments:

- CTRL: The control experiment, where monthly climatological SSTs are employed
- ZMEAN: The perturbed run, where the monthly climatological SSTs have been zonally averaged in the North Atlantic

Both of the above employ a repeated annual cycle of monthly climatological SSTs, sea ice and solar radiation. Temporal linear interpolation is applied throughout the model integrations in order to minimize eventual noise due to sudden changes in the monthly climatological fields. Greenhouse gases are fixed at rates corresponding to 1950-values. The control-run (CTRL) consists of a monthly climatological SST-field obtained from ERA15-reanalysis (Gibson et al. 1997). In the perturbed run (from now referred to as ZMEAN), the monthly climatological SSTs are zonally averaged over the northern Atlantic basin from the equator up to 65N.

Since our wish is to establish the role of the heat transport conducted by the main gyres and currents of the North Atlantic, the SSTs of the Mediterranean Sea remain unchanged in ZMEAN. Moreover, SSTs in the Labrador Sea has not been altered in order to retain a spatially consistent forcing field throughout the year since this area is ice-covered during boreal winter.

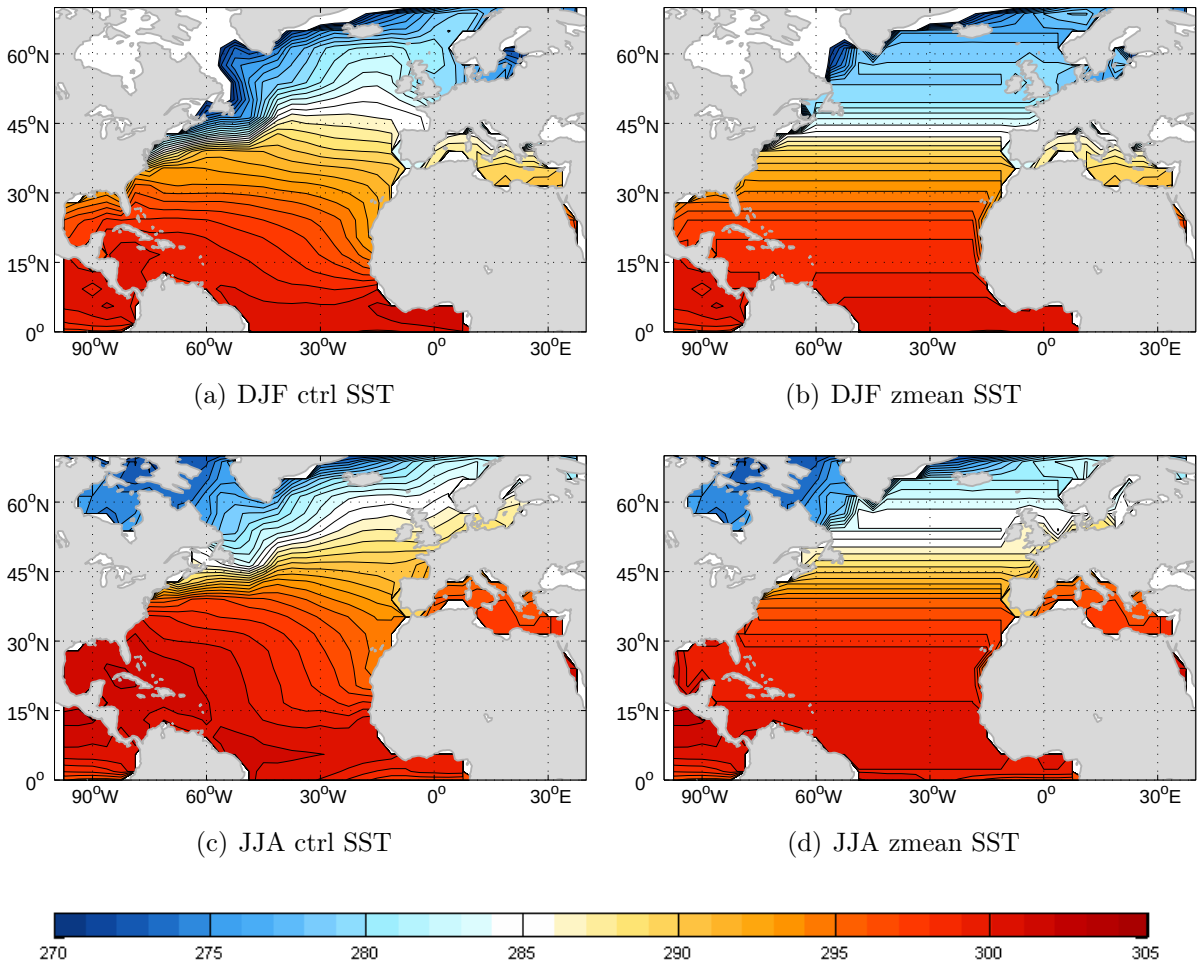

(a) DJF ctrl SST

(b) DJF zmean SST

(c) JJA ctrl SST

(d) JJA zmean SST

Figure 4.1: The winter (DJF) (upper) and summer (JJA) (lower) climatological SST field (left) and these fields zonally averaged (right). Contour intervals at 1 K. *Units in Kelvin.*

Formally, the procedure of zonally averaging the sea-surface temperatures can be described as follows:

$$SST(\lambda, \phi) \rightarrow SST(\phi) \tag{4.1}$$

Here, λ and ϕ are the longitude and latitude, respectively. For the Atlantic sector, the transformation in eq. 4.1 is done by:

$$SST(\phi) = \underbrace{\frac{1}{N_\phi} \sum_{n=1}^{N_\phi} SST(\lambda_n, \phi)}_{'numerical'} = \underbrace{\frac{1}{|\lambda_W - \lambda_E|} \int_{\lambda_W}^{\lambda_E} SST(\lambda, \phi) d\lambda}_{'theoretical'} \tag{4.2}$$

N_ϕ designates the latitude-dependent number of model data points across the width of the basin and λ_W and λ_E the longitude of the western and eastern boundary of the basin,

respectively. It is to be mentioned that the 'numerical' procedure is the one used here as the 'theoretical' requires a completely continuous field of SSTs, obviously not achievable in this context and is thus included here for clarity, only. By following the procedure of Equation 4.2, the longitudinal dependence of the SSTs are removed in order to represent an idealization of a dynamically passive ocean.

Based on what was shown in Figure 1.3(b), it might be argued that this procedure will represent an overestimation of what is observed from the coupled models where the oceanic heat flux is switched off. However, the above procedure is retained as it provides a simple and computationally cheap way of producing the required forcing field as well as enabling us to ascribe atmospheric changes to the dynamical changes of one basin only. This could be a more dubious task if looking into an SST-field from a fully coupled model. What also could be seen as an advantage with our simplified approach is that the total oceanic heat content in the North Atlantic is conserved.

The length of both CTRL and ZMEAN runs is 260 years, and the output from the model are averaged to represent the data on a monthly timescale prior to analysis. To illustrate the operation made on the SSTs, Figure 4.1 shows the mean SST-fields for the boreal winter (DJF) and summer (JJA) in the two model runs.

Figure 4.2 shows the seasonal SST anomalies that constitute the forcing in ZMEAN. For consistency, the anomalies have been averaged over the 3 months in each season.

In general, the forcing constitute a 'quadrupole' pattern, with a negative maximum to the southwestern and northeastern parts of the North Atlantic, and a positive in northwest and southeast. The overall largest amplitude is situated east of Canada, exceeding 8 K in winter. This anomaly is decreased to about 5 K in summer. The largest negative forcing is located just west of the British Isles where the SST in the boreal winter season have been decreased by around 5K when compared to the control-run. In summer and fall this amplitude is reduced to 3K. Another large-scale forcing is west of the North-African continent, where a heating is present with an amplitude of around 3.5-4K in winter. This forcing is restored through much of the year, with a somewhat increased amplitude during summer. All of the Caribbean basin have a wide-spread, but quite persistent cold SSTa with an amplitude of around 2K.

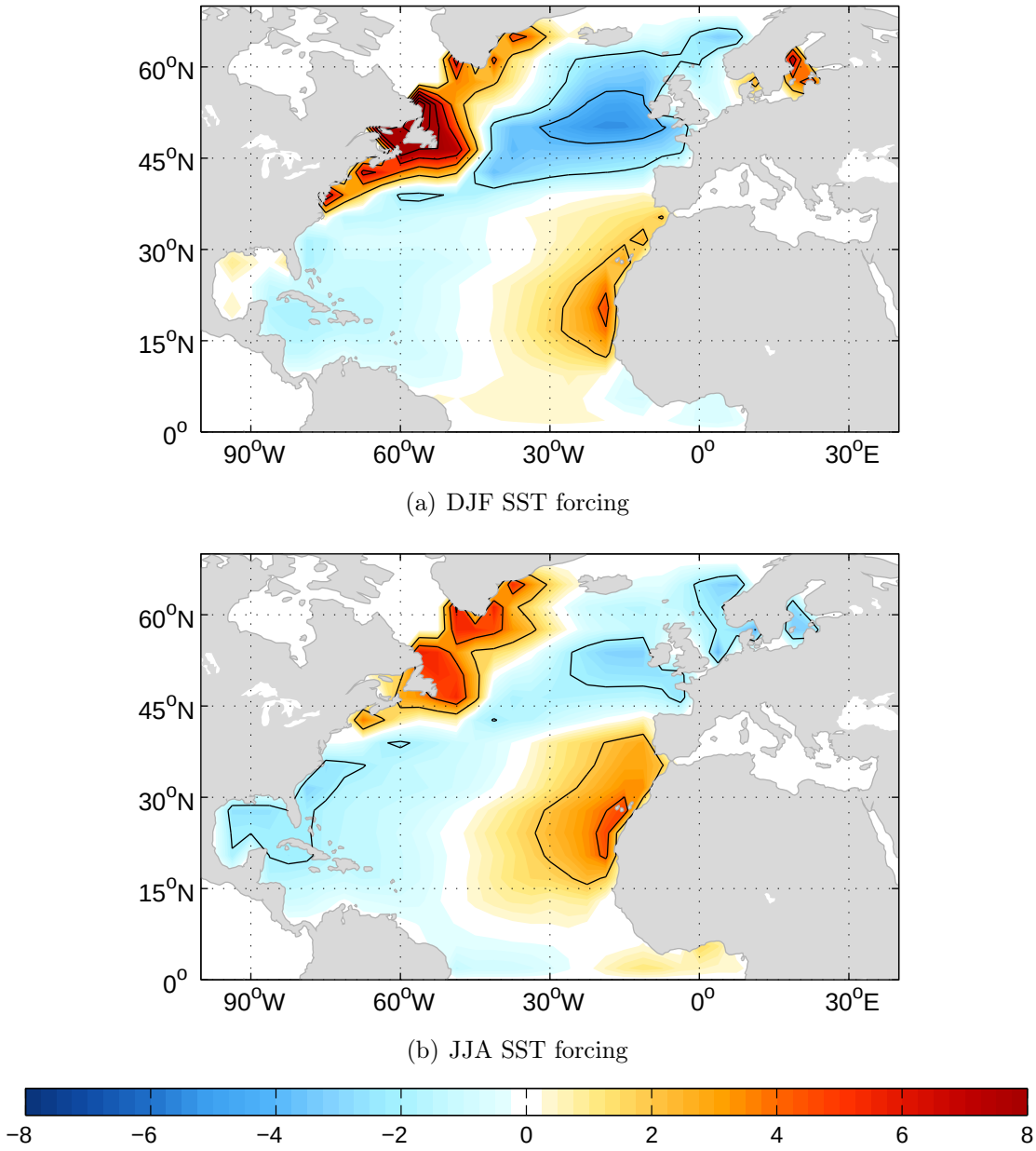

(a) DJF SST forcing

(b) JJA SST forcing

Figure 4.2: The forcing in ZMEAN computed as $SST_{ZMEAN}(x, y) - SST_{CTRL}(x, y)$ in the Sea Surface Temperatures in the North Atlantic Region for the seasons DJF (a) and JJA (b). For clarification, black contours are drawn for every 2 K.

Chapter 5

Equilibrium atmospheric response

Equilibrium atmospheric response

The equilibrium atmospheric response is computed as the seasonal long-term mean of ZMEAN subtracted by the equivalent of CTRL[1]. In the present chapter the mean response of the atmospheric circulation are presented. The main focus will be on the North Atlantic region.

5.1 Mean change of atmospheric circulation

5.1.1 Winter

In Figure 5.1 the winter responses in Mean-Sea Level Pressure (MSLP) is shown. For reference, also the long-term winter mean of CTRL are shown.

A prominent feature arises; the pressure increase west of the British Isles of amplitude above 4 hPa, and the smaller (-2 hPa) and less widespread negative response in the south-eastern parts of Greenland. The former tend to decrease the strength of the southern branch of the Icelandic low, with the latter being an indication of this long-term mean pressure system to be slightly displaced to the north or northwest. It can be mentioned that, associated with the positive response, the near-surface maximum zonal wind is found to be shifted about ~ 5 degrees polewards. One could also observe a low positioned west of the main warm subtropical forcing west of the African west coast. This is consistent with the considerations of Gill (1980) and HK81 as discussed in Section 2.3.1.

An explanation for the positive East Atlantic response could be simply a local and linear one, namely that the negative SST-forcing acts to increase the local air pressure in the

[1]For a variable, X, the response is defined as: $X_{response} = \overline{X}_{zonalSST} - \overline{X}_{climSST}$, where the bar denote the mean of the timeseries for a given season.

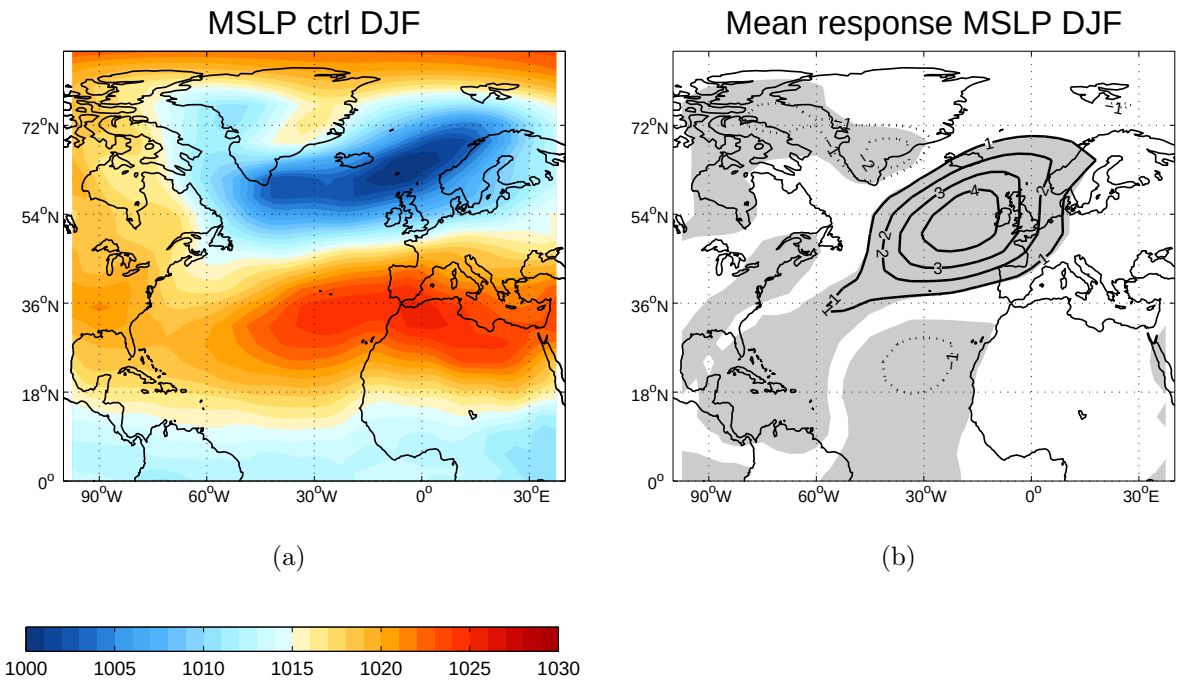

Figure 5.1: The mean winter MSLP-field in CTRL (a) and its response (b). Coloring and contour intervals are 1 hPa. Dotted (solid) contours in (b) correspond to negative (positive) values. The grey shaded areas are statistically significant at the 99 % confidence-level according to a two-tailed t-test.

vicinity, as mentioned in Section 2.2 and in Kushnir et al. (2002). If the direct linear relationship is creating this response, the relative strength would be around $1hPaK^{-1}$ which is comparable to that found in earlier experiments (table 2.2). However, this linear relationship is not found in the western part of the Atlantic.

If taking another view, this positive MSLP response is situated in the (south)eastern end of the North Atlantic storm track, both when measured by means of intensity and track density (Hoskins and Hodges 2002). Therefore, this might be an indication of the storm track to be weakened, either as a consequence of fewer low-pressure systems here, or them being less intense in this area. If this really would be the case, a possible reason could be found by considering the changed baroclinicity through the altered SST-gradients in ZMEAN in the area east of Cape Hatteras, a region of pronounced cyclogenesis. As mentioned in Section 2.5.2, the generation of low pressure systems here is thought to (at least partly) be caused by the sharp SST gradients associated with the Gulf Stream (Hoskins and Hodges 2002). In their figure 14, it is pointed out that the storms moving into the Atlantic region are mainly generated in this particular area, which act to support the emerging hypothesis of the altered SST-gradients to influence the storm track.

There are numerous ways to quantitatively describe storm activity and its mean characteristics. Considering the life-time of such systems, however, the temporal resolution of the data does not allow for the most thorough survey of this matter. Nonetheless, this hypothesis is pursued further by investigating the response in wintertime precipitation shown in Figure 5.2. This is done because precipitation constitute the best proxy available for the storm activity as most of the midlatitude precipitation is directly related to synoptic-scale disturbances. An indication of this is found from the upper panel of Figure 2.2 as the rates of mass-weighted vertical average of diabatic heating (as for instance precipitation) effectively define the North Atlantic storm track (Nigam and DeWeaver 2003).

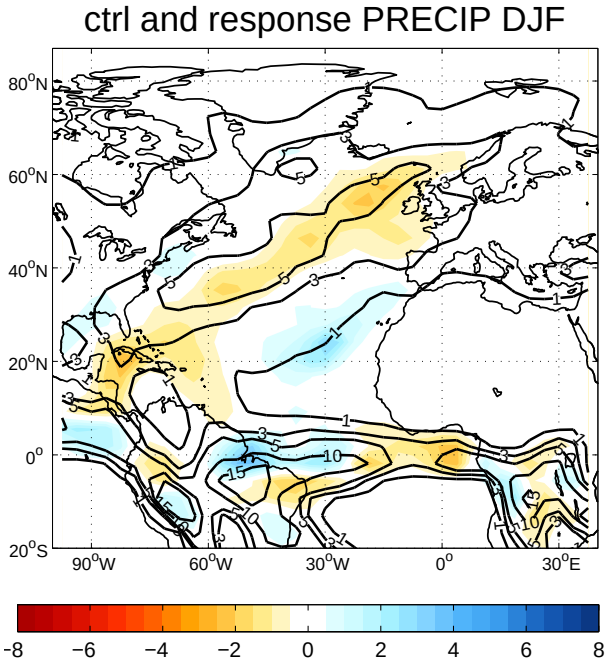

Figure 5.2: Shaded areas show the mean response of precipitation for the winter season, all being significant at the 99% confidence level according to a two-tailed t-test. The black contours show the models winter precipitation climatology taken from the seasonal mean of CTRL. *Units in mm/day.*

As can be seen, there is a decrease in precipitation along the model's storm track, identified as the band of precipitation exceeding ~ 5 mm/day just east of Cape Hatteras and extending northeastwards across the Atlantic. This supports the view of a basin-scale weakening of the North Atlantic storm track when the SST-distribution is zonal.

However, it is to be noted that most of this region of decreased precipitation also coincides with the cooling of the SSTs, leaving the possibility open for this response to be of a more local character. This could be seen from the Clausius Clapeyron relation (Equation 2.10) under the assumption that the air above the negative SSTa is cooled. This local and direct relationship between the SST-forcing and precipitation response was also

considered in the review paper by Kushnir et al. (2002). Moreover, the direct relationship between the SST gradient (or more precisely, its laplacian) and precipitation were in Minobe et al. (2008) identified by means of a high resolution approach. An evident question to be raised is thus if SPEEDY would be able to reproduce such a coupling between the SST gradient and precipitation.

Figure 5.2 also reveals an increase in precipitation southwest of the Canary Islands, a region with low climatological rainfall in CTRL ($\sim 1\ mm/day$). Being in the region of the trade winds coming from the northeast, this response is displaced slightly downstream of the region of maximum forcing, which is consistent with the considerations of Kushnir et al. (2002) regarding earlier GCM experiments. The reason for this response might thus be found directly as the heated surface enhances upward motion (and local temperature) followed by increased condensation which, with the contemporary advective effects, results in intensified precipitation rates downstream of the initial heating.

Further south it can be seen that the eastern Atlantic inter-tropical convergence zone (ITCZ) is weakened in terms of precipitation rates. The western part of the Atlantic ITCZ, however, seems to be shifted slightly northwards, retaining its strength.

From the characteristics of the forcing field it can be seen that the precipitation response near the equator is positively correlated with the forcing, which is consistent with the conclusions of Sutton and Hodson (2007). The absolute change in rainfall, associated with the ITCZ is strikingly much larger than the response found in the subtropics, even if the SST-forcing of the tropics is relatively weak. This indicates that the potential for absolute changes in rainfall is strongly dependent on the background characteristics of the flow. However, as the subtropics is quite dry, the relative response of the latter is quite strong, with around a doubling of the precipitation rate. Therefore, also the strong warm forcing west of Africa is important in shaping the precipitation response.

The winter-response of Z_{500} largely exhibits a dipole structure, with a positive anomaly in the northwest-Atlantic, and one of opposite sign over the European continent, each with a maximum amplitude of around 30 m. The pressure response at 500 hPa is positioned west of the surface pressure response in the central Atlantic, indicating a westward tilt of the perturbed pressure. This is indicative of the response to be of baroclinic structure.

The dipole structure of the Z_{500}-response could be expected from the quasi-geostrophic argumentation of Section 2.3.1, where the mid-level response is shifted downstream relative to the imposed SST-forcing. Assuming that this is true, the first-order estimate of the DJF Z_{500}-response relative to the forcing show that it is below 5 mK^{-1} of amplitude, making it quite weak compared to previous studies (see table 2.2). From this overview

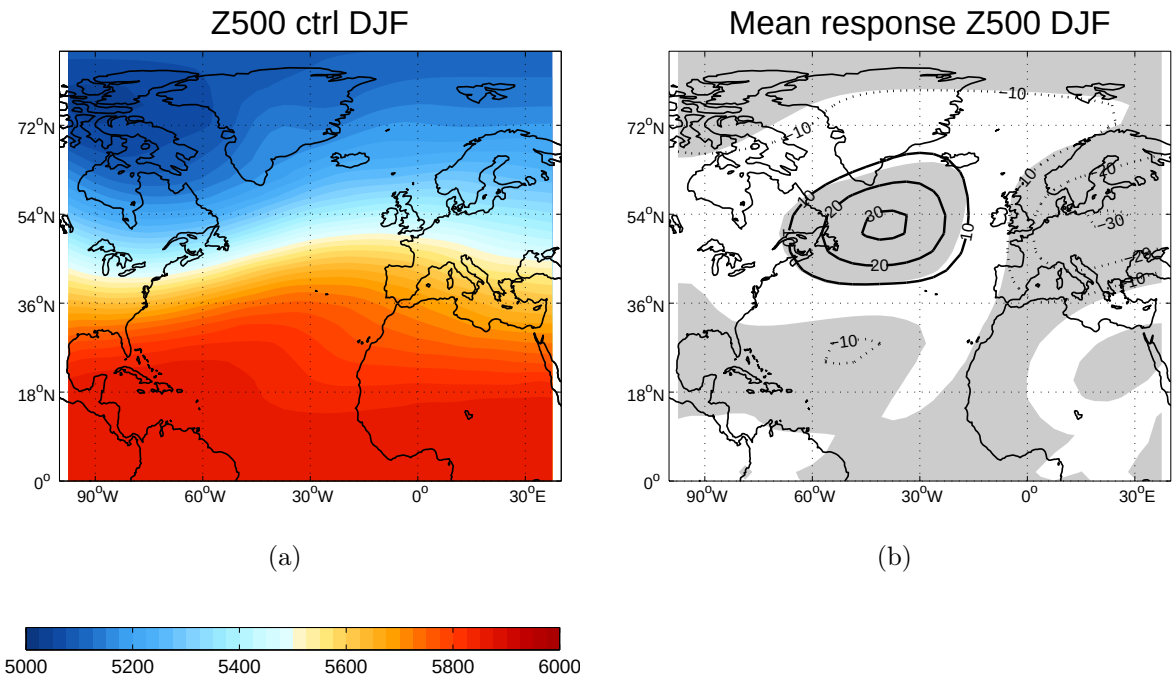

Figure 5.3: The mean winter Z_{500} in CTRL (a) and its response (b). Coloring and contour intervals are 25 and 10 m, respectively. Dotted (solid) contours in (b) correspond to negative (positive) values. The grey shaded areas are statistically significant at the 99 % confidence-level according to a two-tailed t-test.

most of the absolute values of the relative 500-hPa response were 3-4 times as large as the numbers found here.

Due to the large SST-perturbations in our experiment, one could hypothesize that the weak response is a result of an internal damping in the model environment. This could originate from the fact that the model is tuned to represent the atmospheric component of the climate system as closely to the observed as possible. It is to be emphasized that this hypothesis is hard to test for significance, especially when considering the diverse model results in earlier studies mentioned in table 2.2.

Considering now only the northern dipole or the midlatitude part of the forcing, it might also be an intriguing suggestion that SST-anomalies in these two branches together act to dampen the total mid-tropospheric response. However, when holding on to the argument that quasi-geostrophic motions act to balance shallow heating[2] and make use of linear considerations only, such a midlatitude forcing pattern should actually enhance, and not dampen, the mid-tropospheric response. This can be explained by the superposition of

[2]i.e. balanced partly by horizontal temperature advection as discussed in Section 2.3.1

the down- and upstream cores of relatively warm air associated with the western positive and eastern negative forcings, respectively (see Figure 2.3). This would lead to an overall increase in the strength of this atmospheric warm anomaly originating beneath the mid-level high, and consequently increasing the Z_{500}-response through the hypsometric relation (Equation 2.8). Alltogether, this reduces the possibility of explaining the weakness of this response in terms of the spatial structure of the SST-forcing pattern.

Having seen that tropical precipitation anomalies are induced, it might also be hypothesized that nonlocal features originating from the tropics are in some way influencing the midlatitude response.

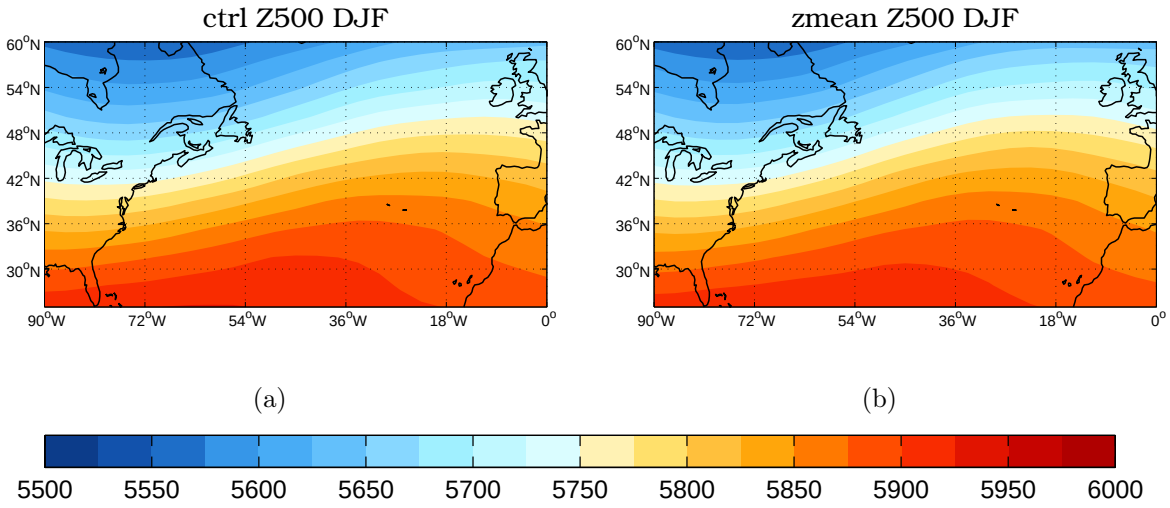

Figure 5.4: The winter Z_{500} field in CTRL (a) and ZMEAN (b). Color interval 25 m.

It might also give some insight to briefly investigate the background flow regime in the 500-hPa level more carefully. From the background fields of CTRL and ZMEAN (Figure 5.4), a westward shift of the 500-ridge above the central Atlantic can be identified in ZMEAN. As the response is weak, this feature is not very strong and thus hard to identify from the figure. However, the Z_{500}-response makes this wave pattern to be of slightly shorter wavelength above the North Atlantic where the signature of ocean currents are removed.

5.1.2 Summer

Investigating now the summer MSLP response of Figure 5.5(c), it can be seen that its pattern is different in most areas compared to the winter case. The winter-time positive

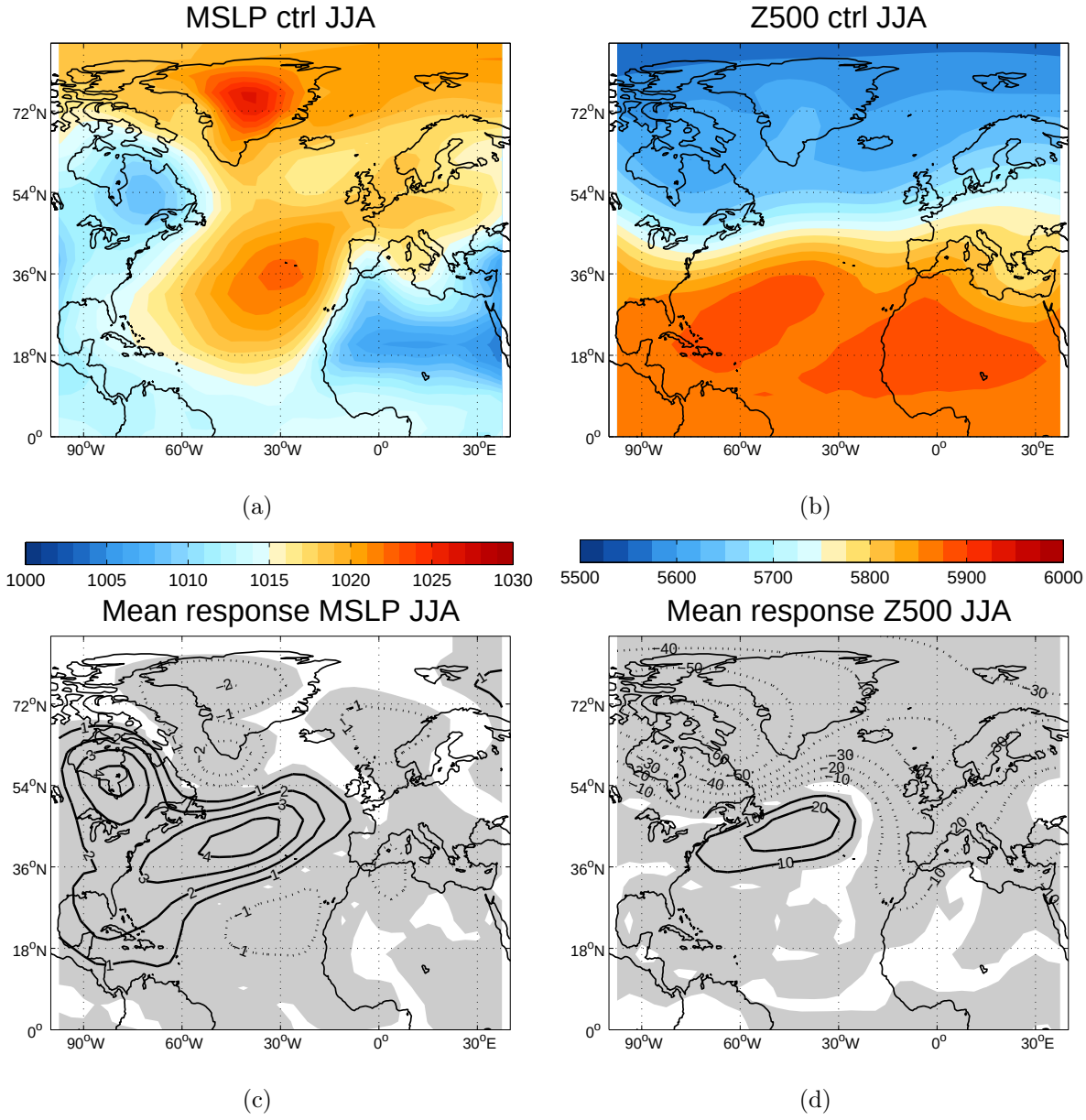

Figure 5.5: The mean summer fields of MSLP (a) and Z_{500} (b). Panels (c) and (d) show the mean summer response of MSLP and Z_{500}, respectively. Contour-intervals in (c) is 1hPa and $10m$ in (d). Dotted (solid) contours correspond to negative (positive) values. The grey shaded areas are statistically significant at the 99 % confidence-level according to a two-tailed t-test.

response west of the British Isles is in summer shifted toward the southwest, more or less retaining its amplitude. This pattern is a result of an intensification of the Atlantic subtropical high which in addition is displaced slightly northwest in ZMEAN. It should be noted that this response is not as spatially consistent with the forcing as was the case in winter, suggesting that this particular response is not generated directly by thermal effects.

A surface low situated in eastern Canada in CTRL appears as a weaker feature in ZMEAN with its center positioned somewhat further to the east. This is manifested in Figure 5.5(c) as the +4 hPa and -2 hPa responses in the southern Hudson Bay and Greenland. The weak negative perturbation in the Norwegian Sea is found to be associated with a strengthened Icelandic low combined with its northeast displacement while the response in central Greenland visualize the weakening of the long term high pressure system occurring there in CTRL. Concurrent with the winter response, the negative pressure perturbation west of North Africa is found also in summer, but in this season with a slightly larger amplitude. In the linear framework, this could be related directly to the relatively stronger positive forcing in this area during summer.

Also for the Z_{500}-response the situation is quite different in summer, a prominent change being the -60m response appearing west of Greenland. This lowering of the 500-hPa-surface is present in the entire North Atlantic region north of 50°N, with a secondary maximum (-40m) positioned in the southern Norwegian Sea with a trough-like extension as far south as Northwest Africa. As the negative forcing is smaller than 2.5 K in the vicinity of this secondary maximum, the relative strength of this response is approximately 15-20 mK^{-1}, which is more in accordance with that of table 2.2.

Compared to winter, the amplitude of the East Atlantic positive Z_{500} response is decreased by around 20% and shifted equatorwards. Furthermore, the position of this response is approximately positioned above the MSLP-response, such that the westward tilt of the response observed in winter is absent in summer. Also, the relatively similar shape suggest that only the strength of the geostrophic wind changes (and not direction) with height, indicating an equivalent barotropic response.

As the summer Z_{500}-field in the central and eastern Atlantic around 40°N is found to be relatively zonally oriented in CTRL (see Figure 5.6), the responses reflects an enhanced wave-pattern in the lower midlatitudes in ZMEAN. This is an interesting observation as one from a linear perspective might have expected that the introduced zonality of the SSTs in ZMEAN to be reflected in the atmospheric temperature, and hence, Z_{500}-field, therefore acting to induce an even more zonal flow. This mechanism is in contrast to that of the winter, where the stationary wave were found to have decreased their wavelength

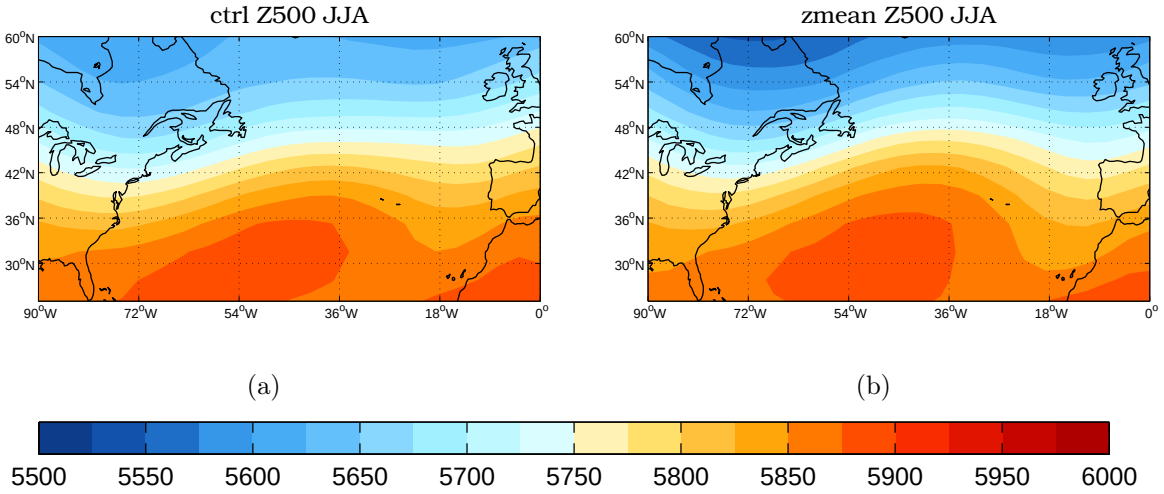

Figure 5.6: The summer Z_{500} field in CTRL (a) and ZMEAN (b). Color interval 25 m.

but retaining their amplitude.

It is seen from the forcing fields of figure 4.2 that, although weak, the SST-distribution near the equator is changed also in summer. Knowing that the ITCZ is generally positioned north of the equator during this season, it operates as a potentially direct pathway for the signals from the SST anomalies to be transported to the upper atmosphere. As one would expect, Figure 5.7 shows that the amplitude of the response in low latitude precipitation is larger in summer than in winter.

Also, a shift in sign of the response is seen compared to winter. Again referring to the forcing pattern, this is consistent with a direct relationship with the sign of forcing in the vicinity as the eastern tropical Atlantic is heated in this season. In addition, the overall tropical forcing amplitudes are generally larger in summer. This general linearity of the tropical response is therefore apparent both in summer and winter in the results.

Due to its relative weakness compared to winter, the summer storm track is not much studied in the literature. An overview of this topic, however, could be found in Mesquita et al. (2008). Under the assumptions that SPEEDY reproduces this summer track fairly well and that this precipitation response is related to the summer storm track, the storm activity is found to be weakened in the summer season. There are also indications of it being shifted northwards, as can be seen from the increase in precipitation south of Greenland.

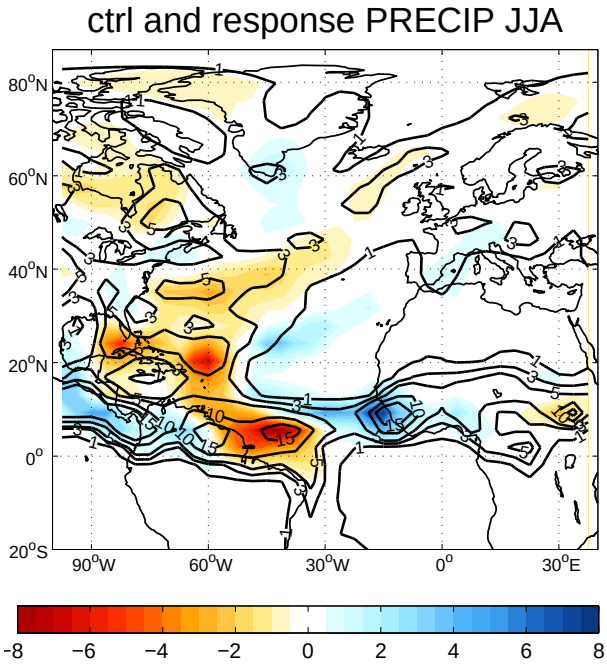

Figure 5.7: Shaded areas show the mean response of precipitation for the summer season, all being significant at the 99% confidence level according to a two-tailed t-test. The black contours show the models summer precipitation climatology taken from the seasonal mean of CTRL. *Units in mm/day.*

5.2 Response in near-surface winds and in the jet

For further clarification of the circulation response introduced in the previous subsection, the changes of wind at (near-)surface and (near-)jet (taken to be 300 hPa) levels are shown in figures 5.8 and 5.9. Here, also the background circulation regimes in the two seasons are shown. The figures include the entire hemisphere, enabling a brief investigation of potential circulation changes well outside the region of forcing.

As can be seen from figures 5.8(a) and 5.8(b) the model reproduces the observed distinct seasonal changes in the flow regimes. For example, can the monsoonal circulation of the Indian Ocean and the convergent tropical flow of the ITCZ during summer be detected. In the North Atlantic region there can be seen a change in the direction of the flow in eastern Canada between seasons. Also, one can identify the generally stronger midlatitude winds in the North Atlantic region during winter.

In terms of the wind fields, one can see that the subtropical high is more defined, although weaker, during summer compared to winter. Associated to this subtropical high, the modeled surface wind climatology in the region west of the African continent (a region of strong positive SST-forcing) is oriented more toward the south during summer. In addition to the local influence of the SST anomalies on the ITCZ mentioned earlier, this northerly wind could be an important feature for explaining the large increase in

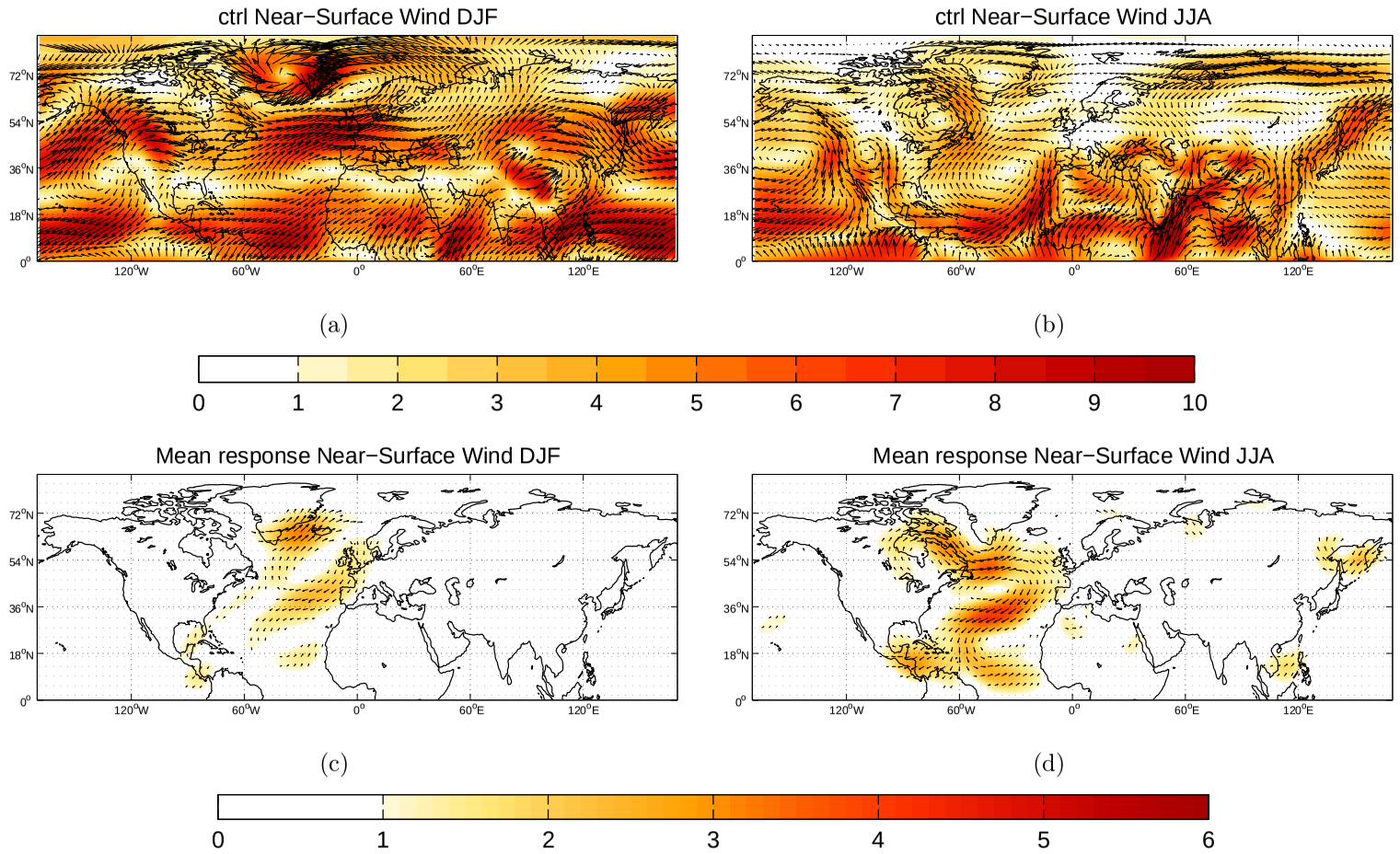

Figure 5.8: The mean near-surface wind fields in the control run for the winter (a) and summer (b). In (c) and (d) the response in these respective seasons are illustrated. Vectors denote wind-direction of winds, shading implies the absolute value of the wind speed. Only the responses where at least one of the wind components exceeds $|1m/s|$ are shown, all being statistically significant at the 95 %-confidence level.

summer precipitation in the eastern Atlantic. It can be argued that the potential increase in specific humidity in this area due to higher SSTs in ZMEAN is advected southwards by the background flow, and close to the convergence zone, increasing the potential for precipitation here. As the forcing is positive also south of the convergence zone, the same argument could be used to explain increased moisture convergence at the ITCZ. It is plausible that these advective effects of moisture play an important role in enhancing the positive precipitation response in area of the eastern Atlantic ITCZ, as the local SST-forcing in this area (see figure 4.2(b)) is reatively weak compared to the forcing north and south of the convergence zone.

When directly comparing the response of the wind in winter (Figure 5.8(c)) and summer (Figure 5.8(d)) the larger changes in the summer wind pattern in the tropical West Atlantic. This reflects the more widespread summer pressure response in this part of the basin, as seen in Figure 5.5(c). Also, a weakened southeasterly flow in the area of Labrador Sea is found during summer.

Figures 5.9(c) and 5.9(d) show the change in wind at the jet level (taken here to be 300 hPa), while figures 5.9(a) and 5.9(b) is the background circulation in CTRL, shown for reference.

For winter (Figure 5.9(c)) the midlatitude dipolar pattern of the Z_{500} response (Figure 5.3(b) is recognized as a reduction in cyclonic wind above the central North Atlantic and increased cyclonic circulation above Europe. Although weak, it can generally be seen that the westerly flow above North Africa and central Mediterranean gain a stronger southerly, or weaker northerly component. An upper level anomalous low situated about 50°W is identified, not so clearly visible from the Z_{500}-response.

For summer (Figure 5.9(d)) the most striking feature is the increase in the jet southwest of Greenland. This feature is consistent with the northwestward shift in precipitation and/or storm track. It also seems that the jet have a slightly larger northerly component in ZMEAN. Furthermore, some of the features from the winter jet-level response are recognized as an induced anticyclonic circulation in central North Atlantic, and cyclonic further south. The summer response is, however, stronger than for winter. This is particularly the case if comparing to the background flow, as the general strength of the upper-level winds is much stronger in winter due to the generally larger meridional temperature gradient in this season (Hartmann 1994). From the anticyclonic character of the response centered north of the Black Sea, one could also observe the inducement of upper-level waves.

In general it can be seen that upper-level winds are mostly affected in, or close to, the

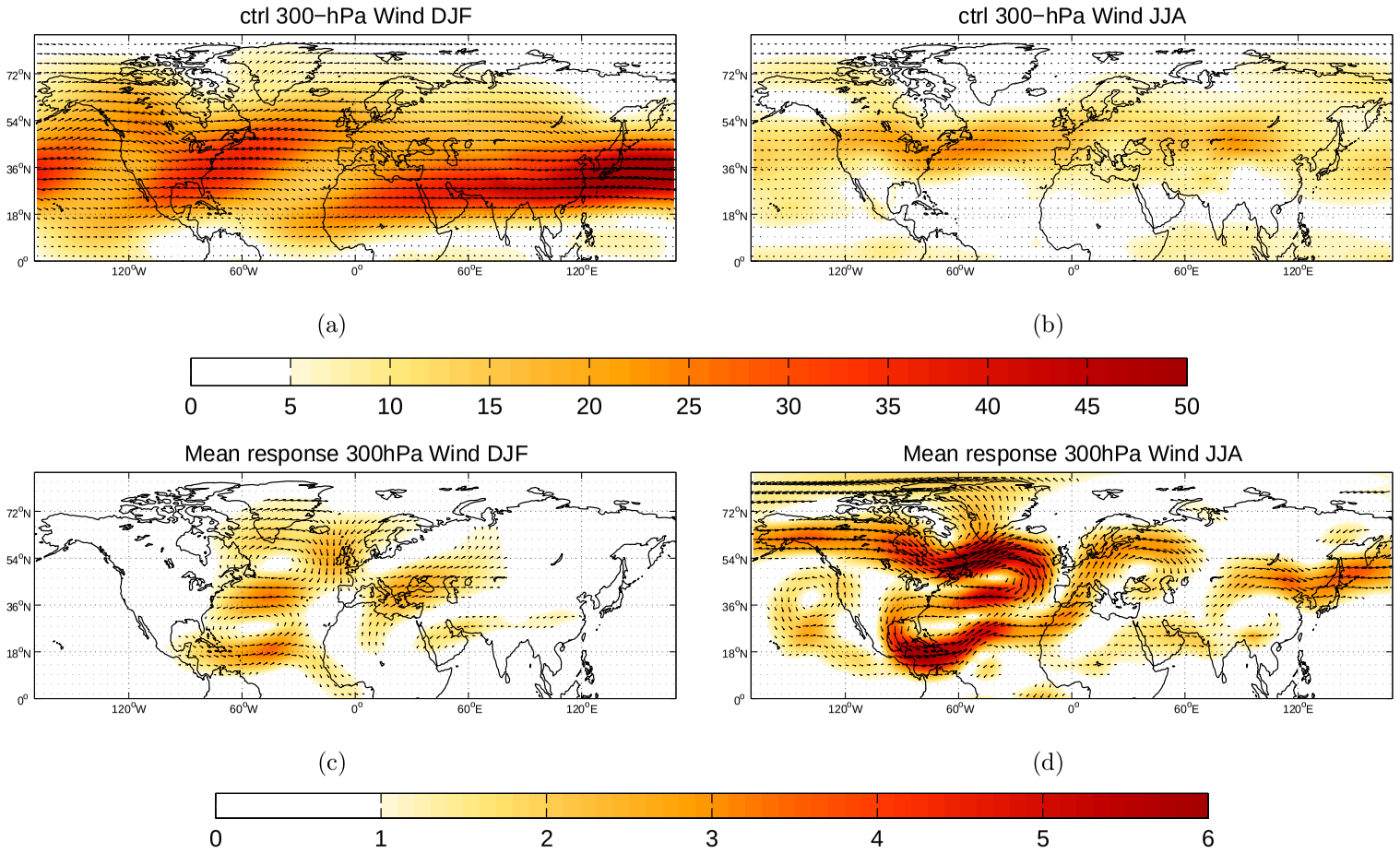

Figure 5.9: The mean near-jet wind fields in the control run for the winter (a) and summer (b). In (c) and (d) the response in these respective seasons are illustrated. Vectors denote wind-direction of winds, shading implies the absolute value of the wind speed. Only the responses where at least one of the wind components exceeds $|1m/s|$ are shown, all being statistically significant at the 95 %-confidence level.

regions of SST-forcing although a stronger and more hemispheric scale of the response is observed during summer season.

5.3 Temperature

It is of interest to see how the temperature anomalies from the SST-forcing are transported up in the atmosphere by the model. In this subsection, the spatial characteristics of the atmospheric temperature response in two different layers are presented. In addition investigate longitude-height cross-sections are investigated in order to examine the vertical signature of the response.

5.3.1 Spatial signature

The atmospheric temperature response in the two intermediate levels of 850 and 700 hPa is illustrated in Figure 5.10. Consistent with the findings discussed earlier, there can be found a seasonal dependence of the response.

Positioned closely to the imposed positive SST-anomalies in the northwestern Atlantic, Figure 5.10(a) shows a region of increased air temperature at 850 hPa with a maximum of about 3.5 K in the eastern parts of Greenland. This pattern is also manifested at the 700 hPa-level in Figure 5.10(b), although with a decreased strength. A cooling occurring above western parts of Europe and the Caribbean Islands can also be seen. For the winter response it can in general be said that the atmospheric temperature response resembles the SST-forcing field geographically. It is also evident that the signal decreases with height.

Based on what already have been established regarding the Z_{500} response in summer, a general cooling is expected north of ~ 50 °N as is shown in figures 5.10(c) and 5.10(d). In the midlatitudes, the signature of the strong West Atlantic positive forcing, seen in figure 4.2(b), is completely absent in the 700 hPa response field. Off the west-coast of Africa a positive response (around 1.5 K) is found at 850 hPa, with a reversed sign at 700 hPa.

For both seasons, the temperature response close to the surface (not shown) is found to be of smaller amplitude compared to the magnitude of the imposed SST-forcing, which is consistent with previous studies, as discussed in Kushnir et al. (2002).

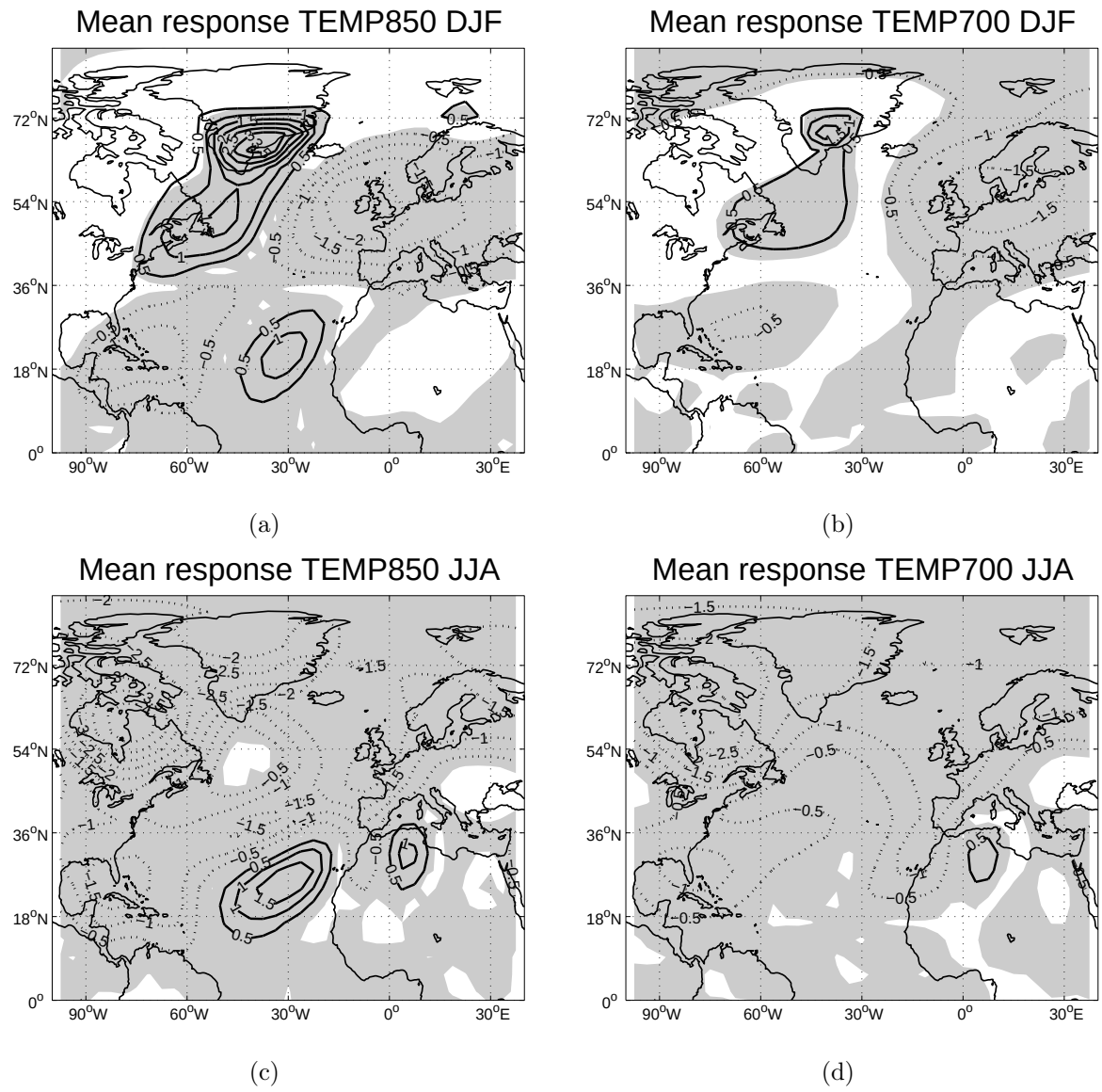

Figure 5.10: The mean response of temperature in winter (a-b) and summer (c-d) for the 850 hPa (left) and 700 hPa (right) levels. Solid contours correspond to a positive response, with the dotted indicating temperatures lower in ZMEAN than CTRL. *Contour intervals are 0.5 K*. The grey shaded areas are statistically significant at the 99 % confidence-level according to a two-tailed t-test.

5.3.2 Vertical signature

The cross-sections of Figure 5.11 show longitude-height diagrams of the temperature response in the two seasons. Considering first the subtropics, the response appears quite

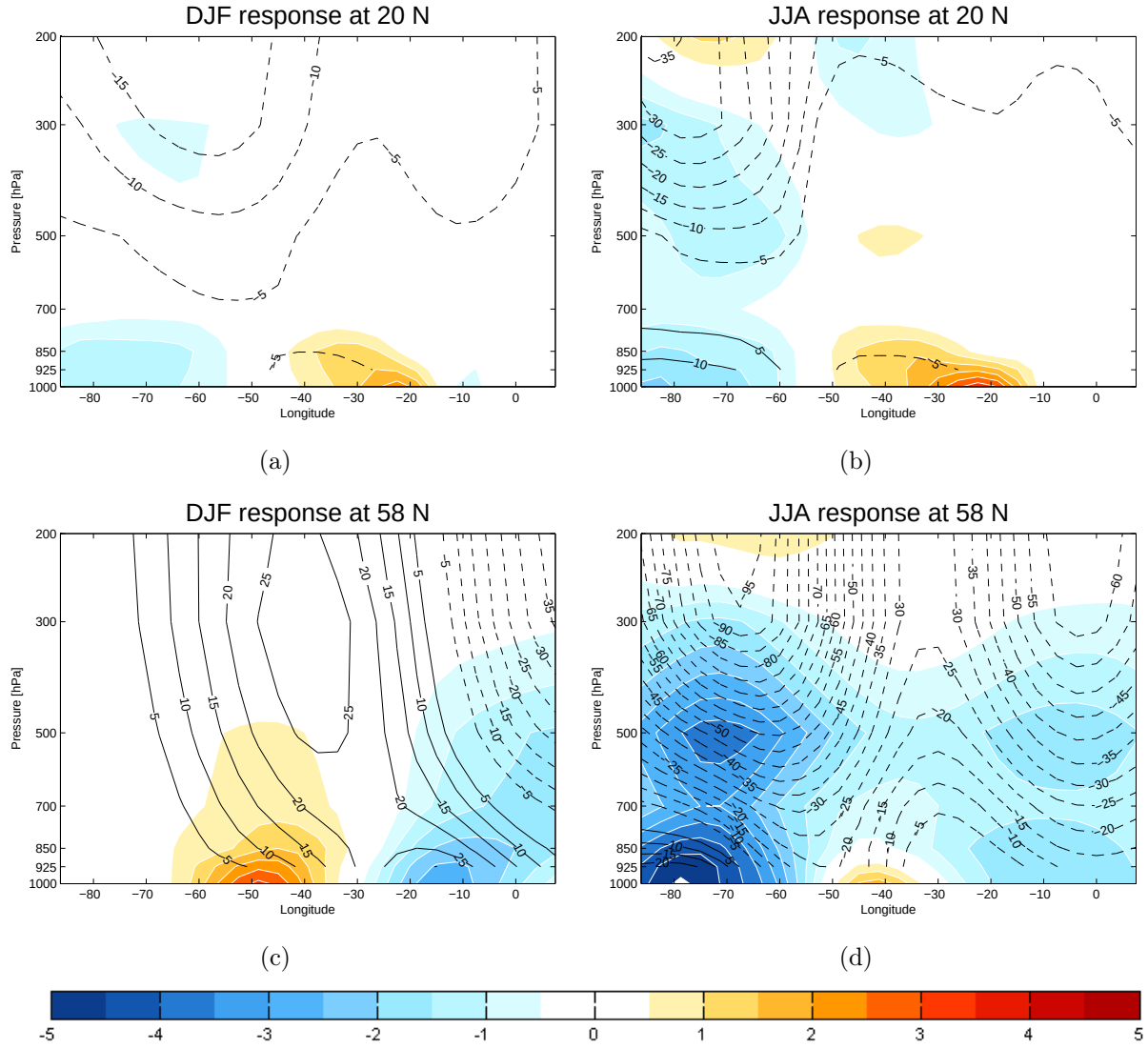

Figure 5.11: The longitude-height mean response of temperature (shaded) and geopotential height (contours, solid (dashed) denote positive (negative) values) in a longitude-height cross-section. Panels (a-b) show the response at 20° N, while panels (c-d) illustrating the response at 58° N. Winter season is shown to the left, summer to the right. Color interval is 0.5 K for temperature. Contour interval for geopotential height response is 5 gph meters with dashed contours marking negative values.

similar between seasons below the 700 hPa-level (figures 5.11(a) and 5.11(b)). Above this level in summer, a negative temperature response is found west of 60°W which might be related to the decreased rainfall (and thus less release of latent heat) here. The temperature response to found to be quite shallow in both seasons.

In the midlatitudes at 58° N (figures 5.11(c) and 5.11(d)) a westward tilt of the geopotential height response is identified in winter. This indicates a change in the direction of the geostrophic wind with height, hence a baroclinic response. This tilt is not as pronounced in summer, suggesting that the response in this season is more of a equivalent barotropic nature. In addition is the relatively larger temperature perturbation in summer, especially at surface and 500 hPa, resulting in the geopotential height response to be deeper in this season, with amplitudes at the 300 hPa level reaching -90 m and -60 m at longitudes of 70° W and 0 ° E.

5.4 Sea-surface heat fluxes

Being the connection between the surface and the above lying air, the changes of sea-surface heat flux is the carrier of the signals that eventually alter the atmospheric state. It is therefore of interest to investigate the changes of this between CTRL and ZMEAN, and this is treated in the present section. The term 'heat-flux' is here associated with the sum of sensible (SHF) and latent (LHF) heat fluxes as well as the contributions from short- and longwave radiation.

In the model, SHF is proportional to the differences in temperature, $T_{sa} - T_{sea}$, and the effective wind calculated as $|V_0| = (U_{sa}^2 + V_{sa}^2 + V_{gust}^2)^{1/2}$, where V_{gust} is a constant representing unresolved wind variability (Kucharski 2007). The subscripts $_{sea}$ and $_{sa}$ denote sea surface and (near-)surface air, respectively. The LHF is also proportional to $|V_0|$ as well as to $min[q_{sa} - q^{sat}(T_{sea}, p_s), 0])$ where ^{sat} denote saturation. Thus, the heat flux associated with latent heat is defined as non-positive meaning that the ocean surface is unable to gain heat from the atmosphere through condensation.

Bearing in mind how this sea-surface heat flux is treated in the model environment, it is apparent that the changes in it constitute a response of the system, and not a direct forcing, as its calculation is dependent on changes in both wind, temperature, and humidity. However, it will be shown that the relationship between the forcing and the heat flux response is quite strong.

Figure 5.12 show the CTRL sea-surface heat fluxes for reference. As can be seen for the winter case, the thermal inertia of the ocean mixed layer provide heating of the above-lying air, hence a net heat loss of the ocean surface. Thus, blue shading indicate ocean heat loss to the atmosphere. In summer, this is reversed as the ocean receive heat from the atmosphere, visualized as red shaded areas.

In Figure 5.13 the response in the flux is presented. Considering first the winter response,

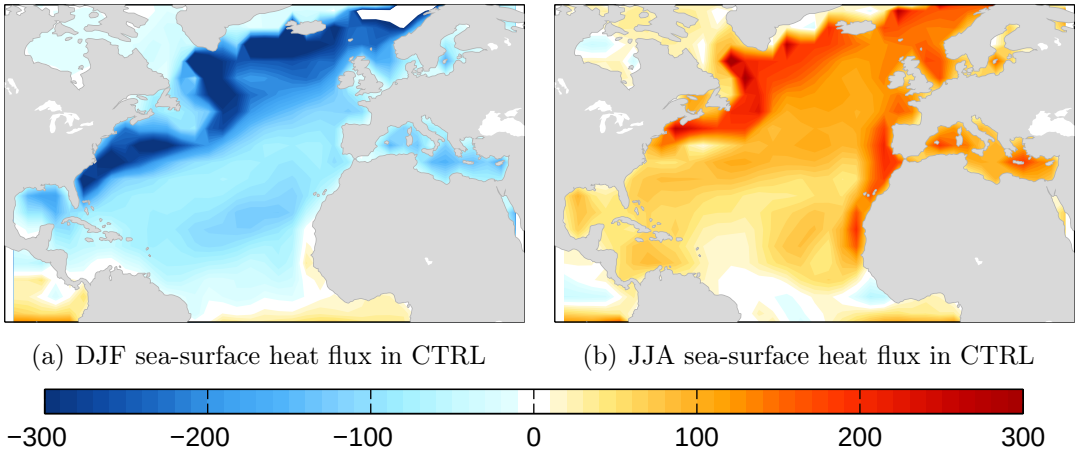

(a) DJF sea-surface heat flux in CTRL (b) JJA sea-surface heat flux in CTRL

Figure 5.12: Sea-surface total heat flux in CTRL for winter (left) and summer (right). Blue shading correspond to net heat loss of the ocean surface, where red represent heat input to the sea-surface. Sea-surface heat fluxes below $|10|$ Wm^{-2} are colored white.

it is evident that the sea-surface heat flux as defined here is negatively correlated with the SST-forcing in most areas. In a coupled system, this would act to dampen the sea-surface anomalies, consistent with the evaluation of Kushnir et al. (2002) concerning earlier GCM-studies[3]. However, this relationship is not directly linear in all areas, as especially can be seen just east of the the zero-forcing line east of New Foundland. Here the forcing is around -2K, but the heat flux response is still of larger amplitude than further east where the forcing is of the order -4.5K. An explanation for this could be as follows:

In a relative manner, the strong zonal gradient of the forcing (positive forcing to the west, negative to the east) tend to heat(cool) the near-surface air west(east) of the zero-forcing line. Remembering from Figure 5.8(a) that the governing flow here is westerly, it is possible for this temperature signal to be advected downstream. Hence, the air entering the area of negative forcing will have a relatively higher temperature, increasing the air-sea temperature difference here. Consequently, this would be reflected as a localized response in the heat flux, slightly downstream of the forcing gradient as observed in Figure 5.13(a).

Moving now on to the summer response, the argument of advective effects can also be used to explain the shape of the heat flux response pattern west of Spain in Figure 5.13. As can be seen, also here the heat flux response is greater (forcing of around +2K) than is the case further south where the forcing is around twice as strong. Since the background

[3]To again visualize the complexity of the fully coupled climate system, it was discussed in Section 2.5.2 that observed SST-anomalies (on the shorter timescales) actually are created from anomalies in the heat flux, induced for example by synoptic weather systems and anomalous wind fields. This would in reality make it hard to distinguish cause and effects from such heat-flux fields.

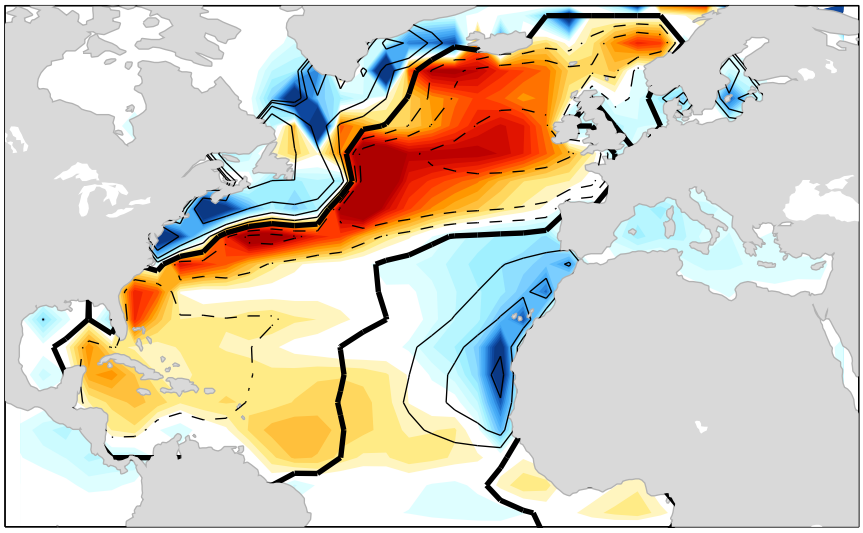

(a) Response in DJF sea-surface heat flux

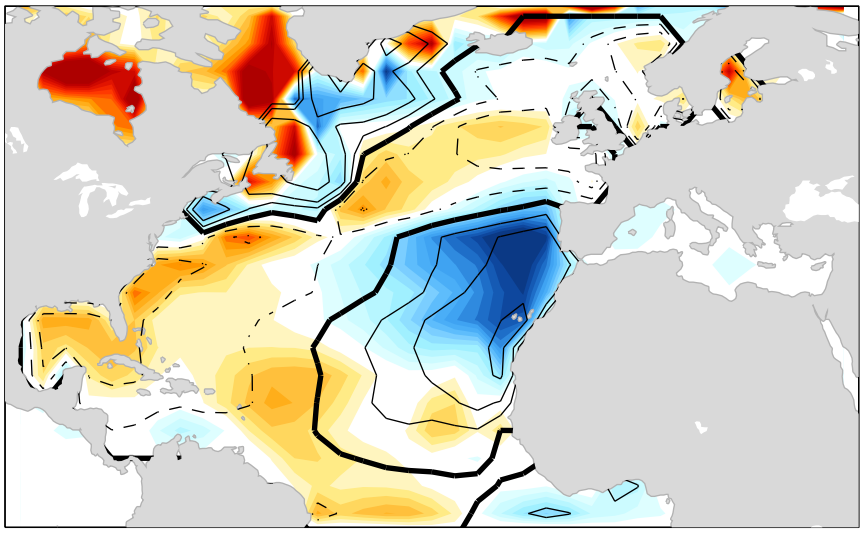

(b) Response in JJA sea-surface heat flux

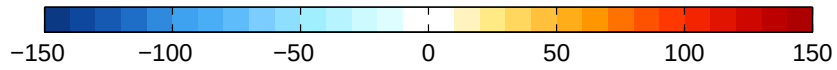

Figure 5.13: Changes in the total heat flux at sea-surface in winter (upper) and summer (lower). Note that the flux are defined as downward. Therefore, blue shading indicate transport of heat from the ocean to the atmosphere (hence a oceanic heat loss). Red shading indicate a heat flux tending to warm the ocean surface. Reponses less than $|10|Wm^{-2}$ are colored white. Solid (dashed) contours denote the positive (negative) SST-forcing. Here, contours are drawn for values of ± 1,± 2,± 4 and ± 8 K with the thick contour visualizing the line of zero forcing.

flow here is from the north, the air which is cooled north of the zero-forcing line will, as it moves southward, eventually come over ocean surface forced to be warmer. Hence, the local air-sea temperature gradient again increases, resulting in the ocean feeding the atmosphere with heat.

Note especially the slightly larger heat flux response close to the equatorial areas in summer than in winter. It is plausible that this effect acts to feed the enhanced tropical precipitation response in summer, again reflecting the direct linear relationship between tropical SST-forcing and precipitation.

The heat flux response in Hudson Bay

Even though well outside the region of forcing, there is a quite drastic change in the heat flux between ZMEAN and CTRL in the area of the Hudson Bay and Labrador Sea during summer. It was found in Section 5.3 that the air temperature here was decreased substantially. In our framework where SSTs are prescribed, and hence constant, a negative heat-flux response is therefore to be expected (i.e. a tendency of the air to be heated by the ocean). However, the sign of this response is reversed with the ocean actually tending to cool the above air, which already is occurring as colder in ZMEAN than in CTRL. Consequently, if the boundary conditions really are constant here, it is not possible to explain this particular heat-flux response by means of the temperature response itself.

In order to explain this inconsistency, one might have to take into account the possibility of a model error, or rather the sensitivity of some of the parameterizations calculating the surface flux. More specifically, it is hypothesized that this response could be caused by the sensitivity of the thermodynamic sea-ice model incorporated to SPEEDY.

From Figure 5.8(b) it could be seen that the wind field of CTRL was cyclonic around a centre situated slightly west of New Foundland. Although this circulation is weakened in ZMEAN (Figure 5.8(d)) the mean circulation is still found to be cyclonic in this region. Therefore, the temperature signal from the positive forcing east and northeast of New Foundland is potentially enabled to be transported with the flow north- and westwards, eventually reaching an area where (fractional) sea-ice cover is present. The summer sea-ice cover used in the model integrations is shown in Figure 5.14 for reference.

Where presence of sea-ice is specified (fractional or total), a thermodynamic sea-ice model described in Kucharski (2007) is triggered in order to calculate the surface energy balance. The sea-surface heat fluxes of Figure 5.13 depend on this calculation, and could therefore be altered if the sea-ice model is sensitive to temperature perturbations or to the radiation scheme used to calculate the balance.

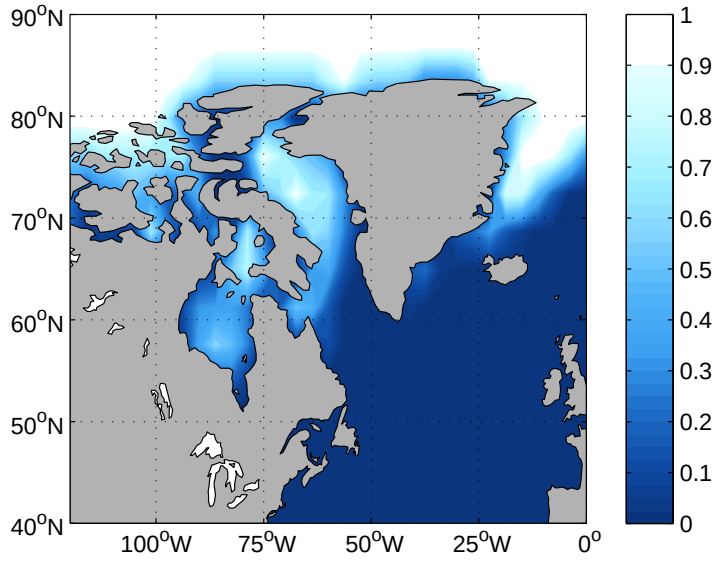

Figure 5.14: Sea-ice cover in boreal summer used as input to SPEEDY. White color indicate sea-ice cover larger than 0.9. Data from Gibson et al. (1997).

It is to be mentioned that if the above argumentation really holds, it might also account for (at least parts of) the positive pressure perturbation in the Hudson Bay in Figure 5.5(c). Therefore, the rest of this thesis will not focus more on this particular region when discussing the atmospheric responses. As the employed SST-forcing is strong, it is assumed that this eventual error have local impacts, only, and that the summer response inside the forcing region (or outside areas covered with sea-ice) still reflect representative circulation changes to the zonally averaged SSTs.

Chapter 6

Response in variability

As have been introduced in sections 2.4.2 and 2.5 it is to be expected that the decadal atmospheric variability should be affected in the absence of ocean circulation. However, in our case such a hypothesis would be hard to test as our model purely represent the atmospheric component of the climate system, therefore not including the complete feedback process schematically shown in Figure 2.8. Nonetheless, it is assumed that the model is capable of producing a representative atmospheric equilibrium response to the realization of no ocean circulation. The shift in variance dealt with here is thus directly connected to the typical SST-pattern in the case of no oceanic circulation. Therefore, it might provide clues of additional low frequency feedbacks intrinsic in the atmosphere to that given in Figure 2.8 in Section 2.5.2.

Firstly, an investigation of the changes in the local variability of the fields of MSLP and Z_{500} at different timescales are performed. The procedure for doing this is to calculate a response matrix on the form $R(x,y) = \frac{var_{ZMEAN}(x,y)}{var_{CTRL}(x,y)}$ from the timeseries consisting of seasonal data from the two different runs. For instance, in the winter case the variance of a variable X is computed in each grid point as:

$$var_{djf}(x,y) = \frac{1}{N}\sum_{t=1}^{N}(X_t^{djf}(x,y) - \overline{X}^{djf}(x,y))^2$$

where $\overline{X}^{djf}$(x,y) is the model's winter climatology and N is the number of seasons.

To investigate the variability changes on the decadal time scales, a running mean filter of 11 years was applied to the time series prior to the calculation of the variances in order to dampen fluctuations on the shorter time scales[1]. It is to be noted that the resulting decadal variance ratio is not tested for significance, as the timeseries (pr. definition)

[1]For this purpose, also a block-averaging approach was performed (i.e. where variances are computed from 10 year block averages, rather than a running mean). This proved not to be a robust method, and is therefore not included.

will be autocorrelated. This act to alter the degrees of freedom (DOF) which is required when calculating the statistical significance.

Some notes are to be mentioned here before looking at the responses. Firstly, in summer, the observed (and modeled) atmospheric variability of the northern hemisphere is generally weaker than is the case for winter. When attributing fractions to describe the change in variability, this fact might yield misleading conclusions as a small absolute change in variance could turn out as a large response. The same could apply for the method of obtaining the decadal variability, as the running mean procedure also act to decrease the variance of the timeseries. However, this method of visualizing the response is applied as it is found to be the most consistent and direct way of investigating the variability changes.

Secondly, if looking into the distribution of the global variance response fields, one would find that it has a quite chaotic nature, but with a tendency of the decadal variability to show a response of larger amplitude than what is found on the annual timescale. However, several aberrations from this is found which is thought to merely reflect the nature of the atmosphere. Therefore, the focus here is more on the local response in variability.

6.1 Mean Sea-Level Pressure

Figure 6.1 show the variance response in the MSLP-field. In winter, the significant variance response on annual timescale seems to reflect somewhat the SST-forcing pattern, where induced negative (positive) SST-anomalies tend to decrease (increase) the annual variability and vice-versa. On the decadal timescale the amplitudes are generally larger, with most of the subpolar Atlantic experiencing decreased variability. In parts of the European continent, however, one could identify the decadal variability in ZMEAN to be enhanced compared to CTRL.

Also the annual summer MSLP variability change is found to coincide with the sign of the forcing in many areas. On the longer timescale however, there is a distinct tendency of the North Atlantic variability to be decreased. In the subtropics south of 40 °N the amplitude of the response is found to be quite insensitive to the time-scale whereas further north there is a marked increased amplitude at low frequency variability. An aberration from this general picture of decreased variability is found west of Greenland where it is increased by around 50%.

6.1.1 Low-frequency variability of the Icelandic Low

In order to gain some insight in how the time-evolution of the circulation looks like, a brief investigation of the winter-time Icelandic Low (IL) in the two model runs is performed.

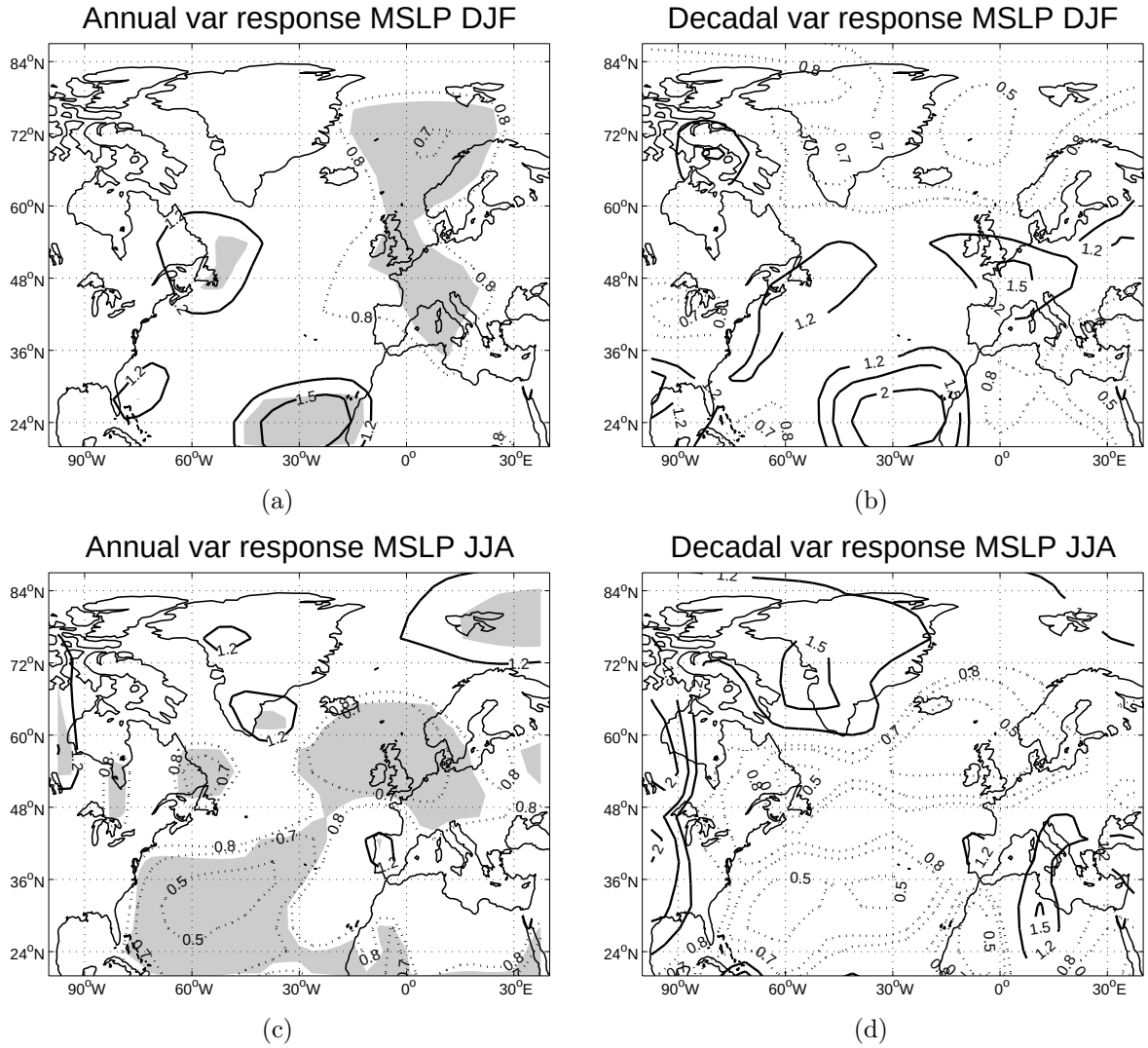

Figure 6.1: The fractional change in MSLP variance in winter (a,b) and summer (c,d) at the annual (a,c) and decadal (b,d) timescale. Values greater than 1 indicate more local variance in ZMEAN than is the case in CTRL. Shaded area on the annual time-scale are statistically significant at the 95% level according to a two-tailed F-test. Nondimensional units for fractional change.

The timeseries of the IL intensity in CTRL (ZMEAN) is shown in the upper (lower) panel of Figure 6.2. The timeseries are computed by extracting the minimum value of MSLP inside the box [50°N - 70°N, 30°W - 10°E] from the season timeseries and thereafter compute their detrended timeseries. Hence, also the position of the IL is captured, enabling an investigation also of the spatial variability of this prominent circulation feature.

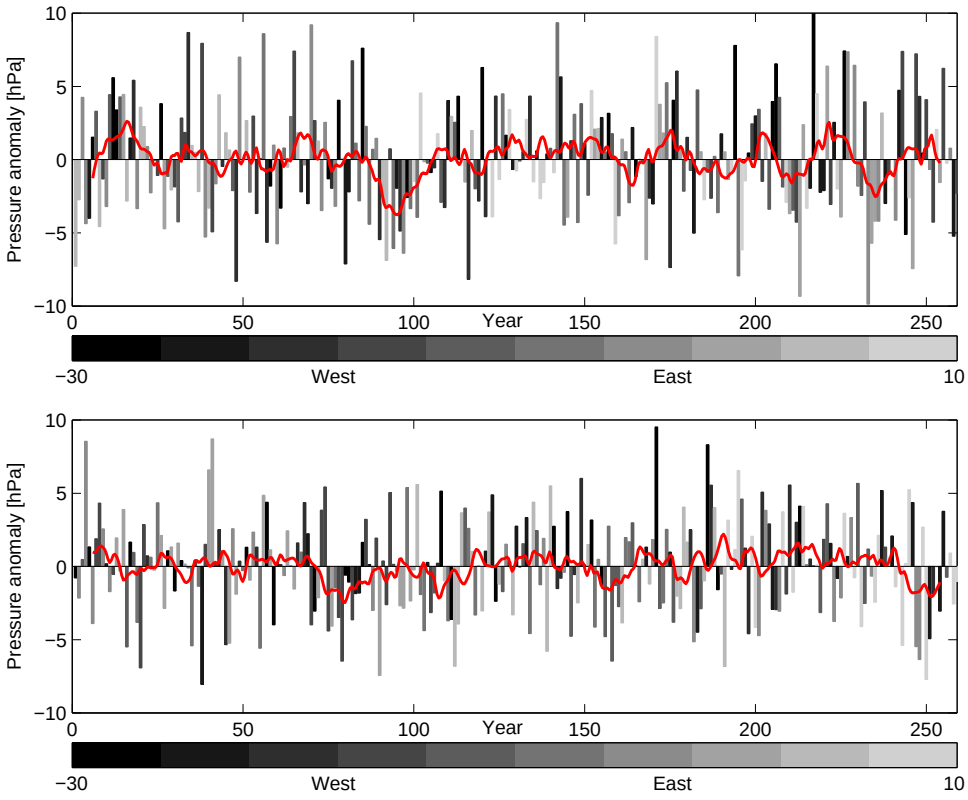

Figure 6.2: Time evolution of the Icelandic Low in CTRL (upper panel) and ZMEAN (lower panel). The y-axis denote the IL pressure anomaly, where negative values indicate a IL-center pressure lower than normal (defined here as the climatological value of the minimum inside the box [50°N-70°N, 30°W-10°E]. The coloring of the bars show the longitudinal position of the low, with darker shading indicating a more western position of the low centre. Red curve is a 11-year running mean of the timeseries. Units in hPa.

Although not very clear, one could identify the variability in CTRL to be of larger amplitude than in ZMEAN. The annual and decadal variance fractions[2] in numbers are 0.71 and 0.60, respectively. This shows that both annual and low frequency variability of the Icelandic Low are less prominent in ZMEAN. It is hard from this picture to state a distinct relationship between the longitudinal position and IL-strength. Such a relation was neither found directly for the latitudinal position of the IL.

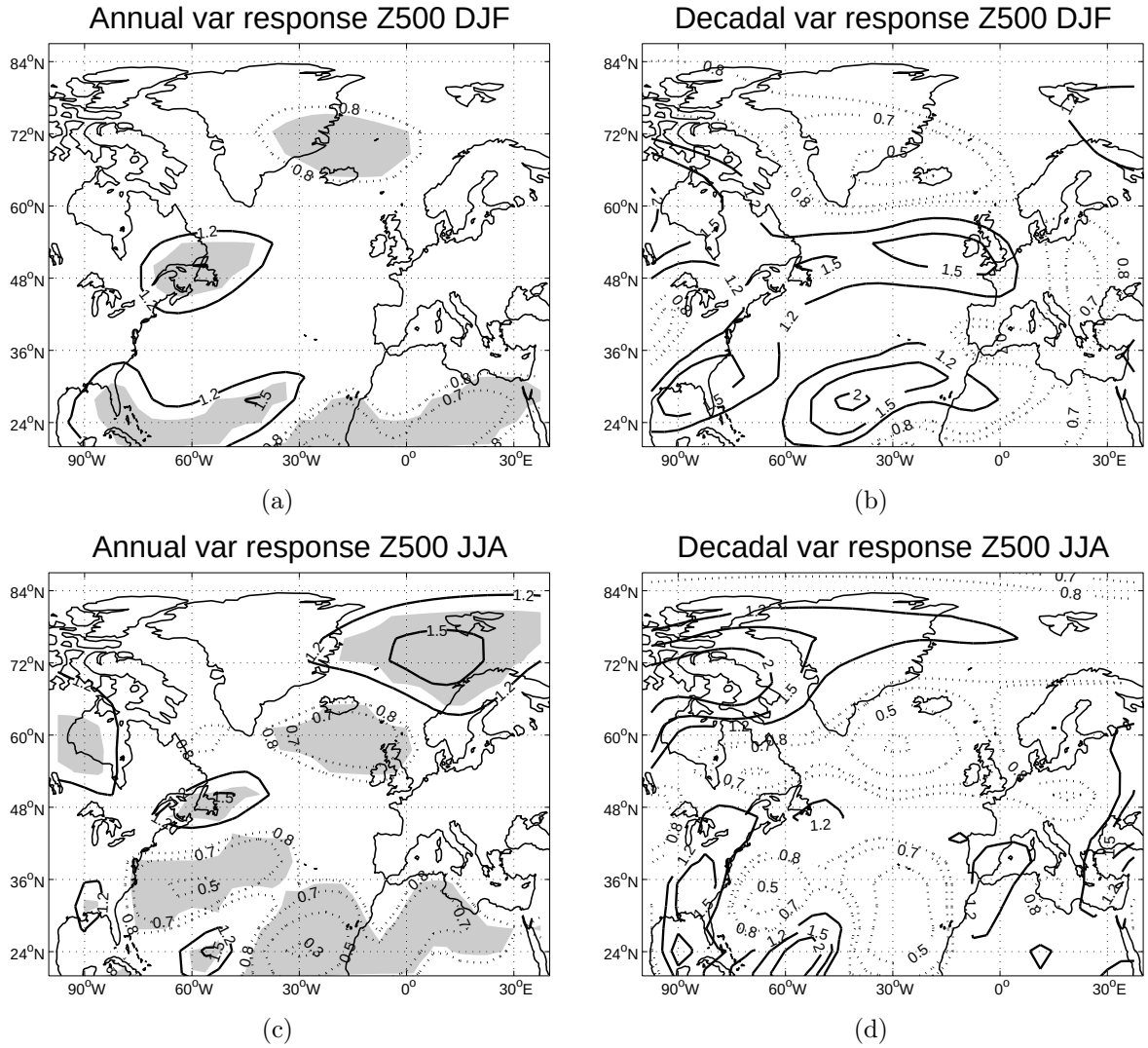

Figure 6.3: The fractional change in Z_{500} variance in winter (a,b) and summer (c,d) at the annual (a,c) and decadal (b,d) timescale. Shaded area on the annual time-scale are statistically significant at the 95% level according to a two-tailed F-test. Nondimensional units for fractional change.

6.2 Geopotential height

Figure 6.3 reveals that the annual winter variability of the 500 hPa height only experience small changes. South of 50° N the low frequency variability of the atmosphere is generally enhanced. Again, the summer annual variance response show generally larger amplitudes

[2]Calculated as explained in beginning of the chapter

than in winter. Moreover, the decreased decadal variability is apparent through most of the North Atlantic basin, which is adding some confidence to the related response in the MSLP-field.

6.3 Changes in the large-scale variability patterns

In this section focus is on the changes in the statistics of the atmospheric internal variability modes. This is done by the decomposition of the data into variability patterns, as described in Section 3.2. The present section concentrates the analysis on MSLP-data and limits it to include the variability patterns resembling the NAO and EA only, as these are the most robust patterns found to explain most of the total variance. In addition, these are the ones found to be the potentially important patterns concerning ocean circulation as depicted in Section 2.4.

Figure 6.4 show the spatial characteristics of the EOFs. We identify the winter-time NAO- and EAP-like patterns (Figures 6.4(a) and 6.4(b)) to be the two patterns explaining most of the variance as also was found from the observational data in Figure 2.6. In summer however, the EOF resembling the EA-pattern is actually the 3^{rd}, and not the 2^{nd} EOF as one would expect from observations. This occurs as a consequence of not subtracting the trend from the timeseries consisting of data from both CTRL and ZMEAN with the result that the 2^{nd} EOF resembles the response pattern itself. In the case where the overall trend is subtracted, indeed the EOF resembling the EA-pattern is the 2^{nd}, spatially consistent to that of Figure 6.4(d). In particular, the large response south of Hudson Bay contributes to this artifact of the 2^{nd} EOF. Therefore, we treat the JJA EOF3 as the EA-pattern.

Even though a limitation of the method to compute the EOFs already have been discussed, the procedure nonetheless provides a compact way of presenting the changes in the statistics of the variability patterns given that their spatial characteristics are robust. In Figure 6.5 the temporal evolution of each spatial patterns is given. The general picture emerges that the NAO is the pattern most affected during summer, as the EA is the pattern most changed during winter. It could be argued that this reveals a seasonal dependence of the atmospheric response to North Atlantic ocean circulation.

Our results show the NAO-index to be significantly increased both in the winter and summer seasons. Under the assumption that the models primary internal variability pattern, taken here to be the NAO, really is reflecting the strength of the Atlantic midlatitude westerlies, this result is in accordance with the Bjerknes' theory of the compensational effects between the atmospheric and oceanic components of the heat transport. Bjerknes (1964) hypothesized, as also is mentioned in Section 2.5.2, that the total meridional heat

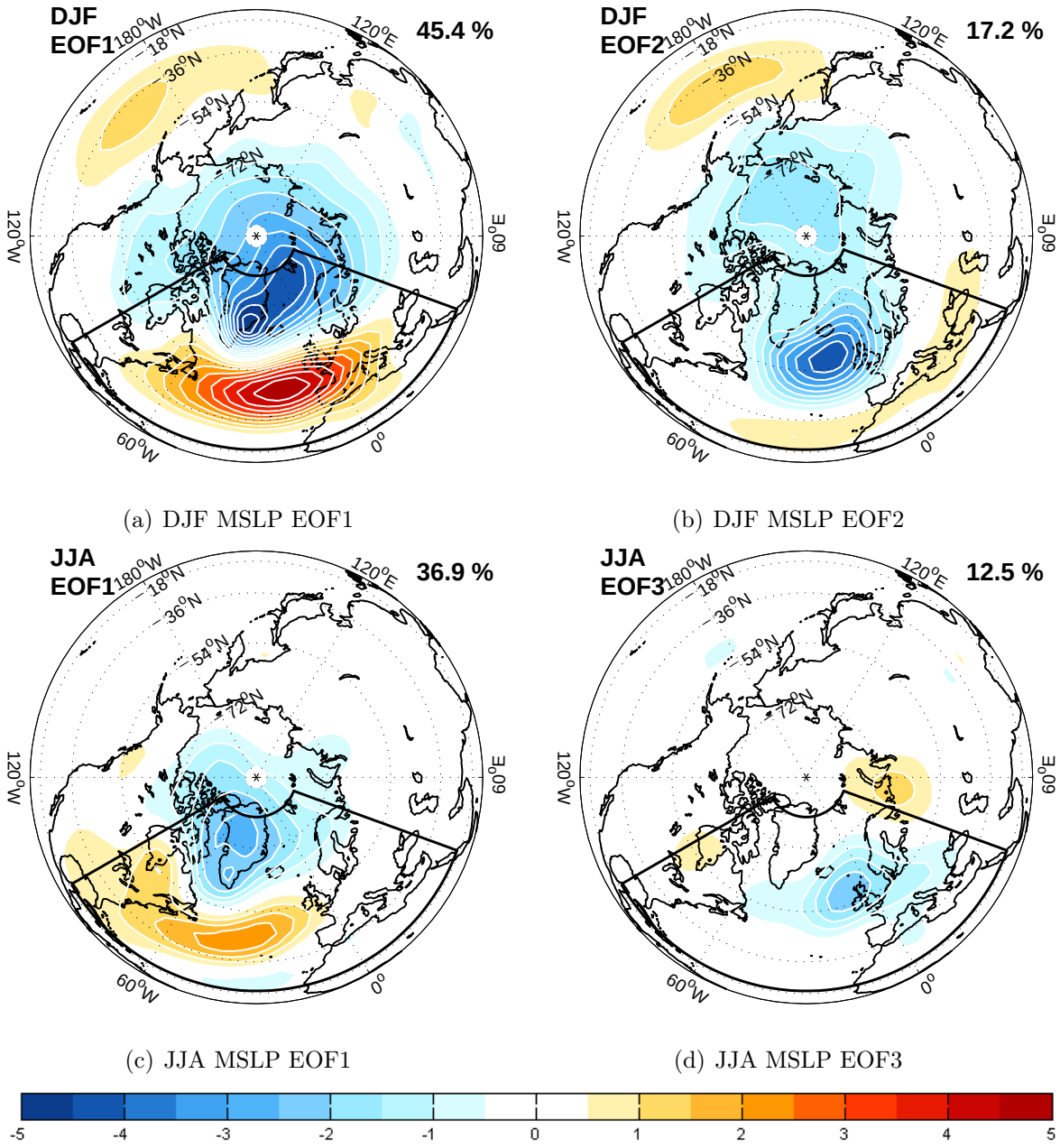

(a) DJF MSLP EOF1

(b) DJF MSLP EOF2

(c) JJA MSLP EOF1

(d) JJA MSLP EOF3

Figure 6.4: Spatial characteristics of the EOFs for winter (upper panel) and summer(lower panel). The amplitude represents hPa pr. standard deviation in their corresponding PC-timeseries. Contour intervals of 0.5 hPa, where amplitudes less than $|0.5|hPa$ shaded white.

transport consisted of opposite fluctuations of its oceanic and atmospheric parts. However, as this is a coupled interaction it would be misleading to make this conclusion based on an idealized and uncoupled model run.

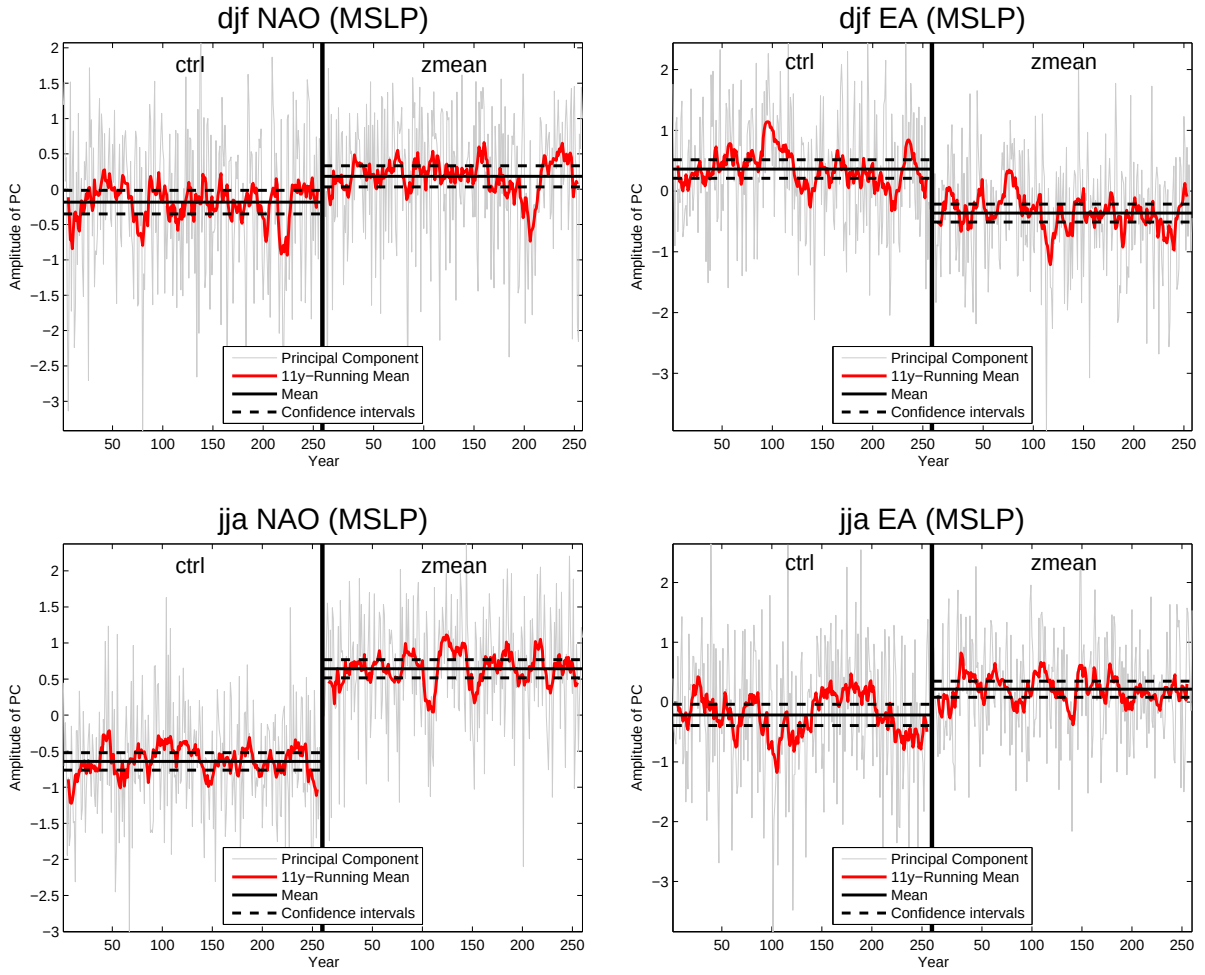

Figure 6.5: Timeseries of the winter (upper) and summer (lower) indices. Left panels illustrate the NAO-index, with the EA-index to the right. Each panel show the index of the CTRL to the left and that of ZMEAN to the right. The grey curves are the unfiltered timeseries with the red curves being a 11-year running mean of the corresponding index. The horizontal solid lines are the mean of the index in the two different runs with the dashed lines being 99% confidence intervals. The vertical axis denote the number of standard-deviations from the total mean of the index.

Given the significant positive NAO response in both summer and winter, it is hard to conclude with the North Atlantic storm track being weakened in the absence of North Atlantic ocean circulation. Under the assumption that the model is able to reproduce the relationship between NAO and the storm track, this could be argued from figure 2.5 regarding the climatic impacts of a positive phase of the NAO. As the mean index

is increased in ZMEAN, this would rather draw the picture of the storm track to be strengthened. The positive NAO response is therefore adding confidence to the precipitation response (and East Atlantic high pressure response) being of a more local character, rather than reflecting a shift in the storm track.

Tables 6.1 and 6.2 show the statistics of the indices describing the temporal evolution of the corresponding spatial pattern. We observe that the temporal mean of all PCs are significantly changed in all seasons, illustrated by the zero p-value.

Both the annual and decadal variance fractions of the indices in the two different model runs are calculated as explained in Section 6.1. The only significant (at the 95%-confidence level) signal found is the decreased year-to year fluctuations in the summer EAP. We also note that this is an even more pronounced feature on the longer timescale. This might be directly related to the shift in summer MSLP variability, as the center of prominent change is situated just in the center of action of the EAP (Figure 6.1(d)). Furthermore, a tendency of a decreased annual variability of the DJF NAO is identified where, interestingly, the decadal signal is absent.

Table 6.1: Statistics for the principal components of the Mean Sea-Level Pressure in the winter (DJF) season. Values are rounded to two decimals.

Pattern	Var. expl.	Mean			Variance fractions		
DJF	(%)	ctrl	zmean	p-value (%)	annual	p-value (%)	decadal
'NAO'	45.42	-0.18	0.18	0	0.8	6.63	1.00
'EA'	17.18	0.36	-0.36	0	0.93	58.18	0.88

Table 6.2: Same as table 6.1 but for summer-season (JJA).

Pattern	Var. expl.	Mean			Variance fractions		
JJA	(%)	ctrl	zmean	p-value (%)	annual	p-value (%)	decadal
'NAO'	36.93	-0.64	0.64	0	1.11	49.19	1.25
'EA'	12.47	-0.22	0.22	0	0.58	0	0.42

A similar approach was also applied to Z_{500}-data which brought qualitatively similar re-

sults as presented above. However, these are not considered as the robustness in the spatial characteristics of the 1st EOF were not found to be satisfactory. In addition, the explained variance from the first EOF where all data were included was found to explain around $\sim$ 20% more than what was the case from the individual CTRL and ZMEAN EOF, indicating that the regime-shift itself between the two model runs explain a large fraction of the total variance of the field. Consequently, such an analysis would lead to circle argumentation.

Chapter 7

Importance of the tropical and extra-tropical SST forcing

As is discussed in the literature (e.g. Hoerling et al. 2001; Sutton et al. 2001; Kushnir et al. (2002); Sutton and Hodson 2007), changes in the midlatitude atmospheric circulation associated with SST anomalies are often found to be connected to tropical forcing, rather than (or in addition to) displaying a direct local response to the extra-tropical forcing. As the imposed SST-forcing in ZMEAN covers a large latitudinal band, this opens for several such teleconnection effects to influence the atmospheric response discussed in the previous chapters. In order to illuminate this eventuality, two additional runs are performed where the forcing are separated into midlatitude and tropical parts, which also was the approach applied in some of the above-mentioned studies. In the next section, these runs are described and some of the results are briefly discussed and compared to that of ZMEAN.

7.1 Description and results from EX-Tr and Tr

The model runs used to separate between the tropical and extra-tropical influence on the atmospheric response to ocean circulation will be referred to as EX-Tr and Tr. EX-Tr consist of the northern branch (north of 38°N) of the SST-forcing in ZMEAN, while Tr employ only the tropical part of the forcing field in ZMEAN, covering the Atlantic south of 35°N and north of the equator. The anomaly patterns themselves are produced identically to that of ZMEAN, hence consisting of monthly zonally averaged climatological SSTs. Each of the two perturbation runs are 100 years long. The forcing fields for the winter and summer seasons are shown in Figure 7.1.

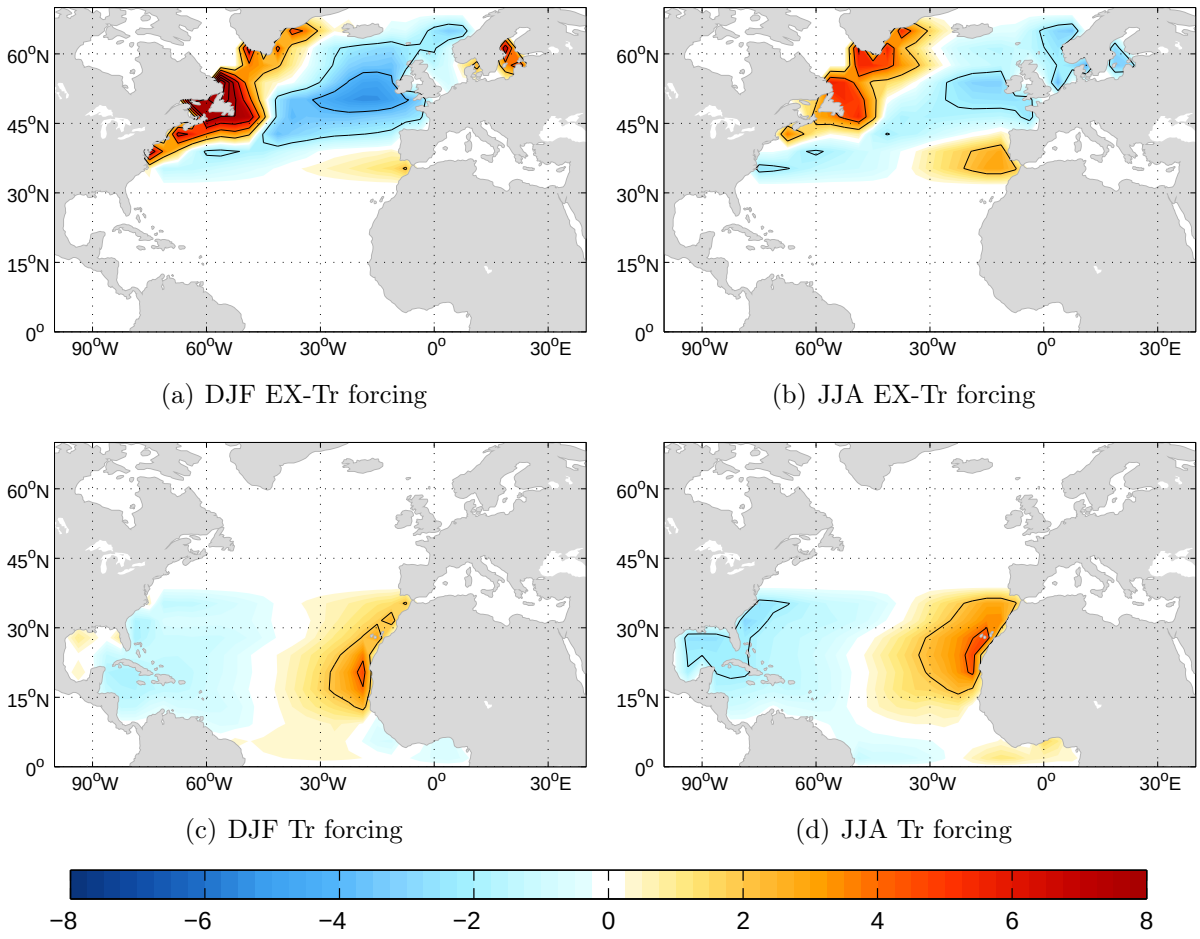

(a) DJF EX-Tr forcing

(b) JJA EX-Tr forcing

(c) DJF Tr forcing

(d) JJA Tr forcing

Figure 7.1: SST-Forcing fields in EX-Tr and Tr. Black contours are drawn for every 2 K.

Mean response

Figure 7.2 shows the winter response (still compared to CTRL) in surface and mid-level circulation in EX-Tr and Tr. From the MSLP-field it can be seen that both the extra-tropical and tropical parts of the forcing result in increased pressure in the eastern Atlantic with amplitudes of 3 hPa and 2 hPa, respectively. In EX-Tr a local and strong negative response (-5 hPa) could be seen in the southeast of Greenland. This particular response is more pronounced here than in Tr and ZMEAN, indicating the ability of the extra-tropical SST-forcing to produce this response locally. Moreover, one could see that no significant MSLP response is found north of 60° N in Tr which is indicative of the atmospheric response at polar latitudes to be primarily driven by the extra-tropical SST-forcing. The induced low pressure response southwest of the Canary Islands is occurring only in Tr, adding confidence to this response being local and in general accordance with that pro-

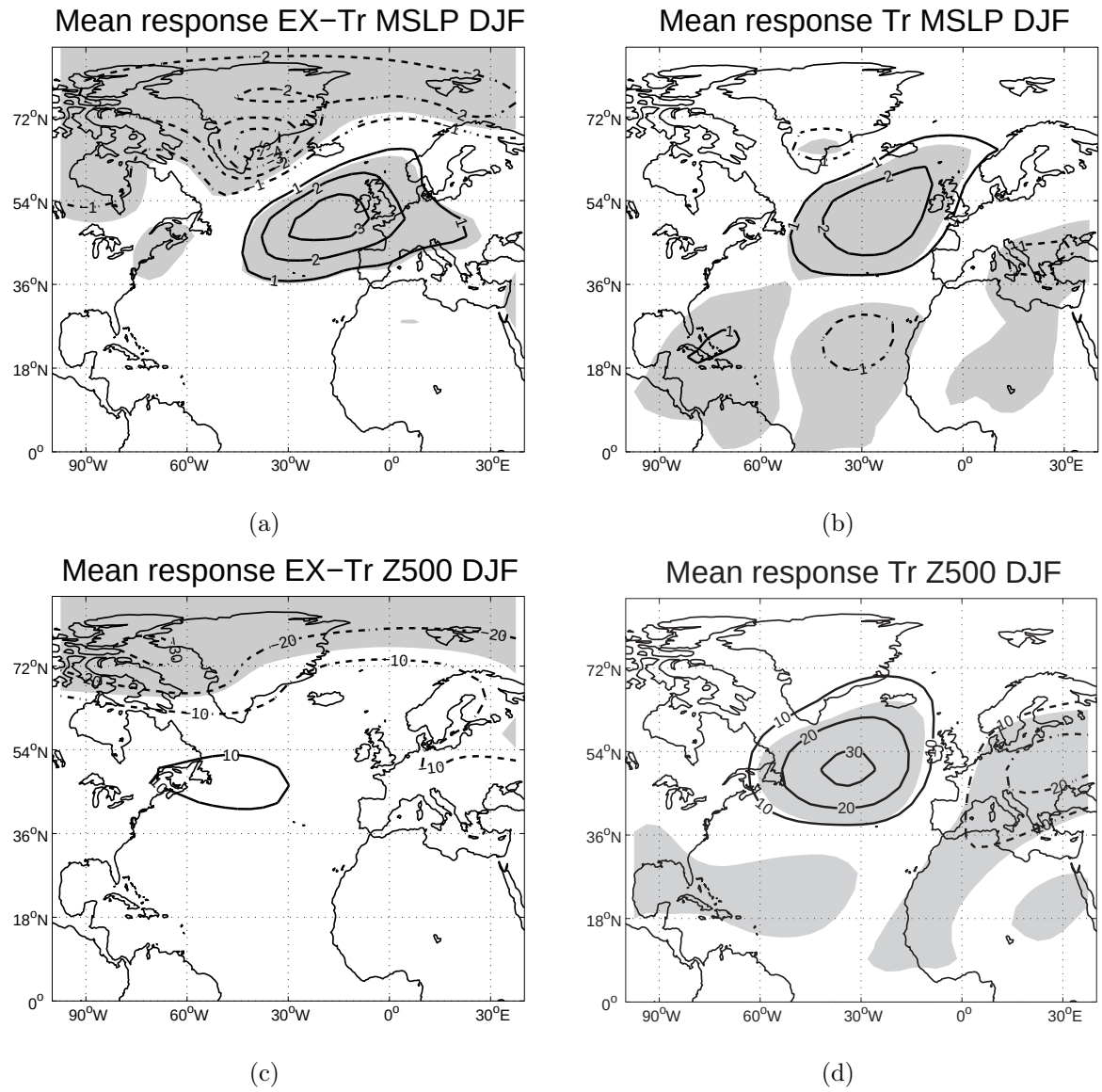

Figure 7.2: Upper panels show the winter MSLP response in EX-Tr (a) and Tr (b) with the corresponding response in Z_{500} shown in panels (c) and (d) when compared to CTRL. Dashed (solid) contours correspond to negative (positive) values. Contour intervals in (a,b) are 1 hPa and 10 m in (c,d). The grey shaded areas are statistically significant at the 99 % confidence-level according to a two-tailed t-test.

posed by Gill (1980).

Perhaps the most interesting result shown in Figure 7.2 is the absence (at least when measured in terms of statistical significance) of the mid-level central Atlantic Z_{500} response in EX-Tr. From the results of ZMEAN (Figure 5.3(b)) this could potentially be explained by means of the QG-theory of Hoskins and Karoly (1981) due to its downstream position compared to the imposed positive forcing. However, as is indicated by the lower panel of Figure 7.2, around 70 % of this response is explained by the tropical forcing alone, visualizing the shallowness of the local extra-tropical atmospheric response to the imposed SST-forcing as well as the limitations of applying QG-theory to presume the local atmospheric response to extra-tropical SSTa.

The above results have two direct implications to the evaluation of this mid-level response in ZMEAN discussed in Section 5.1.1. Firstly, the direct relationship between the extra-tropical SST-forcing and response is even weaker than earlier proposed, thus deviating further from the numbers of table 2.2. Secondly, it visualizes the ability of the tropical SST-anomalies to generate Rossby waves having nonlocal implications for the atmospheric circulation as also is shown by Hoerling et al. (2001) and Sutton and Hodson (2007). Moreover, this response is resembling the negative phase of the EAP-pattern in CTRL, shown in Figure A.2(c), with a spatial correlation of -0.84 (see table 7.2). This is an indication of the potential of this response being affected or driven by the model's internal variability, although projecting on the EA pattern and not the NAO.

The hypothesis of the EA-pattern being important for the atmospheric response to ocean circulation could also be related to some of the results reached by Park and Latif (2005), described in Section 2.4.2. It should, however, be noted that the approach used in the present work is different from the one in Park and Latif (2005). Moreover, the results described here indicate the EAP signal to be of tropical origin and not from signals involving midlatitude ocean circulation as proposed in their study.

Responses in the precipitation patterns (Figure 7.3) display the same general picture as the circulation fields; the tropical response is caused by tropical SST anomalies, whereas there is a tendency for these anomalies to also influence the precipitation pattern somewhat in the midlatitudes. However, most of the precipitation response in the models storm track is created by the extra-tropical forcing, although this decrease is still resembling the forcing pattern of Figure 7.1(a). The tropical influence on the precipitation rates in the model's storm track is quite weak, although indications of decreased rainfall in its southern branch is indicated. Being of nonlocal character, the latter response might be the most interesting; due to its weakness, however, it is not given further attention here.

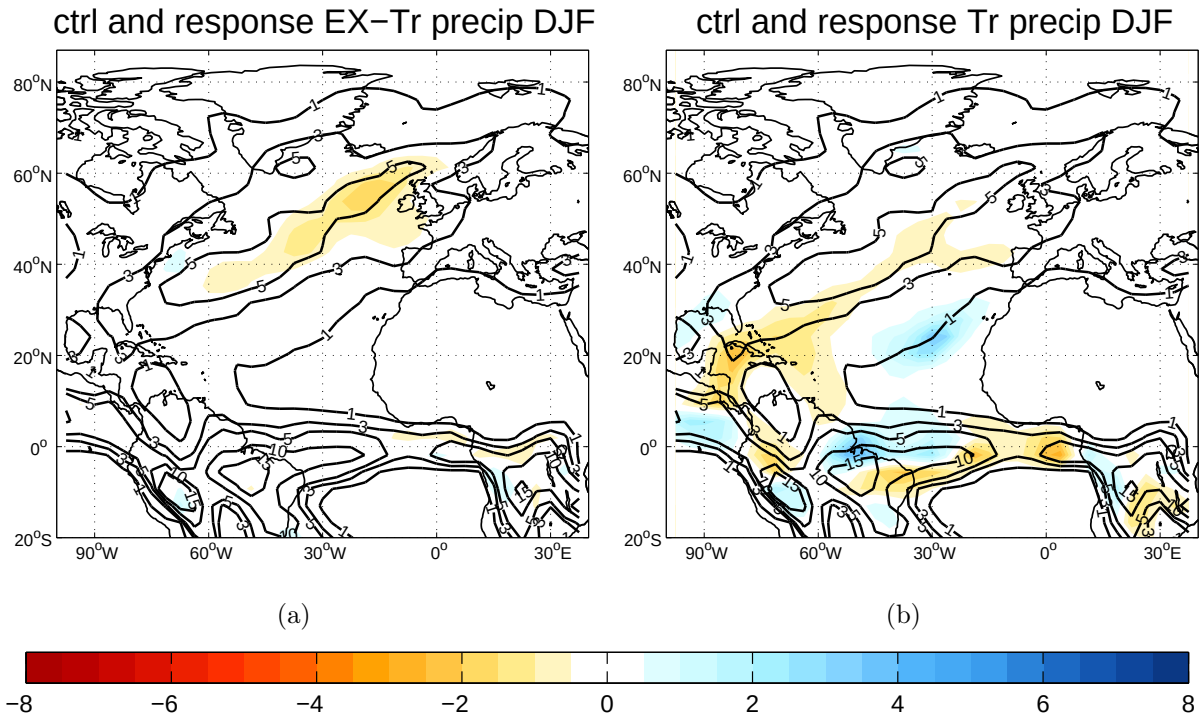

Figure 7.3: Shaded areas show the winter mean response of precipitation in EX-Tr (a) and Tr (b). The black contours show the models winter precipitation climatology taken from the seasonal mean of CTRL. *Units in mm/day.*

As illustrated in Figures 7.4(a) and 7.4(b), the summer pressure field is also mostly affected by the tropical SST-anomalies[1]. Interestingly, this is the case also for the MSLP response in the subpolar and polar areas. The contribution from the tropical forcing to the negative pressure response in the Norwegian Sea is for instance exceeding the one originating from the extra-tropical SST-forcing. Another example more in accordance with the response found in winter (Figures 7.2(a) and 7.2(b)), is the important role of the tropics in shaping the positive pressure perturbation around 40°. The local Gill-type response can be identified west of Africa also in summer, making this a quite robust feature of the atmospheric response to North Atlantic ocean circulation.

Considering the summer Z_{500} response (Figures 7.4(c) and 7.4(d)), it can be seen that the extra-tropical forcing drives a deeper response than what was found during winter. However, also here the tropics act to be the main contributor of the circulation changes. As no particular displacement of the maximum response in MSLP and Z_{500} in the central Atlantic at 40° N is seen, it infers the equivalent barotropic characteristics, concurrent

[1]We here neglect the response in Hudson Bay for discussion, see Section 5.4.

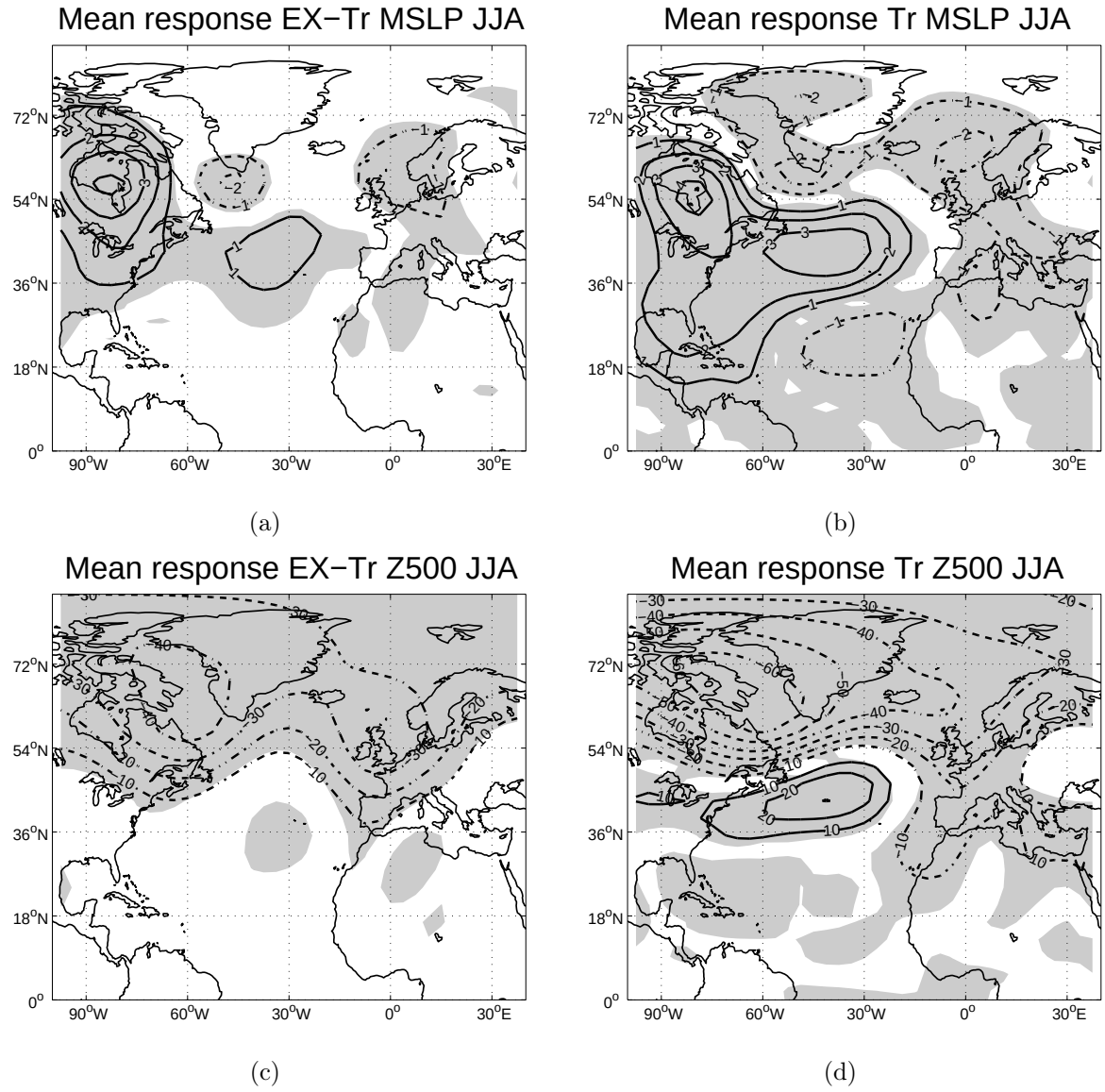

Figure 7.4: Upper panels show the summer MSLP response in EX-Tr (a) and Tr (b) with the corresponding Z_{500} response shown in panels (c) and (d). Dashed (solid) contours correspond to negative (positive) values. Contour intervals in (a,b) are 1 hPa and 10 m in (c,d). The grey shaded areas are statistically significant at the 99 % confidence-level according to a two-tailed t-test.

with that found in ZMEAN.

From the precipitation response during summer in EX-Tr and Tr, the influence of the extra-tropical forcing is found to be quite weak. As one would expect is the tropical precipitation response in Tr coinciding with that of ZMEAN. In addition is most of the precipitation response in the area of [40° N, 40° W] originating from the tropics, in contrast to what was found for the winter season.

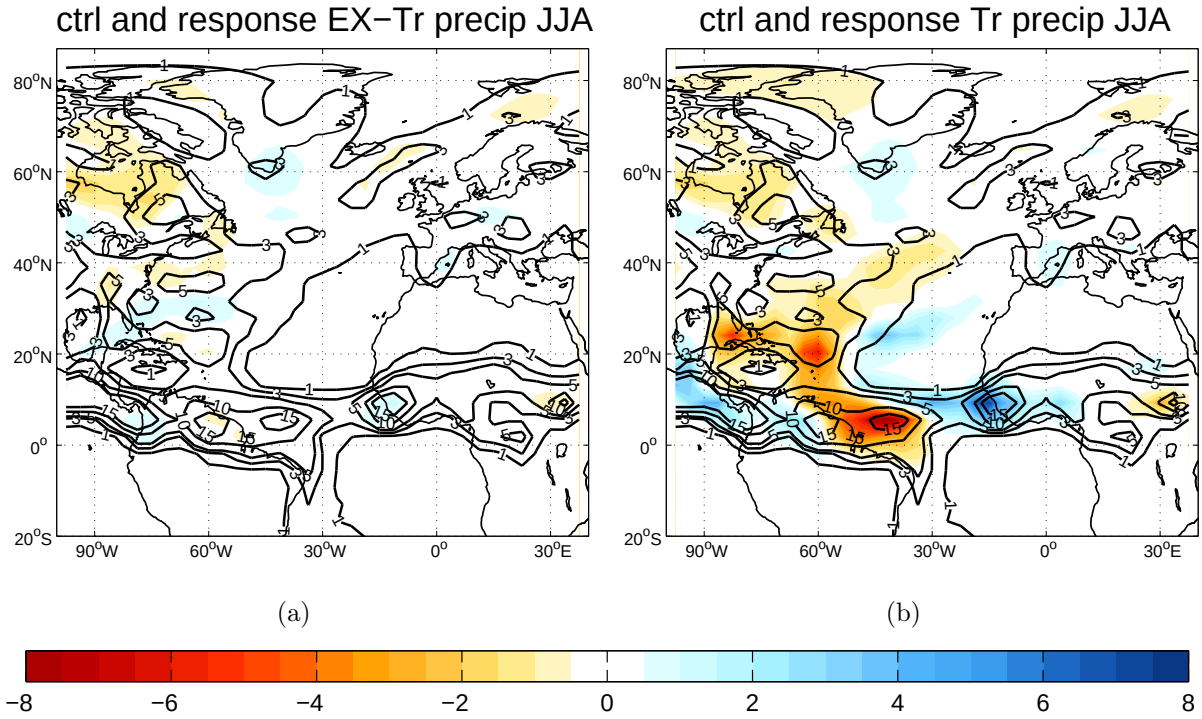

Figure 7.5: Shaded areas show the summer mean response of precipitation in EX-Tr (a) and Tr (b). The black contours show the models winter precipitation climatology taken from the seasonal mean of CTRL. *Units in mm/day.*

Spatial relationship of the responses to the variability patterns

The main aim with quantifying the variability changes caused by the extra-tropical and tropical forcing separately, has been to relate them to the two main variability patterns of the CTRL-run. The spatial characteristics of these modes, which are not equivalent to those given in Section 6.3, can be found in Appendix A.4.

In order to do this, spatial correlation between the response pattern and the variability patterns are computed. Only data within the box mentioned in Section 3.2 have been

used in this analysis. The response matrices have been weighted by the square root of cosine of latitude ($\sqrt{cos\phi}$) before doing the correlation analysis in order to retain the area-independence of the response, as also was done when obtaining the EOFs. Also, only detrended data from CTRL are used for obtaining the EOFs[2].

Table 7.1: Spatial correlation table between the model's intrinsic MSLP variability patterns, represented by the two leading EOFs of the CTRL run, and the responses of the 3 different model runs in the winter and summer seasons. Note that the bold face types are indicating the largest spatial statistical coherence between the patterns only, and not statistical significance.

MSLP	DJF response pattern			JJA response pattern		
Pattern	ZMEAN	Tr	EX-Tr	ZMEAN	Tr	EX-Tr
NAO (EOF1)	0.49	0.32	**0.78**	**0.48**	**0.41**	0.09
EAP (EOF2)	**-0.62**	**-0.66**	-0.15	0.13	0.27	**0.37**

Table 7.2: Same as Table 7.1, but for the Z_{500} data.

$\mathbf{Z}_{500}$	DJF response pattern			JJA response pattern		
Pattern	ZMEAN	Tr	EX-Tr	ZMEAN	Tr	EX-Tr
NAO (EOF1)	0.22	0.22	**0.74**	0.34	0.35	-0.01
EAP (EOF2)	**-0.68**	**-0.84**	-0.02	**0.79**	**0.83**	**0.78**

It can be seen from Tables 7.1 and 7.2 that the correlations in most cases are highly dependent on whether the imposed SST-forcing are only of tropical or extra-tropical origin. The fact that ZMEAN and Tr in most cases display a concurrent statistical relationship to the EOFs might be used as an argument to once again emphasize the general importance of the tropical forcing to induce the atmospheric circulation changes in the North Atlantic region. This is argued as the response of EX-Tr display a quite different behavior based on the spatial correlation analysis.

[2]The EOFs based on JJA Z_{500} data are in this case found to be robust, and are therefore included here

The most interesting to extract from these tables, however, are perhaps the large statistical coherence between the winter circulation response of EX-Tr and the spatial characteristics of the North Atlantic Oscillation in its positive phase, where the correlations for the fields of MSLP and Z_{500} are 0.78 and 0.74, respectively.

As the imposed SST pattern in EX-Tr is thought to represent a realization of the absence of ocean dynamics in the midlatitude North Atlantic, one might once again think of relating this to the discussion introduced in Section 2.5.2 regarding Bjerknes' theory of compensating effects between the oceanic and atmospheric components of the meridional heat transport, as summarized in Figure 2.7. This figure suggest that the presence of a positive anomaly in the westerlies (a positive phase of the NAO) is followed by a positive anomaly of net heat supply by the Gulf Stream. From a statistical point of view it can be argued that this applies also in the present results. This is the case, as the equilibrium atmospheric response to the absence of midlatitude North Atlantic ocean circulation display a signature of increased westerlies in terms of the increased NAO index, which is, according to Bjerknes, the precursor for increased ocean heat transport, and hence ocean circulation. Under the assumption that the model gives a realistic picture of the atmospheric response, this could therefore be described as a negative feedback.

It is here, however, important to remember that the above deduction is based purely on statistical measures and correlations which, even if statistical significant, do not give any information about the real physical relationship(s). Moreover, it is once again to be emphasized that this result is based on an atmosphere being uncoupled to the ocean, and therefore unable to reproduce several mechanisms which might be thought to play a role in shaping the natural atmospheric response to ocean circulation and their interaction.

Chapter 8

Summary and concluding remarks

This thesis has provided an estimate of the atmospheric response to the absence of North Atlantic ocean. The ocean circulation will in the natural system maintain a basin-wide zonal SST-gradient. In order to see how the atmosphere adjusted to a situation without this gradient, an intermediate atmospheric general circulation model was forced with zonally averaged SSTs in the latitude belt between equator and 65°N in the North Atlantic region.

Based on the questions raised in the beginning of the thesis, the main findings are as follows:

- The changes of atmospheric circulation due to the absence of ocean circulation in the North Atlantic is seasonally dependent. In the midlatitudes, this can be seen both from the vertical and spatial structure of the response. In winter, the response is baroclinic and resembling a negative phase of the East Atlantic Pattern. In summer, the response displays a response having a more equivalent barotropic structure, with a horizontal pattern more in accordance with the positive phase of the North Atlantic Oscillation. The spatial similarity of the circulation response to the variability patterns are, however, found to be dependent on position of the imposed forcing as well as season.

- A general tendency of the local atmospheric variability is found to decrease in the absence of ocean circulation, especially is this the case for the summer season. This decrease is more pronounced on the longer timescales. However, there are also identified areas with increased atmospheric variability, as for instance in the lower midlatitudes and the subtropics during winter.

- Based on the model results of ZMEAN and CTRL, one might explain some of the circulation changes in terms of quasi-geostrophic theory. Especially, the induced low pressure situated west of the positive West-African SST-forcing is a robust feature,

consistent with the theory of Gill (1980) and Hoskins and Karoly (1981). Moreover, the changes in precipitation associated with the ITCZ is found to be highly sensitive and linearly related to the magnitude and sign of the imposed SST anomalies. The linearity of the tropical response is consistent with the findings of Sutton and Hodson (2007).

- In the extra-tropics, the model results indicate that care should be taken when presuming the local atmospheric response to extra-tropical SST-forcing based on quasi-geostrophic considerations. This is especially true when the model at the same time is forced by tropical SST anomalies. The direct and local impact of extra-tropical SST anomalies on the atmospheric circulation is in this model found to be weak compared to earlier studies.

- The absence of extra-tropical ocean circulation during winter drives a positive and deep NAO-like atmospheric response, indicating a strengthening in the midlatitude westerlies, which potentially could induce a negative feedback upon ocean heat transport when following the deductions of Bjerknes (1964), although some constraints of this conclusion have already been discussed.

8.1 Future work

Through the work with this thesis some thoughts for future work have been established. For example would a daily output of data from the model enable a more quantitative and thorough way of investigating storm track characteristics and the dynamical features thought to be important in shaping the atmospheric response to extra-tropical SST forcing as argued in Kushnir, Robinson, Bladè, Hall, Peng, and Sutton (2002) and Sutton and Hodson (2007). In addition, conducting such a study would give insight both to the role SST-gradients have in generating these systems as well as how SPEEDY handles these relatively smaller scale features.

As also is explained in this thesis, one looses many aspects of the natural climate system when decoupling the atmosphere from the underlying ocean. For instance is one very important factor, not studied here, the development of sea-ice when ocean heat transport is absent. This is shown, for example by Winton (2003), to be a sensitive factor when investigating the climatic impact of ocean circulation. From the results of Kvamstø, Skeie, and Stephenson (2004) for example, it is plausible that effect of sea-ice changes would have implications for the atmospheric circulation response. Therefore would a further establishment of the atmospheric response to oceanic circulation thus be possible by forcing an AGCM (as SPEEDY) with output data from coupled model integrations, where the oceanic heat flux interior to the ocean were switched off, hence including the effect of changes in sea-ice cover.

Appendix A

Derivations and figures

A.1 Upper limit for linear response in Z_{500}

Starting out with the hypsometric equation describing the 500-hPa height:

$$Z_{500} = \frac{R < T >}{g} \cdot ln(\frac{p}{500})$$

We expand the temperature and pressure to consist as the sum of a background and perturbed state:

$$< T >= \bar{T}_a + T'_{SSTa}; p = p_0 + p'_{surface} \tag{A.1}$$

where p_0=1000hPa and T'_{SSTa} is the imposed anomaly in SST, thus allowing the entire lower half of the atmosphere to adjust to this temperature anomaly in a linear manner. The hypsometric equation may therefore be written as:

$$Z_{500} = \frac{R(\bar{T}_a + T'_{SSTa})}{g} \cdot ln(\frac{1000 + p'_{surface}}{500})$$

$$\Updownarrow$$

$$Z_{500} = \frac{R(\bar{T}_a + T'_{SSTa})}{g} \cdot ln(\frac{1000 + p'_{surface}}{1000} \cdot \frac{1000}{500})$$

$$\Updownarrow$$

$$Z_{500} = \frac{R(\bar{T}_a + T'_{SSTa})}{g} \cdot [ln(1 + \frac{p'_{surface}}{1000}) + ln2]$$

Since $\frac{p'_{surface}}{1000} << 1$, the Taylor expansion of $ln(1 + \frac{p'_{surface}}{1000}) \approx \frac{p'_{surface}}{1000}$ is valid. Hence, the above simplifies to:

$$Z_{500} \approx \frac{R(\bar{T}_a + T'_{SSTa})}{g} \cdot [\frac{p'_{surface}}{1000} + ln2]$$

Neglecting the squared perturbation-terms and expanding the above equation it may be written:

$$Z_{500} \approx \frac{R\bar{T}_a}{g} ln2 + \frac{RT_{SSTa}}{g} ln2 + \frac{RT_a}{g} \frac{p'_{surface}}{1000} \tag{A.2}$$

Expanding the geopotential height of the 500-hPa surface as was done in Equation A.1 for temperature and pressure, we may write:

$$Z_{500} = \bar{Z}_{500} + Z'_{500}$$

where the background state is:

$$\bar{Z}_{500} = \frac{R\bar{T}_a}{g} ln2 \tag{A.3}$$

Substituting Equation A.3 into Equation A.2:

$$Z_{500} \approx \bar{Z}_{500}(1 + \frac{T'_{SSTa}}{\bar{T}_a} + \frac{p'_{surface}}{1000 \cdot ln2})$$

which is the equivalent of:

$$Z_{500} - \bar{Z}_{500} = Z'_{500} \approx \bar{Z}_{500}(\frac{T'_{SSTa}}{\bar{T}_a} + \frac{1}{ln2} \frac{p'_{surface}}{1000})$$

A.2 The quasi-geostrophic assumption

In this section, the considerations concerning the quasi-geostrophic assumption in Section 2.3 are investigated. The derivations in the 2 following subsections are mainly following the steps of Holton (2004), pages 147-152.

In isobaric coordinates, the horizontal momentum equation, the hydrostatic equation, the continuity equation, and the thermodynamic energy equation might be expressed as:

$$\frac{D\boldsymbol{V}}{Dt} + f\boldsymbol{k} \times \boldsymbol{V} = -\boldsymbol{\nabla}\Phi \tag{A.4}$$

$$\frac{\partial \Phi}{\partial p} = -\alpha = RT/p \tag{A.5}$$

$$\boldsymbol{\nabla} \bullet \boldsymbol{V} + \frac{\partial \omega}{\partial p} = 0 \tag{A.6}$$

$$(\frac{\partial}{\partial t} + \boldsymbol{V} \bullet \boldsymbol{\nabla})T - S_p\omega = \frac{Q}{c_p} \tag{A.7}$$

The total derivative in Equation A.4 is defined by:

$$\frac{D}{Dt} \equiv \frac{\partial}{\partial t} + (\boldsymbol{\nabla} \bullet \boldsymbol{V})_p + \omega \frac{\partial}{\partial p}$$

where, $\omega = Dp/Dt$ is the rate of pressure change following the motion and the $_p$-subscript denote that the variables are evaluated on fields of constant pressure. In equations A.4-A.6, $f = 2\Omega sin\phi$ is the Coriolis parameter, Φ is the geopotential and R is the gas constant for dry air. In Equation A.7, $S_p = -T\frac{\partial ln\theta}{\partial p} = -\frac{T}{\theta}\frac{\partial \theta}{\partial p}$ is the static stability parameter, Q is the rate of diabatic heating and c_p is the specific heat of dry air at constant pressure.

A.2.1 The momentum equation

In transforming the momentum equation into the form of Equation 2.4, the first step is to split the horizontal wind into geostrophic and ageostrophic components:

$$\boldsymbol{V} = \boldsymbol{V}_g + \boldsymbol{V}_a \tag{A.8}$$

noting that the ratio $\frac{|\boldsymbol{V}_a|}{|\boldsymbol{V}_g|} \sim \mathrm{O}(10^{-1})$ on the synoptic scale. The geostrophic wind in Equation A.8 is defined as:

$$\boldsymbol{V}_g \equiv f_0^{-1}\boldsymbol{k} \times \boldsymbol{\nabla}\Phi \Leftrightarrow \boldsymbol{\nabla}\Phi = -f_0 \boldsymbol{k} \times \boldsymbol{V}_g \tag{A.9}$$

Here, the constant-f (CF) assumption has been applied, resulting in $\boldsymbol{V}_g$ being nondivergent (Holton 2004). Since synoptic-scale motions in the midlatitude atmosphere are near-geostrophic, $\boldsymbol{V}$ can be approximated by $\boldsymbol{V}_g$, and the advection due to vertical motions, which themselves originate from the ageostrophic component of the motion, can be neglected to the order of the Rossby number; a nondimensional number defined as the ratio of the acceleration- and Coriolis-terms in Equation A.4.[1] Thus, the total derivative may be approximated as:

$$\frac{D\boldsymbol{V}}{Dt} \approx \frac{D_g \boldsymbol{V}_g}{Dt} \tag{A.10}$$

where

$$\frac{D_g}{Dt} \equiv \frac{\partial}{\partial t} + \boldsymbol{\nabla} \bullet \boldsymbol{V}_g = \frac{\partial}{\partial t} + u_g \frac{\partial}{\partial x} + v_g \frac{\partial}{\partial y}$$

Despite the fact that we have used the CF-approximation when defining the geostrophic wind, the latitudinal dependence of the Coriolis parameter in Equation A.4 has to be taken into account (Holton 2004). A 1st-order approximation to include this effect is to expand the Taylor series of f about a reference latitude ϕ_0:

$$f = f_0 + \beta y \tag{A.11}$$

[1] The Rossby number has the form $Ro \equiv U/(f_0 L)$, where U and L denote the typical scales of velocity and length of synoptic disturbances. U, L and f_0 are of the orders $10m/s, 10^6 m$ and $10^{-4}s^{-1}$, respectively. Thereby, the Rossby number are of $\mathrm{O}(10^{-1})$.

where $\beta \equiv (\frac{df}{dy})_{\phi_0}$, and $y = 0$ at ϕ_0. This procedure is commonly known as the *midlatitude β-plane* approximation.

From Equation A.4 it can be seen that it is the difference between the pressure gradient force and Coriolis force which account for the acceleration of motion. This difference is characterized by the departure of the actual wind from the geostrophic wind, thus, in order to retain the prognostic nature of the problem, the ageostrophic component $\boldsymbol{V}_a$ of the wind has to be included in the Coriolis-term.

A combination of equations A.8, A.9 and A.11 into the Coriolis force and pressure gradient force in Equation A.4 can be performed to write:

$$f\boldsymbol{k} \times \boldsymbol{V} + \boldsymbol{\nabla}\Phi = (f_0 + \beta y)\boldsymbol{k} \times (\boldsymbol{V}_g + \boldsymbol{V}_a) - f_0\boldsymbol{k} \times \boldsymbol{V}_g$$

$$\approx f_0\boldsymbol{k} \times \boldsymbol{V}_a + \beta y\boldsymbol{k} \times \boldsymbol{V}_g$$

Here, the ageostrophic wind in the term proportional to βy is neglected. An approximate horizontal momentum equation can therefore be described as:

$$\frac{D_g\boldsymbol{V}_g}{Dt} \cong -f_0\boldsymbol{k} \times \boldsymbol{V}_a - \beta y\boldsymbol{k} \times \boldsymbol{V}_g \tag{A.12}$$

Decomposed in the x- and y-directions, respectively, Equation A.12 can be written (omitting the $\cong$-notation):

$$\frac{D_g u_g}{Dt} - f_0 v_a - \beta y v_g = 0 \tag{A.13}$$

and

$$\frac{D_g v_g}{Dt} + f_0 u_a + \beta y u_g = 0 \tag{A.14}$$

The expression for the quasi-geostrophic vorticity $\zeta_g = \frac{\partial v_g}{\partial x} - \frac{\partial u_g}{\partial y}$ can be obatined by differentiating equations A.14 and A.13 with respect to x and y, respectively, and thereafter subtract the former from the latter (i.e. $\frac{\partial(A.14)}{\partial x} - \frac{\partial(A.13)}{\partial y}$). Doing these operations we get:

$$\frac{D_g\zeta_g}{Dt} + \frac{\partial}{\partial x}(f_0 u_a) + \frac{\partial}{\partial y}(f_0 v_a) + \frac{\partial}{\partial x}(\beta y u_g) + \frac{\partial}{\partial y}(\beta y v_g) = 0$$

$$\Downarrow$$

$$\frac{D_g\zeta_g}{Dt} + f_0(\frac{\partial u_a}{\partial x} + \frac{\partial v_a}{\partial y}) + \beta y\frac{\partial u_g}{\partial x} + \beta y\frac{\partial v_g}{\partial y} + y v_g\frac{\partial \beta}{\partial y} + \beta v_g\frac{\partial y}{\partial y} = 0$$

remembering that the geostrophic wind is non-divergent, and that $\beta \equiv (\frac{df}{dy})_{\phi_0}$, hence independent of y, this simplifies to:

$$\frac{D_g\zeta_g}{Dt} + \beta v_g = -f_0(\frac{\partial u_a}{\partial x} + \frac{\partial v_a}{\partial y}) \tag{A.15}$$

The continuity equation (Equation A.6) can be simplified to:

$$\boldsymbol{\nabla} \bullet \boldsymbol{V} + \frac{\partial \omega}{\partial p} = \boldsymbol{\nabla} \bullet \boldsymbol{V}_a + \frac{\partial \omega}{\partial p} = \frac{\partial u_a}{\partial x} + \frac{\partial v_a}{\partial y} + \frac{\partial \omega}{\partial p} = 0$$

thus, Equation A.15 can be rewritten to the form of Equation 2.4:

$$\frac{\partial \zeta_g}{\partial t} + \boldsymbol{V}_g \cdot \boldsymbol{\nabla} \zeta_g + \beta v_g = f_0 \frac{\partial \omega}{\partial p}$$

A.2.2 The thermodynamic energy equation

Bearing in mind that air is compressible, it is convenient to describe the thermodynamic equation in terms of the potential temperature[2] $\theta = T(p_0/p)^{R/c_p}$ rather than the absolute temperature, since θ is conserved during an adiabatic process. This can be obtained in the following way starting out by substituting S_p in Equation A.7 and follow the approximation of Equation A.10:

$$(\frac{\partial}{\partial t} + \boldsymbol{V}_g \bullet \boldsymbol{\nabla})T + \frac{T}{\theta}\frac{\partial \theta}{\partial p}\omega = \frac{Q}{c_p}$$

and then multiply all terms by the factor θ/T to yield the equivalent of Equation 2.5:

$$(\frac{\partial}{\partial t} + \boldsymbol{V}_g \bullet \boldsymbol{\nabla})\theta + \omega\frac{\partial \theta}{\partial p} = \frac{Q}{c_p}\frac{\theta}{T}$$

A.3 Linearizing equations 2.4 and 2.5 about the zonally averaged flow

The next step is to linearize the equations 2.4 and 2.5 about the zonal mean flow Nigam and DeWeaver (2003). This zonally average is denoted by bars and its deviation by primes. In more general terms, a variable A might be interperated as (Nigam and DeWeaver 2003):

$$A(x, y, p, t) = \bar{A}(y, p) + A'(x, y, p, t) \tag{A.16}$$

By applying this on θ and $\boldsymbol{V}$ in equations 2.4 and 2.5[3], and using subscripts to describe the partial derivatives, thus omitting the $_g$-subscript denoting geostrophic motions, they may be written as:

$$\bar{\zeta}_t + \zeta'_t + \bar{u}\bar{\zeta}_x + \bar{u}\zeta'_x + u'\bar{\zeta}_x + u'\zeta'_x + \bar{v}\bar{\zeta}_y + \bar{v}\zeta'_y + v'\bar{\zeta}_y + v'\zeta'_y + \beta(\bar{v} + v') = f_0(\bar{\omega}_p + \omega'_p)$$

[2]The $_0$-subscript here denote a reference pressure, usually 1000hPa.

[3]The linearization-procedure is omitted in the diabatic heat term of Equation 2.5

and

$$\bar{\theta}_t + \theta'_t + \bar{u}\bar{\theta}_x + \bar{u}\theta'_x + u'\bar{\theta}_x + u'\theta'_x + \bar{v}\bar{\theta}_y + \bar{v}\theta'_y + v'\bar{\theta}_y + v'\theta'_y + \bar{\omega}\bar{\theta}_p + \bar{\omega}\theta'_p + \omega'\bar{\theta}_p + \omega'\theta'_p = \frac{Q}{c_p}\frac{\theta}{T}$$

respectively. From Equation A.16 and the assumption that $\bar{v} = \bar{\omega} \equiv 0$, the above simplifies directly to:

$$\zeta'_t + \bar{u}\zeta'_x + v'\bar{\zeta}_y + \beta v' = f_0\omega'_p \tag{A.17}$$

and

$$\theta'_t + \bar{u}\theta'_x + v'\bar{\theta}_y + \omega'\bar{\theta}_p = \frac{Q}{c_p}\frac{\theta}{T} \tag{A.18}$$

where the squared perturbation-terms have been neglected. Since $v'\bar{\zeta}_y = v'\frac{\partial}{\partial y}(\bar{v}_x - \bar{u}_y) = -v'\bar{u}_{yy}$, Equation A.17 can be rewritten as:

$$\zeta'_t + \bar{u}\zeta'_x + v'(\beta - \bar{u}_{yy}) = f_0\omega'_p \tag{A.19}$$

A.4 Spatial properties EOFs in CTRL

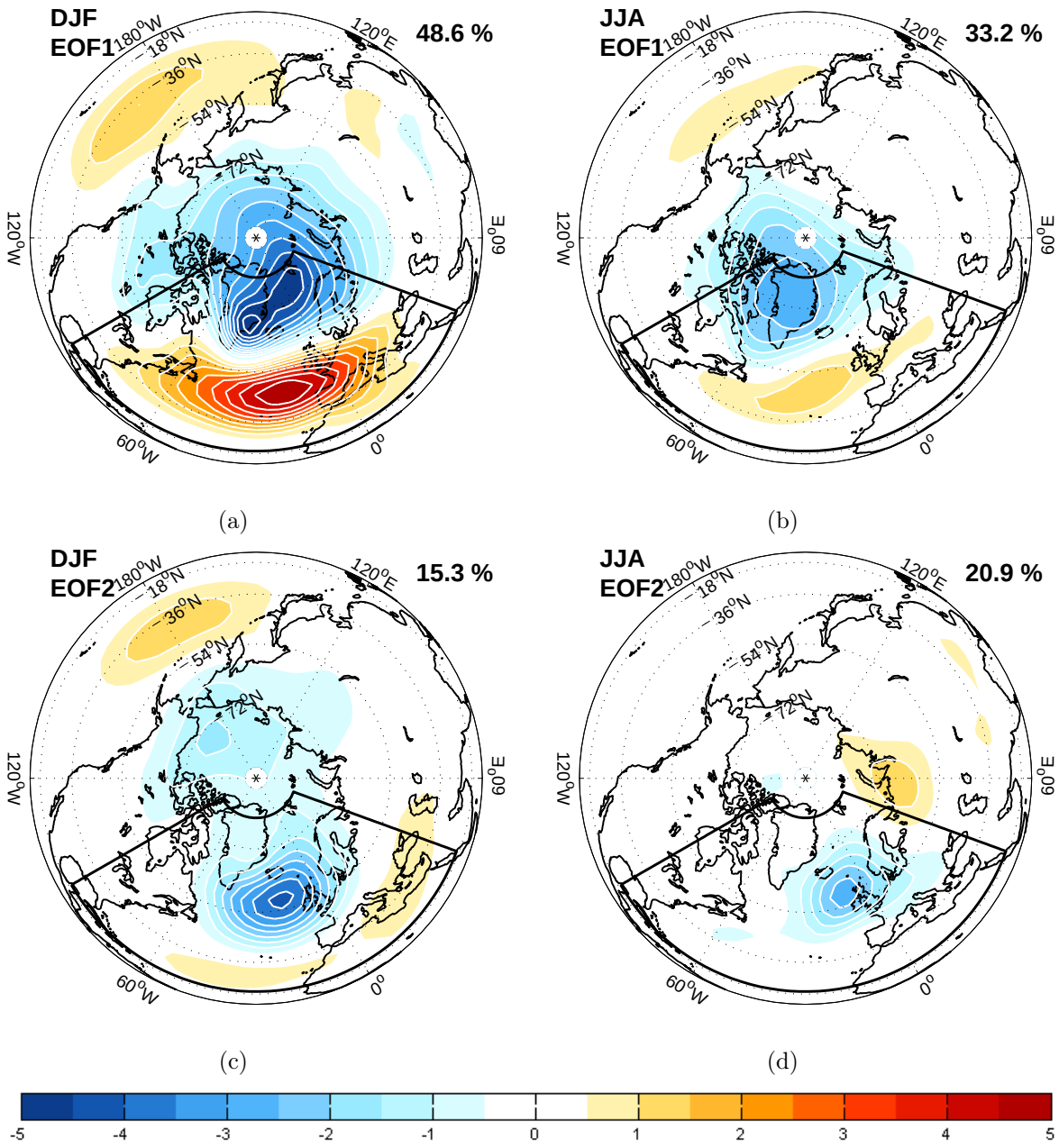

Figure A.1: Spatial characteristics of the first 2 MSLP EOFs in winter (a,c) and summer (b,d). EOFs are computed from the detrended timseries of CTRL inside the sector indicated on the figures. The amplitude represents hPa pr. standard deviation in their corresponding PC-timeseries. Contour intervals of 0.5 hPa, where amplitudes less than $|0.5|hPa$ shaded white.

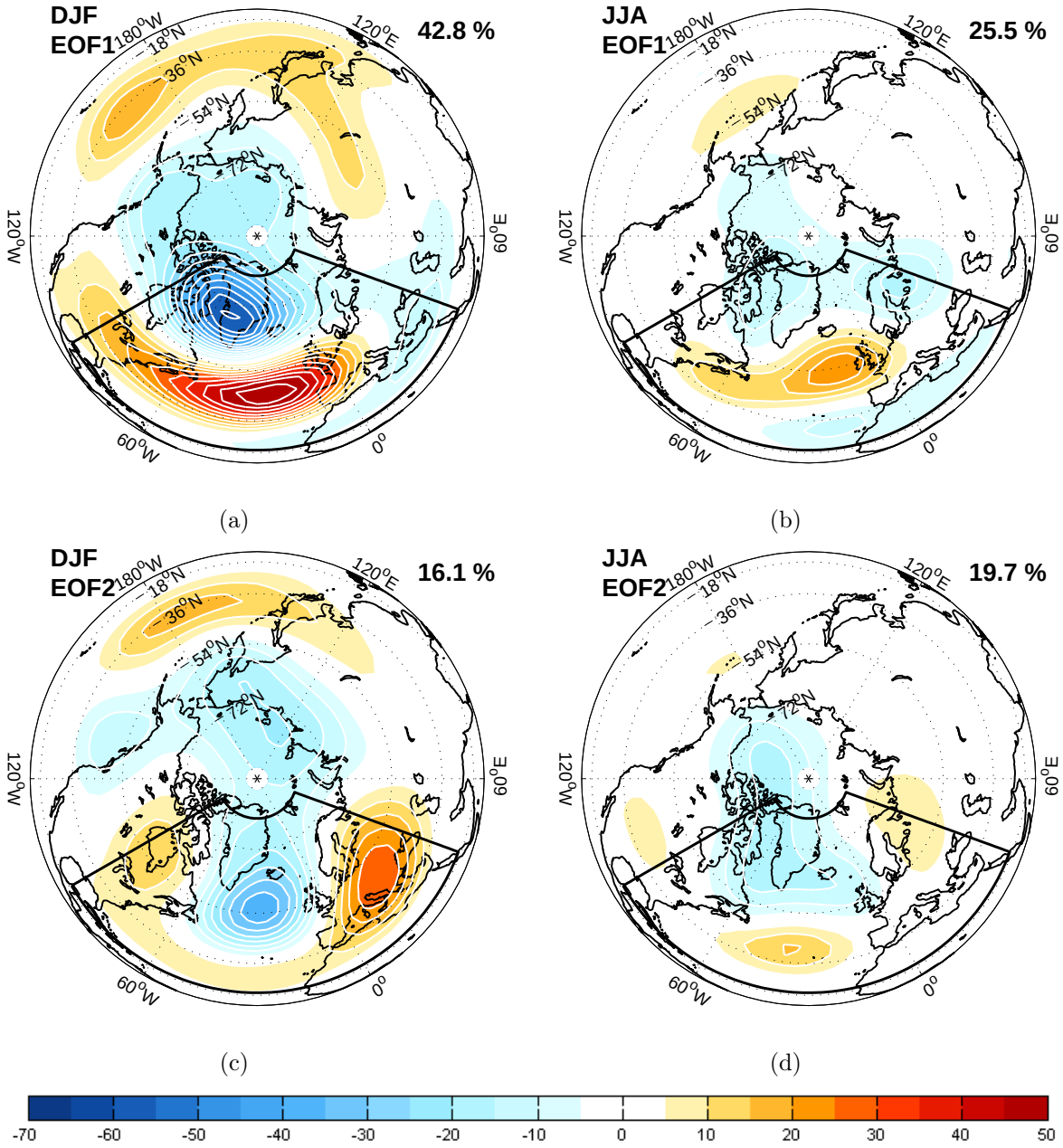

Figure A.2: Spatial characteristics of the first 2 Z_{500} EOFs in winter (a,c) and summer (b,d). EOFs are computed from the detrended timseries of CTRL inside the sector indicated on the figures. The amplitude represents m pr. standard deviation in their corresponding PC-timeseries. Contour intervals of 5 m, where amplitudes less than $|5|m$ shaded white.

Appendix B

List of Figures

1.1 Map overview 2
1.2 Overview of the North Atlantic surface ocean currents 4
1.3 The SST-distribution with and without qflux 4

2.1 Development of surface ridge in response to a warm SST anomaly 8
2.2 Residual of the thermodynamic equation 11
2.3 Thermal forcing response. 12
2.4 Tropical response to SST-forcing 15
2.5 Climatic implications of the NAO-index 18
2.6 The NAO- and EAP patterns 19
2.7 Interannual co-variability of North Atlantic SSTs and atmospheric indices . 23
2.8 Schematic diagram of interactions leading to the interdecadal THC-variability 25
2.9 SST Tripole 26
2.10 Precipitation response to smoothed SSTs 27

3.1 The Gibbs phenomena 31
3.2 SPEEDY resolution 31
3.3 Model bias for Z_{500} 34
3.4 Zonal mean bias for temperature and zonal wind 35
3.5 Model bias for precipitation 36

4.1 SST climatology and zonally averaged SSTs in Northern Atlantic 43
4.2 Seasonal SST-forcing of SPEEDY in ZMEAN 45

5.1 Mean winter response in MSLP 47
5.2 Mean response in winter precipitation 48
5.3 Mean winter response in Z_{500} 50
5.4 The winter Z_{500}-field in CTRL and ZMEAN 51

5.5 Mean summer response in MSLP and Z_{500} . . . 52
5.6 The summer Z_{500}-field in CTRL and ZMEAN . . . 54
5.7 Mean response in summer precipitation . . . 55
5.8 Changes in Near-Surface winds . . . 56
5.9 Changes in winds at 300 hPa . . . 58
5.10 Temperature response at 700 and 850 hPa . . . 60
5.11 Longitude-height crossection of temperature and Z response . . . 61
5.12 Sea-surface heat flux in CTRL . . . 63
5.13 Changes in sea-surface heat flux . . . 64
5.14 Sea-ice cover in boeral summer . . . 66

6.1 Change in the variability of MSLP . . . 69
6.2 Time evolution of the depth of the Icelandic Low in CTRL and ZMEAN . 70
6.3 Change in the variability of Z_{500} . . . 71
6.4 Spatial characteristics of the EOFs . . . 73
6.5 PC-timeseries . . . 74

7.1 Seasonal SST-forcing of SPEEDY in EX-Tr and Tr . . . 78
7.2 MSLP and Z_{500} DJF response in EX-Tr and Tr . . . 79
7.3 DJF precip response in EX-Tr and Tr . . . 81
7.4 MSLP and Z_{500} DJF response in EX-Tr and Tr . . . 82
7.5 JJA precipitation response in EX-Tr and Tr . . . 83

A.1 Spatial patterns of MSLP EOFs in CTRL . . . 95
A.2 Spatial patterns of Z_{500} EOFs in CTRL . . . 96

Appendix C

List of Acronyms

AGCM	Atmospheric General Circulation Model
AMOC	Atlantic Meridional Overturning Circulation
CTRL	Control run
DJF	December-January-February
DOF	Degrees Of Freedom
EA(P)	East Atlantic (Pattern)
ECMWF	European Center for Medium-range Weather Forecast
EOF	Empirical Orthogonal Functions
EqBt	Equivalent Barotropic
EX-Tr	Perturbed run with zonally averaged SSTs in the extra-tropical North Atlantic
IL	Icelandic Low
ITCZ	Inter-Tropical Convergence Zone
JJA	June-July-August
LHF	Latent heat flux
MSLP	Mean Sea-Level Pressure
NAO	North Atlantic Oscillation

NCAR	National Centre for Atmospheric Research
NCEP	National Centres for Environmental Prediction
PC(s)	Principal Component(s)
QG	Quasi-geostrophic
SHF	Sensible Heat Flux
SPG	SubPolar Gyre
SSS	Sea Surface Salinity
SST(a)	Sea-Surface Temperature (anomaly)
STG	SubTropical Gyre
SVD	Singular Value Decomposition
THC	Thermohaline Circulation
Tr	Perturbed run with zonally averaged SSTs in the tropical North Atlantic
WBC	Western-Boundary Current
ZMEAN	Perturbed run with zonally averaged SSTs in the North Atlantic

Bibliography

Barnston, A. G. and R. E. Livezey (1987). Classification, Seasonality and Persistence of Low-Frequency Atmospheric Circulation Patterns. *Monthly Weather Review 115*(6), 1083–1126.

Barsugli, J. J. and D. S. Battisti (1998). The Basic Effects of Atmosphere-Ocean Thermal Coupling on Midlatitude Variability. *Journal of the Atmospheric Sciences 55*(4), 477–493.

Bearman, G. (Ed.) (2002). *Ocean Circulation* (Second ed.). The Open University.

Bjerknes, J. (1964). Atlantic air-sea interaction. In *Advances in Geophysics*, Volume 10, pp. 1–82. Academic Press.

Bourke, W. (1974). A Multilevel spectral model. I. Formulation and Hemispheric Integrations. *Monthly Weather Review 102*(10), 687–701.

Bracco, A., F. Kucharski, R. Kallummal, and F. Molteni (2004). Internal variability, external forcing and climate trends in multi-decadal AGCM ensembles. *Climate Dynamics 23*(6), 659–678.

Bretherton, C. and D. Battisti (2000). An interpretation of the results from atmospheric general circulation models forced by the observed sea surface temperature distribution. *Geophysical Research Letters 27*(6), 767–770.

Charney, J. G. and A. Eliassen (1949). A numerical method for predicting the perturbations of the middle latitude westerlies. *Tellus 1*(2), 38–54.

Czaja, A. (2003, October). Spatial sst variations, ocean dynamics and low-frequency atmospheric variability in midlatitudes. Presentation at the EURESCO conference on 'Achieving Climate Predictability using Paleoclimate Data'.

Czaja, A. and J. Marshall (2000). On the interpretation of AGCMs response to prescribed time-varying SST anomalies. *Geophysical Research Letters 27*(13), 1927–1930.

Czaja, A., A. W. Robertson, and T. Huck (2003). The Role of Atlantic Ocean-Atmosphere Coupling in Affecting North Atlantic Oscillation Variability. In *The*

North Atlantic Oscillation: Climatic Significance and Environmental Impact, Volume 134 of *Geophysical Monograph*, pp. 147–172. American Geophysical Union.

da Silva, A., C. C. Young, and S. Levitus (1994). *Atlas of Surface Marine Data 1994*, Volume 1 of *Algorithms and Procedures. NOAA Atlas NESDIS 6*. U. S. Department of Commerce, Washington DC.

Deser, C. and M. L. Blackmon (1993). Surface Climate Variations over the North Atlantic Ocean during Winter: 1900-1989. *Journal of Climate 6*(9), 1743–1753.

Deser, C., G. Magnusdottir, R. Saravanan, and A. Phillips (2004). The Effects of North Atlantic SST and Sea Ice Anomalies on the Winter Circulation in CCM3. Part II: Direct and Indirect Components of the Response. *Journal of Climate 17*(5), 877–889.

Dole, R. M. (1989). Life Cycles of Persistent Anomalies. Part I: Evolution of 500 mb Height Fields. *Monthly Weather Review 117*(1), 177–211.

Emery, W. and R. Thomson (2001). *Data Analysis Methods in Physical Oceanography* (Second and Revised ed.). Amsterdam, The Netherlands: Elsevier B.V.

Ferranti, L., F. Molteni, and T. N. Palmer (1994). Impact of localized tropical and extratropical SST anomalies in ensembles of seasonal GCM integrations. *Quarterly Journal of the Royal Meteorological Society 120*(520), 1613–1645.

Gibson, J. K., P. Kallberg, S. Uppsala, A. Hernandez, A. Nomura, and E. Serrano (1997). ERA description ECMWF Re-Analysis Project Series 1.

Gill, A. E. (1980). Some simple solutions for heat-induced tropical circulation. *Quarterly Journal of the Royal Meteorological Society 106*, 447–462.

Gill, A. E. and E. M. Rasmusson (1983). The 1982-83 climate anomaly in the equatorial pacific. *Nature 306*, 229–234.

Hannachi, A., I. T. Jolliffe, and D. B. Stephenson (2007). Empirical orthogonal functions and related techniques in atmospheric science: A review. *International Journal of Climatology 27*(9), 1119–1152.

Hartmann, D. (1994). *Global Physical Climatology*. Academic Press.

Held, I. M. and M. J. Suarez (1994). A proposal for the intercomparison of the dynamical cores of atmospheric general circulation models. *Bulletin of the American Meteorological Society 75*(10), 1825–1830.

Hendon, H. H. and D. L. Hartmann (1982). Stationary waves on a sphere: Sensitivity to thermal feedback. *Journal of the Atmospheric Sciences 39*(9), 1906–1920.

Hoerling, M. P., J. W. Hurrel, and T. Xu (2001). Tropical origins for recent North Atlantic climate change. *Science 292*, 90–92.

Holton, J. R. (2004). *An Introduction to Dynamic Meteorology* (Fourth ed.), Volume 88 of *International Geophysics Series*. Elsevier Academic Press, London, UK.

Hoskins, B. J. and D. J. Karoly (1981). The steady linear response of a spherical atmosphere to thermal and orographic forcing. *Journal of the Atmospheric Sciences 38*(6), 1179–1196.

Hoskins, B. S. and K. I. Hodges (2002). New Perspectives on the Northern Hemisphere Winter Storm Tracks. *Journal of the Atmospheric Sciences 59*(6), 1041–1061.

Hurrell, J. W., Y. Kushnir, G. Ottesen, and M. Visbeck (2003). An overview of the North Atlantic Oscillation. In *The North Atlantic Oscillation: Climatic Significance and Environmental Impact*, Volume 134 of *Geophysical Monograph*, pp. 1–35. American Geophysical Union.

Kalnay, E., R. Kistler, W. Collins, D. Deaven, L. Gandin, M. Iredell, S. Saha, G. White, J. Woollen, Y. Zhu, M. Chelliah, W. Ebisuzaki, W. Higgins, J. Jonawiak, K. Mo, C. Ropelewski, J. Wang, A. Leetmaa, R. Reynolds, R. Jenne, and D. Joseph (1996). The NCEP/NCAR 40-Year Reanalysis Project. *Bulletin of the American Meteorological Society 77*(3), 437–471.

Kucharski, F. (2007, Visited November, 2007). ICTP Atmospheric General Circulation Model SPEEDY-Net Homepage. http://users.ictp.it/∼kucharsk/speedy-net.html.

Kucharski, F., F. Molteni, and A. Bracco (2006). Decadal interactions between the western tropical Pacific and the North Atlantic Oscillation. *Climate Dynamics 26*(1), 79–91.

Kushnir, Y. (1994). Interdecadal variations in North Atlantic sea surface temperature and associated atmospheric conditions. *Journal of Climate 7*(1), 141–157.

Kushnir, Y. and I. M. Held (1996). Equilibrium atmospheric response to North Atlantic SST anomalies. *Journal of Climate 9*(6), 1208–1220.

Kushnir, Y. and C. Lau (1992). The general circulation model response to a North Pacific SST anomaly: Dependence on time scale and pattern polarity. *Journal of Climate 5*(4), 271–283.

Kushnir, Y., W. A. Robinson, I. Bladè, N. M. J. Hall, S. Peng, and R. Sutton (2002). Atmospheric GCM Response to Extratropical SST Anomalies: Synthesis and Evaluation. *Journal of Climate 15*(16), 2233–2256.

Kvamstø, N. G., P. Skeie, and D. B. Stephenson (2004). Impact of Labrador Sea ice extent on the North Atlantic Oscillation. *International Journal of Climatology 24*(5), 603–612.

Latif, M. and T. P. Barnett (1994). Causes of decadal climate variability over the North Pacific and North America. *Science 266*(5185), 634–637.

Latif, M. and T. P. Barnett (1996). Decadal climate variability over the North Pacific and North America: Dynamics and predictability. *Journal of Climate 9*(10), 2407–2423.

Latif, M., E. Roeckner, M. Botzet, M. Esch, H. Haak, S. Hagemann, J. Jungclaus, S. Legutke, S. Marsland, U. Mikolajewicz, and J. Mitchell (2004). Reconstructing, monitoring, and predicting multidecadal-scale changes in the North Atlantic thermohaline circulation with sea surface temperature. *Journal of Climate 17*(7), 1605–1614.

Lindzen, R. S. and S. Nigam (1987). On the role of sea surface temperature gradients in forcing low-level winds and convergence in the tropics. *Journal of the Atmospheric Sciences 44*(17), 2418–2436.

Lorenz, E. N. (1956). Empirical orthogonal functions and statistical weather prediction. Scientific Report 1, Air Force Cambridge Research Center, Air Research and Development Command. Cambridge Mass.

Mesquita, M. S., N. G. Kvamstø, A. Sorteberg, and D. Atkinson (2008). Climatological properties of summertime extra-tropical storm tracks in the Northern Hemisphere. *Tellus 60A*(3), 557–569.

Minobe, S., A. Kuwano-Yoshida, N. K. Komori, S. P. Xie, and R. J. Small (2008). Influence of the Gulf Stream on the troposphere. *Nature 452*, 206–209.

Molteni, F. (2003a, Visited September, 2007). Appendix to: Atmospheric simulations using a GCM with simplified physical parameterizations. I: Model climatology and variability in mutli-decadal experiments. http://users.ictp.it/∼moltenif/speedy-doc.html.

Molteni, F. (2003b). Atmospheric simulations using a GCM with simplified physical parameterizations. I: Model climatology and variability in multi-decadal experiments. *Climate Dynamics 20*(2-3), 175–191.

Namias, J. (1959). Recent seasonal interaction between north pacific waters and the overlying winds. *Journal of Geophysical Research 64*(6), 631–646.

NAO-webpage (2007, May). http://www.ldeo.columbia.edu/NAO.

Nigam, S. and E. DeWeaver (2003). Stationary Waves (Orographic and Thermally forced). In *Encyclopedia of Atmospheric Sciences*, pp. 2121–2137. Academic Press, Elsevier Science, London.

Palmer, T. and Z. Sun (1985). A modelling and observational study of the relationship between sea surface temperature in the north-west atlantic and the atmospheric general circulation. *Quarterly Journal of the Royal Meteorological Society 111*, 947–975.

Park, W. and M. Latif (2005). Ocean dynamics and the nature of air-sea interactions over the north atlantic at decadal time scales. *Journal of Climate 18*(7), 982–995.

Peng, S. and S. Li (2002). North Atlantic SST forcing of the NAO and relationships with intrinsic hemispheric variability. *Geophysical Research Letters 29*(8), 117 (1–4).

Peng, S., L. A. Mysak, H. Ritchie, J. Derome, and B. Dugas (1995). The differences between Early and Midwinter Atmospheric Responses to Sea Surface Temperature Anomalies in the Northwest Atlantic. *Journal of Climate 8*(2), 137–157.

Peng, S. and W. A. Robinson (2001). Relationships between atmospheric internal variability and the responses to an extratropical SST anomaly. *Journal of Climate 14*(13), 2943–2959.

Peng, S., W. A. Robinson, and M. P. Hoerling (1997). The modeled atmospheric response to midlatitude SST anomalies and its dependence on background circulation states. *Journal of Climate 10*(5), 971–978.

Pitcher, E. J., M. L. Blackmon, G. T. Bates, and S. Munoz (1988). The effect of North Pacific sea surface temperature anomalies on the January climate of a general circulation model. *Journal of the Atmospheric Sciences 45*(2), 172–188.

Press, W. H., S. A. Teukolsky, W. T. Vetterling, and B. P. Flannery (2003). *Numerical Recipes in Fortran 77* (Second ed.). Cambridge University Press.

Randall, D. A., R. A. Wood, S. Bony, R. Colman, T. Fichefet, J. Fyfe, V. Kattsov, A. Pitman, J. Shukla, J. Srinivasan, R. J. Stouffer, A. Sumi, and K. E. Taylor (2007). Climate Models and Their Evaluation. In *Climate Change 2007: The Physical Science Basis. Contribution of Working Group 1 to the Fourth Assessment Report of the Intergovernmental Panel on Climate Change [Solomon, S., D. Qin, M. Manning, Z. Chen, M. Marquis, K.B. Averyt, M.Tignor and H.L. Miller (eds.)]*, pp. 589–662. Cambridge University Press, Cambridge, United Kingdom and New York, NY, USA.

Rhines, P. B. and S. Häkkinen (2003). Is the oceanic heat transport in the North Atlantic irrelevant to the climate in Europe? *ASOF Newsletter No. 1*, 13–17.

Robinson, W. A. (2000). Review of WETS - The workshop on extra-tropical SST anomalies. *Bulletin of American Meteorological Society 81*(3), 567–577.

Rodwell, M. J., D. P. Rowell, and C. K. Folland (1999). Oceanic forcing of the winter North Atlantic Oscillation and European climate. *Nature 398*, 320–323.

Seager, R., D. S. Battisti, J. Yin, N. Gordon, N. Naik, A. C. Clement, and M. A. Cane (2002). Is the Gulf Stream responsible for Europe's mild winters? *Quarterly Journal of the Royal Meteorological Society 128*(586), 2563–2586.

Seierstad, I. A. and J. Bader (2008). Impact of a projected future arctic sea ice reduction on extratropical storminess and the nao. *Climate Dynamics Submitted*.

Seierstad, I. A., D. B. Stephenson, and N. G. Kvamstø (2007). How useful are teleconnection patterns for explaining variability in extratropical storminess? *Tellus 59A*(2), 170–181.

Sutton, R. T. and D. L. R. Hodson (2007). Climate response to basin-scale warming and cooling of the North Atlantic ocean. *Journal of Climate 20*(5), 891–907.

Sutton, R. T., W. A. Norton, and S. P. Jewson (2001). The North Atlantic Oscillation - What role for the ocean? *Atmospheric Science Letters 1*(2), 89–100.

Thompson, D. W. J., S. Lee, and M. P. Baldwin (2003). Atmospheric processes governing the Northern Hemisphere Annular Mode/North Atlantic Oscillation. In *The North Atlantic Oscillation: Climatic Significance and Environmental Impact*, Volume 134, pp. 81–112. American Geophysical Union.

Thompson, D. W. J., J. M. Wallace, and C. H. Hegerl (2000). Annular modes in the extra-tropical circulation. Part II: Trends. *Journal of Climate 13*(5), 1018–1036.

Timmermann, A., M. Latif, R. Voss, and A. Groetzner (1998). Northern Hemisphere interdecadal variability: A coupled air-sea mode. *Journal of Climate 11*(8), 1906–1931.

Vallis, G. K. (2006). *Atmospheric and Oceanic Fluid Dynamics* (First ed.). Cambridge University Press.

Wallace, J. M. and D. S. Gutzler (1981). Teleconnections in the geopotential height field during northern hemisphere winter. *Monthly Weather Review 109*(4), 784–812.

Wallace, J. M. and P. V. Hobbs (1977). *Atmospheric Science, an introductory survey.* Academic Press.

Walpole, R., R. Myers, S. Myers, and K. Ye (2002). *Probability and statistics for engineers and scientists* (Seventh ed.). Prentice-Hall.

Winton, M. (2003). On the climatic impact of ocean circulation. *Journal of Climate 16*(17), 2875–2889.

Xie, P. and P. A. Arkin (1997). Global precipitation: A 17-year monthly analysis based on gauge observations, satellite estimates, and numerical model outputs. *Bulletin of American Meteorological Society 78*(11), 2539–2558.